**Evolution of the South Dakota Tornado Outbreak**

**of 24 June 2003**

JAY TROBEC

*Sioux Falls, SD*

*Corresponding author address*:  Dr. Jay Trobec, KELO-TV, 501 South Phillips Avenue, Sioux Falls, SD  57104. E-mail:  jtrobec@keloland.com

**Abstract**

Several intriguing factors contributed to the single-day record tornado outbreak in South Dakota on 24 June 2003. One-half of the 67 tornadoes occurred in a warm sector which was weakly-sheared due to a substantially unidirectional flow. Strong surface heating and very steep low-level lapse rates promoted initiation of these tornadoes, many of which then exhibited unusual southeast-to-northwest movement. It was not the trochoidal curl motion documented in many previous events at the end of a longer-track tornado life cycle; radar data suggest it was instead the mechanism of mid-level mesocyclonic rotation which caused the tornado vortexes to veer cyclonically to the left (northwest quadrant) of the parent storm's movement throughout their lifetimes. Another supercell during the outbreak, near a surface-low pressure center, also produced a tornado which moved left of observed storm motion - though it was not as deviant as the tornado movement that occurred in the warm sector, and appeared to be related to the rear-flank downdraft and a preexisting convergence boundary. The anomalous tornado movements confirmed to operational forecasters that storm motion and tornado motion are not equivalent.

There are many papers in the meteorological literature about other notable tornado outbreaks, such as the 3 May 1999 outbreak around Oklahoma City (e.g. Thompson and Edwards, 2000; Edwards et al., 2002B), and the "Super Outbreak" on 3 April 1974 (Corfidi et al., 2004). But currently there is no such comprehensive study of the South Dakota outbreak. This paper will explore its evolution, including the cyclic supercell and cell mergers preceding the Manchester F-4. Additionally, a radar examination of conditions near Sioux

Falls airport quantifies extreme wind shear conditions and rapid tornadogenesis along the glidepath flown by a commercial jetliner as it attempted a landing near the conclusion of the outbreak.

## 1. OVERVIEW

The South Dakota tornado outbreak of 24 June 2003 occurred in a convectively unstable environment on the warm side of a southwest-northeast oriented stationary front. The outbreak began at approximately 2200 UTC, lasting six hours. During that time, 67 tornadoes were reported and confirmed in post-event surveys (refer to Appendix A). The event began with a supercell tornado near Mitchell. As the initial cell moved downstream (northeast) along the front, a series of supercell mergers and interactions took place. The result was an F-4 tornado that destroyed the town of Manchester.

Simultaneously, a series of cells moving out of northeast Nebraska created a cluster of generally-weak tornadoes in the warm sector in southeast South Dakota. These tornadoes formed in an area of weak flow, with the cluster moving slowly to the north toward the city of Sioux Falls. As a squall line approached from the west, tornadoes of F-0 to F-2 intensity occurred west and north of the Sioux Falls airport. We will discuss the individual tornadic events in the same general order as they developed during the outbreak.

We would like to acknowledge that, in addition to studies cited in this paper, there have been other studies of widely varying facets of this outbreak. For example, Passner and Noble (2004) measured acoustic energy generated by the tornadoes. Boustead and Schumacher (2004) examined the warm sector tornadoes in the context of the lack of a discernible surface boundary. Patterson and Cox (2005) used a supercomputer to create an artistic, 3D visualization of the airflow within the Manchester tornado. With an outbreak the magnitude of this one, there is much to study and much to discover.

## 2. THE FIRST SUPERCELL

An examination of the first supercell is essential to the study of the outbreak of 24 June 2003 because it was the first convective activation of the unstable environment that would produce the record tornado day. It occurred before other neighboring storms began to modify the atmospheric conditions in which the subsequent tornadoes formed.

The first cell requiring a severe thunderstorm warning in South Dakota developed rapidly in Davison County south of Mount Vernon and Mitchell. At 2122 UTC, the cell returned a 45 dBZ maximum reflectivity to the KFSD WSR-88D radar, distance 124 km (Fig. 1a), and was moving north-northeast at 16.5 m s$^{-1}$ (32 kt or 37 mph). By 2158 UTC, a circulation (adjacent regions of inbound and outbound Doppler velocities) was identified by the radar's mesocyclone detection algorithm (MDA; Stumpf et al., 1998). At 1.5 deg elevation, the supercell also exhibited a three-body scatter spike (TBSS; Fig. 1b), a radar signature indicating large hail (Lemon, 1998). The TBSS radar artifact is also referred to as a flare echo (Wilson and Reum, 1988). In either nomenclature, the radar returns depict three body scattering of hydrometeors first explained by Zrnic (1987). In this instance, several local storm reports received by the NWS reported hail sizes as large as 4.4 cm diameter north of Mitchell beginning at 2216 UTC.

In order to classify different types of supercells, Thompson and Edwards (2005) set the following characteristics of environmental conditions for a "classic supercell" - in contrast to an HP (high precipitation) or LP (low precipitation) supercell:

-Cloud base between 1-2 km

-Convective available potential energy (CAPE; Moncrieff and Miller, 1976) of 1500-3500 J kg$^{-1}$ and lifted index (LI; Galway, 1958) of -4 to -10

-Midlevel SR (storm relative) winds 10-18 m s$^{-1}$ (20-35 kt) and SR helicity >250

-Moderate precipitation efficiency, well-defined wall cloud, inflow region, and rear flank downdraft.

The initial supercell of this outbreak was appropriately described as a good fit for Thompson and Edwards' definition of a classic supercell because of the following factors:

a) The 1800 UTC meso-Eta model projected a cloud base of 1.1 km, surface-based CAPE of 3769 J kg, and LI of -7.5 (referenced in Part I of this thesis).

b) The 2300 UTC RUC analysis indicated 30 kt SR winds at 1 km. The 0-1 km SRH of 224.8 m$^2$ s$^{-2}$ (Barker, 2003) was just short of Thompson's 250 SR helicity threshold.

c) The storm produced precipitation, had a wall cloud reported by spotters, and exhibited an inflow region suggested by a tight radar reflectivity gradient on the south side of the cell. It also had a rear flank downdraft as evidenced by the resulting hook echo signature observed on radar.

Supercells classified as "classic" are somewhat more likely than low-precipitation or high-precipitation supercells to produce tornadoes (Davies-Jones et al., 2001), and that was the result here. The storm had 41 m s$^{-1}$ (80 kt) of gate-to-gate shear in storm relative mean (SRM) velocity at 0.5 degree at 2217 UTC (Fig. 2a and Fig. 2b) 8 km northeast of Mount Vernon. At 2220 UTC, emergency management reported "4 to 5 structures were impacted" by a tornado,

with large trees downed and at least one person injured (NOAA-SPC, 2003).

Base reflectivity of the storm remained ≥55 dBZ as detected by the KFSD radar at the 0.5 deg beam height continuously for 35 minutes until 2252 UTC. During this time it traveled 24 km (15 mi) to the north, with the resulting tornado leaving behind a path of damage ([Fig. 3](#)) rated as F-2 on the Fujita scale (Fujita, 1981).

## a. Anomalous tornado motion

Throughout the life cycle of the tornado, the NEXRAD combined attribute table estimated the cell was moving to the northeast. In the pre-event tornado watch issued by the Storm Prediction Center (SPC), mean storm motion was estimated from 230 degrees at 15 m $s^{-1}$ (30 kt). Since the tornado would be expected to travel with the parent supercell, a similar movement would be expected from the tornado vortex. But with the first tornado of the evening, the *tornado* damage path was mostly northward, appearing to deviate from the expected path of storm motion, resulting in a NEXRAD-based tornado vortex path forecast that was incorrect. This case confirms that tornado motion and supercell motion may differ significantly, as discussed in WDTB (2002) and documented by many, including high resolution Doppler studies such as Marquis (2006).

Typically, storm motion prediction vectors are derived from various components of RAOB sounding data. In recent years, the Bunkers ID (internal dynamics) method (Bunkers et al., 2000), utilizing storm advection by mean winds plus interaction of the convective updraft with the sheared environment, has gained acceptance operationally (Edwards et al., 2002;

Ramsay and Doswell, 2005). Previously, most storm motion predictions were variations of a method first proposed by Maddox using mean direction (and 75% of the speed, accounting for the storm's mass) of winds occurring through the 0-6 km layer, adjusted to the right by 30 degrees to allow for supercell dynamics (30R75; Maddox, 1976). Precision and reliability of either of these methods is obviously limited by the fact that RAOB soundings come from balloon launches that often occur several hours before, and many miles distant, from where storms occur.

In this case the tornado occurred in relatively close proximity (173 km) north of the Neligh, Nebraska vertical wind profiler. Real-time Doppler radar wind data at 36 sampling heights up to 16.25 km AGL was available from the profiler, which is part of the NOAA National Profiler Network (http://www.profiler.noaa.gov/jsp/profiler.jsp). The Neligh profiler winds appear to be a fair representation of the wind flow approaching the tornado in Mount Vernon, especially since surface orographic effects between the two locations are minimal.

Profiler data from Neligh was available at 2200 UTC, just as severe convection was beginning (Fig. 4). Winds in the lowest 1000 m were from the south, veering to southwest at 2000-3000 m AGL. At higher levels, the winds continued to veer through 9000 m, although the wind speed at that height was only 18 m s$^{-1}$ (35 kt). Those vectors were similar to the output of the KFSD NEXRAD VAD (velocity azimuth display) wind profile generated 122 km to the east of where the first supercell was located.

Given these layer wind directions and speeds, both the Bunkers method (Fig. 5) and the Maddox 30R75 storm motion method would move the supercell and resulting Mount

Vernon tornado in a northeast direction. The forecast was correct (NEXRAD

identified cell motion 220 deg at 8.2 m s$^{-1}$) - yet most of the damage path was oriented north,

approximately 40 deg to the left of what would be expected if the tornado moved in the same

direction as its parent thunderstorm.

Multiple factors may have contributed to the discrepancy between tornado motion and

supercell motion in this case. One may involve a subtle boundary that appeared in an

examination of 1 km visible satellite imagery. Towering cumulus was seen near Mitchell

beginning at 1815 UTC (Fig. 6a-b). By 1915, convective cells seemed to be forming along a

north-south oriented boundary (Fig. 6c). This boundary remained stationary for the next hour,

as the time series indicates (Fig. 6d-f). At 2115 UTC, a thunderstorm with anvil cloud has

developed on the boundary (Fig. 6g). It appears that the tornado vortex followed that

boundary due north as the supercell matured between Mount Vernon and Mitchell.

As the parent storm moved into the central part of Davison County at 2218 UTC, it

began swerving to the right. Most supercells do move to the right, due to the pressure gradient

on the right flank of the rotating updraft (Rotunno and Klemp, 1985). From here it assumes

the forecasted northeast path, with a backsheared anvil evident on satellite imagery (Fig. 6h). It

appears the original movement of the initial *tornado* was atypical, not following the expected

northeast path. It instead followed the north-south boundary.

Operationally, the difference between supercell motion and tornado motion with this

cell was difficult to detect in real time. In fact, the tornado warning statement issued by the

National Weather Service (NWS) at 2212 UTC mentioned, "a tornadic thunderstorm near Mt.

Vernon… moving northeast at 20 mph" which was true, although the *tornado* path

of threat was to the north. Forecasters were not alerted at this time by the NEXRAD radar

tornado vortex signature (TVS) and elevated tornado vortex signature (ETVS) algorithms,

which were not triggered by this cell. But the mesocyclone detection algorithm (MDA; Stumpf

et al., 1998) did pick up the midlevel rotation of the broader storm, and may provide some

further clues about the supercell's behavior.

The midlevel circulation that activated the MDA is apparent in a time series of

NEXRAD level 3 SRM velocity images from the KFSD WSR-88D radar. At 2153 UTC a

mesocyclone was detected and given the identifier R9, indicated by a red circle marker in the

display (Fig. 7a). The MDA embedded within the NEXRAD combined attribute table placed

the center of the circulation south of Mount Vernon. At 2158 UTC (Fig. 7b) the MDA moves

the mesocyclone center to the north-northeast, identifying its direction of movement from 207

deg, or slightly to the left of anticipated storm motion (a left-mover). The following volume

scan at 2203 UTC showed significant dealiasing failure, seen in the SRM product in the 2.4 and

3.4 deg elevation tilts (Fig. 7c), causing R9 to disappear temporarily. This loss of data proves

significant because we cannot tell if the algorithm would have continued to move the

mesocyclone center to the north-northeast prior to tornadogenesis, or if the cell had already

begun to move to the right. Visually, the 1.5 deg tilt puts the center of the midlevel circulation

south of Mount Vernon based on the placement of opposing gates of 28 m s$^{-1}$ inbound and 13

m s$^{-1}$ outbound. Storm R9 regains its radar attributes at 2208 UTC (Fig. 7d), with the center of

the midlevel rotation now east of Mount Vernon. At 2213 UTC (Fig. 7e) the MDA marker

jumps sharply to the east, along with a gate-to-gate shear couplet that is seen on the SRM 1.5

deg and 2.4 deg elevations 7 km east of Mount Vernon. However, it should be

noted that the strongest shear at the 1.5 deg elevation actually appeared 3 km east of Mount

Vernon, near where the RFD side of the hook echo is located. That is where there is a couplet

of 23 m s$^{-1}$ inbound and 18 m s$^{-1}$ outbound at 4 km AGL, collocated with a similar circulation

at the lower level 0.5 deg SRM elevation (previously referenced in Fig. 2b). That is also the

location of a tornado damage report time stamped 2215 UTC by the NWS.

After this, the path of the mesocyclone center and the tornado damage path rapidly

diverged. At 2218 UTC (Fig. 7f), the MDA marker is 8 km northeast of Mount Vernon,

moving 212 deg at 8.7 m s$^{-1}$ according to the NEXRAD attribute table. Through the next two

volume scans at 2223 UTC (Fig. 7g) and 2228 UTC (Fig 7h), the mesocyclone assumes more

of a right movement (eastward) at 222 deg. By 2233 UTC, the MDA tracking of mesocyclone

R9 ceased (Fig. 7i) although the remaining thunderstorm continued moving to the northeast.

Radar evidence of the anomalous movement of the tornado associated with

mesocyclone R9 can be deduced with NEXRAD level 2 data. We can see how the tornado

followed this weak convergence/boundary almost due north by examining the spectrum width

(SW) returns. Spectrum width is a measure of the velocity dispersion within the pulse volume

(Lemon, 2005). Tornado vortexes are one of the atmospheric conditions which produce high

SW values.  Herald and Drozd (2001) suggest areas of SW >6 m s$^{-1}$ (12 kt) be scrutinized for

tornado presence. In this case, radar returns beginning at 2208 UTC (Fig. 8a) show SW

maxima >7 m s$^{-1}$ (14 kt) on the east side of Mount Vernon, where there were confirmed

tornado touchdowns. The next volume scan at 2213 UTC (Fig. 8b) shows the high SW area

moving to the north, a path it continued over the next three volume scans, covering

a total of 20 minutes and approximately 10 km (Fig. 8c-8e) before the vortex detected with SW

dissipates.

It must be noted that there was also a large region of high SW values east of the

tornado closer to the mass centroid of the supercell. They were produced by the inflow

notch/updraft region of the storm, as evidenced by the tight reflectivity gradient along the S

side of the cell. One limitation of the use of SW data is that intense updrafts, three body

scattering, and deep convergence zones (DCZ; Lemon and Burgess, 1993) within the supercell

can also produce high SW values (Lemon, 2005). Operationally, the product also tends to be

quite noisy. As a result efforts have been made to integrate spectral and velocity data in a fuzzy

logic and neural network to improve tornado detection and lower the false alarm rate (Wang

et. al, 2006).

If we overlay the SW maxima (ignoring the SW maxima associated with the

precipitation cascade region of the supercell) and the MDA markers on the map of tornado

damage (Fig. 9), we get a clearer indication of what happened. The SW maximums on the rear

flank of the storm are collocated with the tornado path charted by the NWS damage survey.

Again the path of the tornado vortex appears to be primarily north - not northeast. Such

anomalous tornado motion is not unprecedented. During the VORTEX study (Rasmussen,

1994), for example, there were two days in which tornadoes moved to the north while their

parent thunderstorms moved to the northeast (WDTB, 2002), which appears to be exactly the

case here. An opportunity for further study might be the frequency with which tornado vortex

motion occurs to the left of the parent supercell's motion, and the tornado's

location relative to the parent mesocyclone.

## b. Tornadoes near the "triple point"

The strongest supercell remained in close proximity to the surface low and

stationary/warm front, eventually making its way through Sanborn County. Multiple tornadoes

were reported, especially around Forestburg, where a "large tornado with lots of debris" was

reported by an off-duty NWS meteorologist (NOAA-SPC, 2003). New storms initiated 32 km

(20 mi) to the northwest along an existing boundary near Woonsocket by 2245 UTC. A

strengthening tornado produced a swath of F-1 to F-3 damage (Fig. 10)

Just as the strongest supercells were moving to the north-northeast, so too did the

surface low, which appeared for the next two hours to remain slightly southwest of where the

tornadoes were occurring. The surface low pressure center was near Forestburg at 0000 UTC

(Fig. 11a), then continued to slowly drift in a northeast direction. The low deepened to an

ASOS-observed 999.9 hPa at 0100 UTC (Fig. 11b), and maintained that pressure at 0200 (Fig.

11c), when it was located just east of Huron. The attendant stationary-warm front was where

the strongest tornadoes would occur before the pressure gradient began to ease at 0300 UTC

(Fig. 11d), and by 0400 UTC only an inverted trough remained in South Dakota (Fig. 11e).

The nearness of the surface low appeared to be a factor not only in the strongest

tornadoes during this outbreak, but also in most violent tornadoes in the Northern Plains.

When studying tornadoes ≥ F-4 in the Northern Plains 1993-1999, Broyles et al. (2002) found

they were all within 400 km (250 mi) of the surface low. In this case, the proximity

was even closer, with all of the F-3 and F-4 tornadoes located within 50 km of the surface low.

This is a similar distance as was between a surface low and the long-track Chandler-Lake

Wilson-Leota F-5 tornado in southwest Minnesota in 1993.

Surface pressure falls are known to increase horizontal vorticity, leading to increased

storm relative helicity (Meted, 2006). In the South Dakota outbreak, the approach of the

surface low may have helped overcome initially weak shear in the environment to promote

tornadogenesis. The backing of surface winds near the low increased directional shear with

time. The SPC's significant tornado parameter (STP; Thompson et al., 2004) picked up on

these factors, and with the 2300 UTC and 0000 RUC runs the STP increased in this area to

extremely high values (>10 unitless).

## 3. THE MANCHESTER TORNADO

In addition to their close proximity to the surface low, the interaction of a group of

supercells near the surface low contributed to generation of the only F-4 tornado of the

outbreak. This is where the strongest tornadoes would be expected, because by this time

helicity, shear, and CAPE were all substantial.

### a. Cell mergers

Three distinct storms (0.5 deg base reflectivity > 40dBZ) were discernable at 2308

UTC from the KFSD radar (labeled #1, #2, and #3 on Fig. 12a).  Storm #1 was located six

miles west of Woonsocket, storm #2 was near Alpena, and storm #3 was farther southeast,

near Artesian. At this time the storms were all approximately 140 km (87 mi) from

the KFSD radar, and exhibited maximum reflectivities ~60 dBZ. The KFSD radar algorithm

estimated storm motion as northeast at 9-11 m s$^{-1}$ (20-25 mph). The strongest storm was #1,

with an attributed VIL (vertically integrated liquid) of 67 kg m$^2$, and storm top height of 13624

m (44,700 ft). There was also a strong cyclonic couplet on the SRM (storm relative mean)

velocity product (Fig. 12b).

The Baron shear algorithm (Wilson and Lemon, 2000) processes NIDS data from all

available WSR-88D radars in real time, integrates velocity values from the lowest two

elevations of those radars, outputs a cyclonic shear value in knots, and places a marker at the

location of the shear maximum on a radar display for use by television stations and other end-

users. At this time, the algorithm detected and marked 47 m s$^{-1}$ (92 kt) of low-level shear in

storm #1, especially significant because the storm is 138 km (86 mi) from the KFSD radar.

That distance is beyond the range at which the WSR-88D's tornado vortex signature algorithm

(TVS; Brown et al., 1978) is calculated. But tornado damage of F-3 severity occurred

coincident with where the Baron shear marker was placed.

Ten minutes later, at 2318 UTC, storm #2 appears to be entraining precipitation and

cold air from the forward flank of the stronger storm #1 in a destructive merger (Fig. 13 a-b).

Storm #1 now has a VIL attribute of 76 kg m$^2$, a top of 15330 m (50,300 ft), and exhibits a

hook echo as it continues to moves to the northeast at 9 m s$^{-1}$ (20 mph). Northeast of the

hook, there is a bounded weak echo region (BWER), 23 miles (37 km) southwest of

Manchester. The BWER was in close proximity to an echo overhang at higher elevations

(cross-section, inset of Fig. 13a), indicating the presence of a strong, nearly vertical, updraft suspending precipitation aloft.

By 2338 UTC (Fig. 14 a-b), storm #1 is returning 60 dBZ with a VIL of 78 kg m$^2$ and storm top of 15.4 km (50,600 ft). It is moving north-northeast at 11.2 m s$^{-1}$ (25 mph) toward the town of Manchester. Storm #3 has reorganized and moved to the north, heading into the projected path of storm #1. The two cells merge by 2353 UTC (Fig. 15a), with KFSD radar indicating 41.2 m s$^{-1}$ (80 kt) of cyclonic shear 27 km (17 mi) southwest of Manchester (Fig. 15b). Because the two storms both had inflow from the south or southeast, as evidenced by the tight reflectivity gradient and SRM data, it appears this merger was a constructive one, strengthening the now-combined supercell (Fig. 16 a-b).

A reflectivity hook echo is observed at 0023 UTC (Fig. 17a), and SRM velocity has a strong cyclonic shear couplet (44 m s$^{-1}$, or 86 kt of base velocity shear at the location of the shear marker) on the southwest side of Manchester (Fig. 17b). Storm spotters reported "two tornadoes on the ground concurrently" at 0027 UTC (NOAA-SPC, 2003) co-located with that shear.

**b. Discussion of the cyclic nature of the Manchester supercell**

The two simultaneous tornadoes appeared to result from the regenerative cycling process of the supercell. One of the tornadoes was weakening as the other was strengthening, occurring just before the tornado went through Manchester.

A cyclic supercell is described in various ways. In the NWS Advanced Spotters' Field

Guide it is described as a supercell which undergoes the mesocyclone formation-tornado formation-rear flank downdraft formation process a number of times (NOAA-NWS, 1992). As one tornado dissipates, another tornado develops to the east where the evaporatively-driven rear flank gust front and a stationary/warm front (in this instance called the pseudo-warm front) intersect (WW2010, 2004). This evolution is diagrammed in an idealized schematic (Fig. 18). The tornadogenesis occurs as storm inflow is refocused into this region to the east, causing the tornado coincident with the newly-dominant updraft and possible vorticity maximum. Dowell and Bluestein (2002A) concluded that a wind shift is not necessary for the second tornado to develop, contrary to previous conceptual models. In either case the original tornado dissipates because, as speculated by Dowell and Bluestein (2002B), it either has become disconnected from the warm sector or has had its low level wind field disrupted (lacking vorticity).

The cycling process in the Manchester supercell can be observed in 0.25 km resolution level 2 velocity data from the KABR radar 113 km to the north. The center beam height of the 0.5 deg tilt at this distance is 2188 m AGL. To this data we applied a storm motion vector of 240 deg at 10.3 m s$^{-1}$ to obtain the SRM velocity output. Note this is different from the NEXRAD level 3 data, because we wanted to utilize the finer resolution of the level 2 data.

At 0003 UTC, a strong cyclonic couplet is collocated with the hook echo (Fig. 19), but no tornado was reported at this time. In the next volume scan, the hook is filling (Fig. 20) and a brief, F-0 tornado was reported southeast of Cavour. At 0013 UTC (Fig. 21), SRM velocity indicates the cyclonic circulation southeast of Cavour has weakened and another circulation

seems to be forming south of Iroquois. By 0018 UTC (Fig. 22) the Cavour

circulation has dissipated, and the circulation south-southeast of Iroquois has taken over. The

tight reflectivity gradient in the same area indicates this is now the inflow region. Continuing

with the evolution, the next scan shows a new hook echo forming at 0023 UTC (Fig. 23). As

the new hook wraps around at 0028 UTC, a strong cyclonic couplet appears just southwest of

Manchester (Fig. 24). By 0033 UTC, the couplet, hook, and F-4 tornado are all moving into

Manchester itself (Fig. 25).

Earlier in its lifecycle, the Manchester supercell had exhibited multiple RFD surges, as

documented by a mobile mesonet array (Lee et al., 2004; Finley, 2004; Grzych, et al., 2004), all

of whom classified Manchester as a cyclic supercell.

But whether this case meets guidelines for a cyclic supercell is not a closed question.

Although there is no clear, definitive definition of the term, Adlerman (1999), Dowell and

Bluestein (2002A), and Beck et al. (2004) specifically describe the initiation of new

mesocyclones along the occlusion point and the demise of the original mesocyclone in cyclic

supercells.

There was no complete dissipation of the mesocyclone involved in the Manchester

tornado. If one looks at the higher tilts of radar, particularly the 1.5 deg velocity scan from

KFSD with Gibson Ridge dealiasing algorithm applied (Fig. 26), one finds a continuous

cyclonic signature in every volume scan from 2338 UTC to 0033 UTC, traveling a distance of

43 km to Manchester. While this signature is not seen continuously in the lowest, 0.5 deg tilt

(beam height 1645 m) during the cell mergers previously described, the 1.5 deg signatures at

beam height 3810 m appear to meet the criteria for single Doppler radar detection

of mesocyclones. Specifically, there was Doppler velocity shear $\geq$6 m s$^{-1}$ and differential

velocity $\geq$30 m s$^{-1}$ (Donaldson, 1970), and the circulation was 2-10 km wide (Glickman, 2000).

Since the mesocyclone is persistent for 1 h, this would call into question whether the repeated

mesocyclone formation-tornado formation-rear flank downdraft formation process in the

NWS description of a cyclic supercell was realized.

To carry the argument further, one might assert that even though the mid level

mesocyclone remained intact, the *low level* mesocyclone formed, occluded, and reformed. That

would explain the discontinuity between the 1.5 deg and 0.5 deg radar data. It is because of the

low level cycling and repeated tornadogenesis that Lee and Finley classified the Manchester

storm as a cyclic supercell (Lee and Finley, personal communication). This fits with the

mesocylogenesis described by Adlerman et al. (1999), who made a clear distinction between a

persistent mid-level (3-7 km) mesocyclone and the shorter lived low-level rotation.

Perhaps if there is any uncertainty, one might use the more generic term "cyclic

tornadogenesis" (Rasmussen et al, 1982; Wicker and Dowell, 2000; Dowell and Bluestein,

2002A and 2002B) when describing the Manchester storm.

**c. F-4 tornado**

At 0033 UTC, the tornado entered Manchester from the south, with KFSD base

reflectivity displaying a pronounced hook echo (Fig. 27a). Simultaneously, SRM velocity

indicated a maximum velocity of 26 m s$^{-1}$ (50 kt) into the hook, just in front of the rear flank

downdraft (Fig. 27b). Immediately to the east of that couplet is a gate 21 m s$^{-1}$ (40 kt) inbound toward the KFSD radar, creating an accompanying anticyclonic vortex. This might also be an indication of a gust front associated with the occlusion of the mesocyclone (L.R. Lemon, personal communication). Such an occlusion would be centered on or near the cyclonic shear signature.

At 0042 UTC, base velocity from KFSD had a divergent couplet (adjacent gates of opposing velocities on the same radial) of 36 m s$^{-1}$ (70 kt) of shear directly over Manchester (Fig. 28a). A slowly moving tornado passed directly through Manchester (Fig. 28b), inflicting F-4 damage.

The depth of the rotation and upright stature of the storm are of particular interest, because they are more pronounced than the other storms in the outbreak. Looking at a range-height indicator (RHI) side view from the south (Fig. 29), the cyclonic circulation over Manchester is exceptionally vertically stacked and at least 6100 m (20,000 feet) deep. Most of the time, mesocyclones are tilted and the radar-detected rotation is displaced from the vertical with height (Speheger and Smith, 2006). At this time the storm top was also began descending, from 16.2 km (53,100 ft) to 13.7 km (44,900 ft).

Engineer and storm chaser Tim Samaras deployed five turtle-like weather probes on the west side of Manchester in advance of the storm (Samaras, 2004). Two of the probes were near or under the tornado itself (Fig. 30a). One of them recorded a 100 hPa barometric pressure fall, thought to be the greatest pressure drop ever recorded in the field by an in-situ weather instrument (Fig. 30b).

As the storm moved north of Manchester it was still producing a tornado, although the maximum velocities were no longer as tightly packed as they were in Manchester. Visually, the tornado began to "rope out" as it decayed (Fig. 31a-b).

The tornado created F-4 damage from 2.4 km south of Manchester to 3.6 km north of the town. The total continuous damage path was 40 km long (NWS-FSD, 2003). In addition, several short-lived F-0 to F-2 tornadoes F-0 to F-2 occurred as the right-moving supercell that went through Manchester completed another cycle of tornadogenesis (Fig. 32).

## 4. WARM SECTOR TORNADOES

At the same time the Manchester tornado touched down, thunderstorms developed in the warm sector in the southeast corner of South Dakota. While this was an area of high instability, it would not have been considered exceptionally favorable for tornado development.

### a. Shear and buoyancy

Environmental winds in southeast South Dakota showed limited directional shear. In the 1800 UTC 24 June 2003 meso-Eta model sounding for KYKN (Yankton), valid at 0000 UTC 25 June (Fig. 33), the vertical wind profile veered only from southeast to southwest with height. Consequently, storm relative helicity (SRH) was diminished. SRH in the 0-3 km layer was 230 $m^2$ $s^{-2}$; a value of 150 to 299 is considered weak for tornado potential (Sturtevant, 1994). SRH in the 0-1 km layer was only 64 $m^2$ $s^{-2}$; for that layer a value greater

than 100 should be reached for an increased threat of tornadoes with supercells

(Thompson, 2003).

What the area near the Nebraska border lacked in wind profile was compensated for

with buoyancy. Table 1 shows lapse rates based on meso-Eta temperatures at specific

pressure surfaces (e.g. 950 hPa-900 hPa, 850 hPa-700 hPa) for KYKN. Destabilization is

suggested by very steep lapse rates which had increased through the afternoon to 10-11°C

km$^{-1}$ in the lowest 100 hPa of the atmosphere. In addition, the LCL and LFC were both very

low, near 1200 m AGL. CAPE was 4623 J kg$^{-1}$, of which 196 J kg$^{-1}$ was in the 0-3 km layer.

That is significant because 0-3 km CAPE around 200 J kg$^{-1}$ is considered quite large, and

may contribute to weak or low-end significant tornadoes in weaker shear environments

(Davies, 2002).

The imbalance between buoyancy and shear skewed the bulk Richardson number

(BRN), a unitless severe weather parameter which has long been used as a supercell

predictor. Weisman and Klemp (1982) concluded that BRN < 50 favored supercells, while

BRN > 50 favored multicellular storms. Here the BRN was 61, yet supercells were

produced.

Even forcing for thunderstorm initiation was an issue in the warm sector, since there

were no existing convergence boundaries apparent on radar or satellite (refer back to Fig. 6).

But initiation was supported by significant solar heating. The 1800 UTC meso-Eta forecast a

convective temperature of 31.9°C at 2200 UTC at Yankton. By 2300 UTC, the KYKN

observed temperature was 32.8°C.

Thirty-three tornadoes - accounting for approximately one-half of the outbreak - occurred in this area. Most of the tornadoes were short-lived, and produced F-0 to F-2 damage (Fig. 34). Note that many of the damage paths are unusually oriented southeast to northwest.

## b. Anomalous tornado motion

The southeast to northwest directed damage paths are intriguing, because winds aloft veer directionally from the south at 18 m s$^{-1}$ (35 kt) at 850 hPa to southwest at 21 m s$^{-1}$ (40 kt) at 500 hPa. The only layer that has prevailing southeast winds is the surface (Fig. 35) from the northwest corner of Iowa through southeast South Dakota (including Turner County). The multiple southeast-northwest oriented tornado tracks may appear to come from left-moving supercells, but left movers are rarely known to produce tornadoes (Bunkers, 2002).

One storm chaser who observed and photographed the Turner County tornadoes north of Centerville described those tornadoes as coming from large, northward moving supercells. He said tornadoes formed as the rear flank downdraft suddenly strengthened, on the southeast (inflow) side of the storms, and moved around the parent circulation counter-clockwise as in a "merry-go-round." When the tornadoes reached the northwest side of the large mesocyclone, new tornadoes re-formed on the southeast flank and began a similar, circuitous movement around the storm (Jeff Piotrowski, personal communication). The concept is somewhat analogous to the motion of suction vortices with a large scale tornado.

Radar data seems to support this contention. During the tornado touchdowns in

Turner County, between 0040 UTC and 0140 UTC (25 June 2003), KFSD radar

algorithms generated more than a dozen storm cell identification and tracking (SCIT)

markers, categorized as mesocyclone and TVS. In every case, algorithms identified the

direction of cell movement as either north or northeast. This would be consistent with

storms occurring within the southerly, 35 kt low-level jet depicted by the RUC model at 850

hPa (Fig. 36).

But an examination of radar-indicated shear (combined base velocity and SRM

velocity) shows curved paths consistent with those that tornadoes circling around northward

moving mesocyclones would take. A mosaic of maximum cyclonic shear during the tornadic

period (Fig. 37) shows a cyclonic curve in the shear pattern. The shear maxima match the

damage paths well, as indicated during the post-event survey.

Such leftward-moving tornadoes are not unheard of, though documented cases seem

to favor the leftward swing during the dissipation phase of longer track tornadoes. One

occurred during the Kellerville, TX during the VORTEX study (Wakimoto et al., 2003). In

that case, while the mean storm motion was from southwest to northeast, the tornado did

swerve in a northwest direction (trochoidal track) toward the end of its life. A trochoid is a

curve created by a fixed point along the radius of a rotating circle (Weisstein, 2006). The

theory posited is that the leftward-swerving damage paths were caused by the tornado

revolving around the larger-scale mesocyclone.  But it should be noted that the Kellerville

tornado had been creating F-5 damage during its mature stage, while northwestward-moving

southeast South Dakota tornadoes never produced more than F-2 damage.

Several leftward-swings were detected in the family of tornadoes

documented in the McLean, TX storm during VORTEX (Dowell and Bluestein, 2002A).

Again the movement appears at the end of the longer, southwest to northeast track of the

damage path. The difference in this event is that the tornadoes were associated with a cyclic

supercell, so each regeneration of the tornado vortex had the similar trochoical curl during

dissipation. Burgess et al. (1982) specifically included this curl in diagramming what they

called mesovortex core evolution.

Agee et al. (1976) also detected leftward moving tornadoes during an examination of

the 1974 Super Outbreak in Indiana, describing them as multiple vortices embedded within a

parent tornado cyclone system. During the Super Outbreak, there were several damage paths

that moved in a cycloid direction, either to the left or the right depending on which quadrant

of the parent circulation they were located.

Potts and Agee (2002) point out different types of mesocyclone vortexes are

associated with different types of tornado damage paths, and they attempted to classify

them. One of the ten types they identified is an M-I, a mesocyclone with mini-tornadoes that

produce curtate cycloidal damage patterns. A curtate cycloid (Fig. 38), a subset of trochoids,

consists of a path traced out by a fixed point along the radius *inside* a rolling circle (Weisstein,

2006).

The relevance of this study to the 24 June 2003 warm sector tornadoes can be

demonstrated with a hodograph and a curtate cycloid diagram (Fig. 39). The hodograph is

the BUFKIT forecast of winds from the 1800 UTC meso-Eta, plotted for the 0100 UTC

time frame that evening at KYKN. The profile shows a 0-6 km mean wind

calculation of 200 deg at 13 m s$^{-1}$. This represents the mean wind within the cloud-bearing

layer of the storm, a fair approximation of the movement of the mid-level mesocyclone

(Stumpf et al., 1998). If we apply the 200 deg vector and assume a curtate cycloid movement

of the resulting tornado, we see that tornadoes that form on the east (inflow) side of a storm

can move in a southeast to northwest direction as the storm as a whole propagates forward.

The parallel paths of the smaller tornadoes were probably due to continuous formation of

multiple tornadoes by other mesocyclones.

With the correct location of the storm along the mesocyclone radius, the tornado can

actually move in a somewhat straight southeast to northwest path, rather than a curved one.

A close examination of NEXRAD level 3 KFSD Doppler radar velocity data pertaining to

the F-2 tornado near Centerville in southern Turner County seems to support this assertion.

The NWS damage survey confirmed the F-2 started 1 mi (1.6 km) northwest of Centerville.

Spotter reports placed it there at 0057 UTC, after which it traveled from southeast to

northwest (NWS-FSD, 2003). To visualize the actual tornado location, we imported the

NWS damage path map into a radar PPI display, and compared the path of that tornado and

others to the location of the mesocyclone. We found the best view of the midlevel

circulation centers of the storm at the 2.4 deg radar beam elevation (tilt 3 of level 3 data),

intercepting the storm at a height of approximately 2500 m AGL.

It should be noted that quality of the velocity field from this storm was degraded by

significant range folding, and an inability to properly resolve velocities through dealiasing.

The NEXRAD mesocyclone detection algorithm (MDA) was able to generate mesocyclone markers in some cases, but it did not recognize all circulations due to range folding observed in a comparison of the level 3 data and level 2 output of the radar. We focused on the F-2 tornado because it had the most distinct radar signature. Nearby smaller, weaker tornadoes were difficult to discern, given their size and distance (55 km) from the radar.

At 0043 UTC (Fig. 40), a developing mid-level circulation is seen in the storm relative velocity field (lower right panel of each image), with 46 m s-1 (90 kt) of shear. Tighter gate-to-gate shear is located directly over Centerville, a signature of the developing F-2 tornado. The following volume scan, 0048 UTC (Fig. 41), shows the developing mesocyclone in approximately the same location, while the tighter circulation has moved to the northwest. This is where the first tornado touchdown was reported, on the north side of Centerville. An MDA (mesocyclone detection algorithm) marker is generated during the 0053 UTC volume scan (Fig. 42), placed just east of Centerville in line with that circulation's north-northeast (200 deg) movement. The shear associated with the F-2 tornado continued moving due northwest along the post-event damage path. The divergent movements continued at 0058 UTC (Fig. 43), with the tornado now east of Viborg. The location of the tornadic shear cannot be discerned from the 0.5 deg level 3 images due to incomplete dealiasing. The location is implied by damage path, as well as the location of vertically stacked shear in level 2 velocity data from the same time period (not shown) at 0.4, 1.4, 2.4, and 3.4 deg. Meanwhile the mesocyclone was still moving away to the northeast. At this point, the mesocyclone circulation had considerable depth, from a base of 2166 m, to a top

of 9518 m AGL. Low-level shear coincident with a new tornado has formed on the northwest side of the MDA marker, collocated with the southeast to northwest F-1 damage path of the second tornado.

Dealiasing problems also dampen the tornado signature at 0.5 deg at 0103 UTC (Fig. 44) and 0108 UTC (Fig. 45). In each case, ground location of the damage paths was compared with level 2 velocity data to set the tornado location and time. During the life cycle of the mesocyclone (0053 UTC-0108 UTC) the center of the mesocyclone circulation travelled northeast (190 deg) 11.1 km, at a speed of 12.4 m s$^{-1}$. The associated tornado moved northwest (310 deg) 10.2 km at a speed of 11.3 m s$^{-1}$. In this case of the F-2 tornado near Centerville, the mid-level mesocyclone moved at approximately the forecast mean speed and direction, while the tornado produced by that circulation moved in a generally straight line in a divergent direction.

## c. Discussion of the anomalous motion

We can examine the movement of the tornado analogous to an object rotating around the circumference of a rotating disk. While a disk is solid and a mesocyclone is a viscous fluid of air, we can at least compare the speed of mesocyclone rotation to the location of the tornado to see if our thesis is mathematically plausible.

A map locating the mid-level circulation centers and F-2 tornado (Fig. 46) shows the divergent paths, with time stamps determined by a combination of radar-indicated rotation, MDA circulation centers, and NWS damage reports. In each of the four volume scans 0048-

0103 UTC, the mesocyclone and associated tornadoes were approximately 12 km

apart. If vectors are drawn between each tornado and the coincident location of the

mesocyclone circulation center, they veer cyclonically. Combining those vectors results in a

schematic storm-relative view of the mesocyclone (Fig. 47a). This rotational movement is

the mechanism resulting in the curvilinear direction of tornado movement in the northwest

quadrant of the mesocyclone.

Tangential velocity is the linear velocity of a point (in this case, a tornado) on a

rotating disk at a radius ($r$) from the axis of rotation. It can be calculated by taking

circumference of the full circle ($2\pi r$) divided by the time period it would take for one

complete revolution. The tornado location veered 45 deg (1/8 of a circle) in 15 min.

$$\frac{2\pi r}{8(15\ min)} = \frac{2(3.14)12000\ m}{120\ min} = \frac{75{,}360\ m}{120\ min} = \frac{628\ m}{min} = \frac{10.5\ m}{sec}$$

A tangential velocity of 10.5 m s$^{-1}$ seems reasonable, especially compared with the

radar data examined previously. At 0058, when shear maxima in the storm were stacked

most vertically upright, the 3.3 deg elevation of storm-relative velocity from the KFSD radar

resulted in a beam height of 3048 m AGL (Fig. 47b). Rotation can be quantified by the

azimuthal shear across the outermost opposing gates of the 12 km disk at this elevation.

$$\frac{(+12\ m\ s^{-1}) - (-15.5\ m\ s^{-1})}{12\ km} = \frac{27.5\ m\ s^{-1}}{12000\ m} = .0023\ s^{-1}$$

The broad area of radar outbound gates ranging from 7-15 m s$^{-1}$ at this radar level

(red area circled in figure) appears consistent with the circulation producing the leftward-

movement and speed of the tornadoes. Although tornado damage paths and radar

TVS locations do not always match up due to storm tilt and other factors (Speheger and

Smith, 2006), there appears to be fair agreement in this case.

## 5. TORNADOGENESIS NEAR SIOUX FALLS AIRPORT

By 0300 UTC, a north-south oriented squall line had formed, and with sunset it

appeared the event was starting to transform into an MCS (mesoscale convective system). But

the tornado outbreak was not over yet.

### a. Bow echo development

As the squall line rapidly moved east, the squall line bulged out into a bow, with

Doppler velocities of 20-25 m s$^{-1}$ (40-50 kt) behind the apex of the reflectivity gradient.

Those values may be underestimated, because the bow echo was moving slightly across the

beam, not quite radially toward the radar beam. Since the KFSD radar was operating in VCP

(volume coverage pattern) 11, new volume scans were completed every five minutes and the

lowest elevation scans, here referred to as BREF1 (base reflectivity) and SRM1 were both

gathered at 0.5 deg beam height, or ~500 m AGL at the bow.

Strong cyclonic shear developed on the northern end of the bow apex south of

Pumpkin Center, north of Parker at 0308 UTC (Fig. 48a-b). This is the favored region for

tornado development associated with a bow echo (Fujita, 1978). During this time a brief F-1

tornado was produced with wind damage reported along the bow apex west of Sioux Falls.

Note that east and southeast of the circulation, KFSD is exhibiting range folding problems,

also known as "purple haze" (OFCM, 2005) on the radar display.

The circulation moved to the northeast along the northern side of the bow echo at 0313 UTC (Fig. 49a-b). The cyclonic shear increased to over 41 m s$^{-1}$ (80 kt) as the circulation continued along the "comma head" of the bow as it moved northeast toward Hartford (Fig. 50a-b). A tornado touched down as the circulation crossed Interstate 90 on the east side of Hartford with ~41 m s$^{-1}$ (80 kt) of cyclonic shear (Fig. 51a-b). Sixteen homes were damaged or destroyed by an F-1 tornado.

Baron shear markers were not generated by the 0328 UTC volume scan (Fig. 52a-b), probably due to processing problems with the aliased data. Strong inbound velocity bins were noted as the squall line approached the WSR-88D, and the level 3 radar data is filled with spurious data. Velocity dealiasing failure occurs in the level 3 KFSD data, continuing through the next volume scan at 0334 UTC (Fig. 53a-b) as the storm passed just north of Sioux Falls airport.

During that time period, a passenger jet carrying one hundred passengers from Minneapolis was scheduled to land at Sioux Falls airport. At 0333 UTC the plane was making an approach to runway 15, which brought it toward the airport from the northwest, in close proximity to where the tornado was located.

Airport and onboard wind shear alert systems both sounded. The aircraft swerved and rolled before the pilot pulled out of the landing and was re-routed to Omaha. Shortly after the aborted landing, the control radioed the aircraft that a tornado had been reported

four miles northwest of the airport. The co-pilot replied, "Copy, I think we got a nice glance at it." (Trobec, 2003)

Shortly thereafter, the outbreak transitioned into a heavy rain event. Widespread rainfall of 1-2 inches (2.5-5 cm) occurred in eastern South Dakota.

**b. Volumetric radar analysis**

Because the Hartford and airport tornado occurred within 17 km of the KFSD RDA, we are presented with an excellent opportunity to review a three-dimensional volumetric radar analysis of the storm, especially by processing 0.25 km velocity range bins available in the level 2 archive.

Due to the close proximity of the radar targets, some quality control work with the data is required. We are unable to discern the highest elevations of the storms because of the so-called "cone of silence" directly above the radar. Even the maximum radar tilt (19.5 deg) only intercepted the tornadic storms to a height of 8000 m. Neighboring radars such as KABR show storm top reflectivity actually exceeded 14,600 m.

In addition, the high radial velocities at close range meant there would be folding in the unprocessed level 2 velocity data. Velocity folding occurs when the velocity of the target exceeds the Nyquist velocity of the radar (Glickman, 2000). In the WSR-88D operating in VCP 11, it occurs approximately above 25 m s$^{-1}$, so significant velocity dealiasing needed to be performed on this data. We did this utilizing a Gibson Ridge analyst edition level 2 viewer with its proprietary dealiasing algorithm, assuming a storm motion of 240 degrees at 10.3 m

s$^{-1}$ (20 kt) to create a storm relative velocity product.

In the 0318 UTC volume scan (Fig. 54), a strong cyclonic couplet is immediately apparent 21 km west of the radar. (Note there is also dealiasing failure on the squall line southwest of the radar, in the general area where the anticyclonic bookend vortex would be expected.) Maximum cyclonic velocities were -43 m s$^{-1}$ (-84 kt) inbound and +15 m s$^{-1}$ (+30 kt) outbound, totaling 58 m s$^{-1}$ (114 kt) of shear in the 0.25 km storm relative data field. The radar beam was able to sample the very lowest part of the storm, because at that distance the 0.5 deg beam height is only 200 m AGL. In a 3D view of all radar tilts, the reflectivity data (Fig. 55) shows strong reflectivities ≥50 dBZ to a height of 8000 m in the leading edge of the approaching squall line/bow echo. A reflectivity notch is seen where storm inflow is developing in the bookend vortex. That notch is also seen in the storm relative velocity fields (Fig. 56) when the 20.5 m s$^{-1}$ (40 kt) isosurface is plotted.

The line of strong inbound velocities not only bulged toward the radar, but clearly sloped upward in the direction of the rear inflow jet behind the line. As the vortex formed, +21 m s$^{-1}$ (+40 kt) outbound winds appear farther to the north, away from the center of the circulation, from a height only as low as 1700 m AGL (5.2 deg beam angle). The outbound winds rapidly dropped off to a maximum of only +13 m s$^{-1}$ (+25 kt) at 1400 m AGL (4.2 deg beam angle), suggesting that the strongest part of the circulation was still suspended aloft, not yet surface-based.

Moving ahead to the next volume scan at 0323 UTC, the circulation moved 7 km to the northeast, on the east side of Hartford (Fig. 57). Dealiased maximum velocities were -40

m s$^{-1}$ (-78 kt) inbound and +25 m s$^{-1}$ (+49 kt) outbound, a total 63 m s$^{-1}$ (127 kt) of shear in the 0.25 km storm relative data field. The center beam height was only 200 m AGL at the 0.5 deg tilt.

In a 3D look at the base reflectivity field, one can see a band of 50 dBZ reflectivity that has encircled an area of weaker reflectivity (Fig. 58). In a plan position indicator (PPI) view, this would be the hook echo. It is reflectivity that has wrapped all the way around an area of weak reflectivity, or weak echo vault. On higher radar elevations, this would be seen as a bounded weak echo region (BWER; Lemon and Doswell, 1979). In this case it was a vault that extended to 5000 m (16.6 deg beam height). Inside the hook in the 20.5 m s$^{-1}$ (40 kt) storm relative isosurface view (Fig. 59) is a "trunk" of outbound returns, depicting air being evacuated up and out of the hook echo region very near the tornado and vented through the storm top. The base of this trunk is very near the location of F-1 tornado damage. Such a tornado would be expected just upwind of the rotating updraft in the Lemon and Doswell (1979) supercell model.

The movement of air around the right rear flank of the storm, the surge of the RFD, can also be seen in the same imagery as viewed from the south (Fig. 60). Downdrafts are known to play a significant role in tornadogenesis, with tornadoes most likely to form after the downdraft has reached the ground (Davies-Jones, 2006). At this point there is also an upward curl in the inbound velocity, suggesting the RFD has wrapped all the way around to where the low level storm inflow is entering the southeast part of the hook. The tornado moved to the east, as seen in the damage path (Fig. 61).

The velocity data from that tornado becomes somewhat difficult to interpret due to significant aliasing problems created by the combination gust front and cyclonic signatures. In addition, the features of interest begin moving more easterly, so we now use base velocities rather than SRM velocity data. The 0328 UTC volume scan from KFSD (Fig. 62) shows continuity of the Hartford mesocyclone, with a maximum inbound of -41 m s$^{-1}$ (-79 kt) and maximum of + 32 m s$^{-1}$ (+62 kt) outbound at a distance of 14 km from the radar, where the 0.5 deg beam is only 100 m AGL. At this point if there is a tornado, it is near the end of its verified damage path. Just southeast of the circulation center, between the cyclonic signature and the radar, there is a broad area of -31 to -36 m s$^{-1}$ (-60 kt to -70 kt) winds, a surging gust front which produced significant straight line wind damage. Along this line on the radar is a large region of blank velocity gates, due to dealiasing failure. An examination of the raw Nyquist velocities shows there was velocity folding. The inset of Fig. 62 shows the non-dialiased velocities west-northwest of the radar. There are several velocity gates >15.4 m s$^{-1}$ (30 kt) ahead of the bowing line, and the presence of weak inbounds ahead of them suggest they are folded, actually strong outbounds headed toward (into) the squall line. There is at least one 36 m s$^{-1}$ (70 kt) shear couplet present in the noisy field. Witnesses reported a tornado in this area, moving in an east-northeast direction, though no damage path was reported in the post-event survey.

The Hartford tornado had ended by the next volume scan, at 0333 UTC (Fig. 63). But the storm still has a strong mesocyclonic signature, with maximums of -20 m s$^{-1}$ (-38 kt) inbound and -27 m s$^{-1}$ (+53 kt) outbound across a 2.8 km circulation located north of the town of Crooks. A number of large trees were reported down from strong winds in the

nearby town of Colton. Farther south, the trailing gust front moved 4.6 km in five minutes, a forward speed of approximately 65 km/hr.

## c. Aviation issues

Let us examine that same volume scan in relation to Sioux Falls airport, where the commercial jet was attempting to land. Timing is crucial to determining the wind field through which the DC-9 flew. The FAA tower tape (refer to Appendix B) indicates the pilot was cleared to land at 03:32:18. A time-stamped audio tape from Minnehaha County Metro Communications shows that a 911 telephone call from storm chaser Jeff Piotrowski began at 03:28:22 UTC, vividly describing a "jetliner going right by the tornado" 3:50 later, at 03:33:10 UTC. The 0333 UTC (25 June 2003) volume scan is marked in the Archive2 data as beginning at 0333:29 UTC, with the 0.5 deg base velocity product time stamped at 0333:48 UTC. If the radar archive, FAA tower recorder, and 911 call center time stamps are accurate, the 0333 UTC 0.5 deg velocity data was sampled within one minute or less of the plane's final approach to runway 15 at Sioux Falls airport, and can be considered a proximate state of the low level atmosphere in the airliner's path.

A close-up view of the 0333 UTC base velocity data (Fig. 64) shows three distinct circulations at the 0.5 deg height. Circulation #1 is the remnants of the Hartford mesocyclone, which is now 12 km northwest of the airport, directly inline with runway 15. Circulation #2, with 32 m s$^{-1}$ (63 kt) of rotational shear, is 5.7 km north of the runway, and circulation #3 is 3.3 km from the end of the runway, with 35 m s$^{-1}$ (69 kt) of shear. At this proximity to the KFSD airport, the 0.5 deg tilt is sampling the atmosphere at <50 m AGL,

extremely close to the surface. Similar cyclonic signatures are seen on the adjoining elevated tilts (not shown). Either or both circulation #2 and circulation #3 produced a tornado, witnessed by Piotrowski and meteorologists standing outside the NWS office at the base of the KFSD radar (Todd Heitkamp, personal communication). Only one short path of F-0 damage was reported north of the airport (refer back to Fig. 61).

If the time stamps on the radar imagery are correct, the jetliner probably flew through the front flank of the broad mesocyclone 12 km northwest of the airport. At this point, the pilot reports encountering what he described as a "sideslip," and decided to abort the landing (FAA, 2004). Unfortunately, the go-around vector he had been given by the tower was to the southeast (heading 150), taking the plane directly into the path of circulation #2 and #3, and at least one tornado. Weather radar alone cannot determine whether the plane went through the tornado vortex itself. But based on the eyewitness report, timing coincidences, and 0.25 km radar data, we can conclude it was very close.

Since the pilot reported multiple wind shear events during his missed approach (FAA, 2004) it is conceivable the plane may have encountered at least portions of all three radar-identified circulations.

**SUMMARY AND CONCLUSIONS**

While the outbreak was a record one in numbers of confirmed tornadoes, no fatalities occurred, in part due to an average lead time of 16.7 minutes reported for the 44 tornado warnings issued by the NWS office in Sioux Falls (NWS-FSD, 2003). 87% of the tornadoes

were weak, ≤F-1. Several of the tornadoes exhibited unique characteristics, although

they seemed to loosely fit into three general groups based upon location.

1) <u>Near the surface low</u>: This is the region where the outbreak initiated, in a region of

abundant surface moisture. The first tornadic supercell, classified a classic supercell, moved in

a northeast direction as anticipated based on environmental profiles. But the tornado on its

rear flank deviated from that motion, swerving to the north along a preexisting low-level

convergence boundary. Radar-indicated shear values confirm previous studies concluding that

tornado motion and supercell motion are not necessarily identical.

2) <u>Along the warm front</u>: The strongest tornadoes of the outbreak occurred on the

warm side of a southwest to northeast oriented warm front. Parameters such as $EHI_{0-1}$ and

STP correctly identified the tornado-favorable environment. A series of cell mergers acted

upon what has been described as a cyclic supercell, resulting in the Manchester F-4. This slow-

moving supercell was exceptionally erect vertically, rather than tilted as often seen with storms

of this type.

3) <u>In the warm sector</u>: Surface heating that reached the convective temperature

combined with steep low-level lapse rates (10-11°C) in an area with a very low LCL (1200 m)

to produce four supercells, resulting in numerous weak tornadoes. Several of these tornadoes

exhibited highly unusual motion for the Northern Plains, moving in a southeast to northwest

direction. We believe the anomalous motion was due to circular movement (curtate cycloid) of

the vortexes around circulation centers of the parent mesocyclone, in a region of weak

midlevel flow. This contention was supported by storm chasers and with 0.25 km WSR-88D

data, although there was significant aliasing in the velocity fields.

The outbreak concluded with the rapid development along and ahead of a surging squall line. Three of the tornadic vortexes were aligned along the glidepath of a passenger jet as it attempted to land in Sioux Falls. The landing was ultimately aborted.

In an operational sense, a review of these tornadoes shows that even with keen situational awareness, radar identification of small tornadoes and prediction of tornado movement can be a challenge. The task is even more difficult when it occurs within the compressed time and space of an outbreak of this magnitude.

# REFERENCES

Abbs, D.J., and R. Pielke, 1986: Thermally forced surface flow and convergence patterns over northeast Colorado. *Mon. Wea. Rev.*, **114**, 2281-2296.

Adlerman, E.J., K.K Droegemeier, and R.P. Davies Jones, 1999: A numerical simulation of cyclic mesocyclogenesis, *J. Atmos. Sci.*, **56**, 2045-2069.

Agee, E.M., J.T. Snow, and P.R. Clare, 1976: Multiple vortex features in the tornado cyclone and the occurrence of tornado families. *Mon. Wea. Rev.*, **104**, 552-563.

Atkins, N.T., M.L. Weisman, and L.J. Wicker, 1999: The influence of preexisting boundaries on supercell evolution. *Mon. Wea. Rev.*, **127**, 2910-2927.

Barker, E., cited 2003: Wxcaster.com. [Online at http://www.wxcaster.com/weather.php3, accessed 2004.]

Beck, J., J.L. Schroeder, J. Wurman, and C. Alexander, 2004: High-resolution dual-Doppler analysis of a cyclic supercell. Preprints, *22$^{nd}$ Conf on Severe Local Storms*, Hyannis, MA, Amer. Meteor. Soc., 13.3.

Brown, R.A., L.R. Lemon and D.W. Burgess, 1978: Tornado detection by pulsed Doppler radar. *Mon. Wea. Rev.*, **106**, 29-38.

Broyles, C., N. Dipasquale, and R. Wynne, 2002: Synoptic and mesoscale patterns associated with violent tornadoes across separate geographic regions of the United States: Part 1 – low-level characteristics. Preprints, *21$^{st}$ Conf. on Severe Local Storms*, San Antonio, TX, Amer. Meteor. Soc., J65-J68.

Boustead, J.M., and P.N. Schumacher, 2004: Warm sector tornadoes without discernible surface boundaries and with minimal deep layer shear. Preprints, *22$^{nd}$ Conf. on Severe Local Storms*, Hyannis, MA, Amer. Meteor. Soc., 2.1

Bunkers, M.J., and J.W. Zeitler, 2000: On the nature of highly deviant supercell motion. Preprints, *20th Conf. On Severe Local Storms*, Orlando, FL, Amer. Meteor. Soc., 236-239.

_____, B.A. Klimowski, J.W. Zietler, R.L. Thompson, and M.L. Weisman, 2000: Predicting supercell motion using a new hodograph technique. *Weather and Forecasting*, **15**, 61-79. [COMET module version of this paper available online at http://www.comet.ucar.edu/modules/scmotion.htm, accessed 2004.]

_____, 2002: Vertical wind shear associated with left-moving supercells. *Wea. and Forecasting*, **17**, no. 4, 845-855.

Burgess, D.W., V.T. Wood, and R.A. Brown, 1982: Mesocyclone evolution statistics. Preprints, *12th Conf on Severe Local Storms*, Amer. Meteor. Soc., San Antonio, TX, 422-424.

Cheresnick, D.R., and J.B. Basara, 2005: The impact of land-atmosphere interactions on the Benson, Minnesota tornado of 11 June 2001. *Bull. Amer. Meteor. Soc.*, **86**, 637-642

Corfidi, S.F., J.J. Levit and S.J. Weiss, 2004: The Super Outbreak: Outbreak of the Century. Preprints*, 22nd Conf. Severe Local Storms*, Hyannis MA.

Curtis, L., 2003: Mid-level dry intrusions as a factor in tornado outbreaks associated with landfalling tropical cyclones from the Atlantic and Gulf of Mexico. *Wea. and Forecasting*, **19**, 411-427.

Davies, J.M., 1993: Hourly helicity, instability, and EHI in forecasting supercell tornadoes. Preprints, *17th Conf. on Severe Local Storms*, St. Louis, MO, Amer. Meteor. Soc., 107-111.

_____, 2002: On low-level thermodynamic parameters associated with tornadic and nontornadic supercells. Preprints, *21st Conf. Severe Local Storms*, San Antonio, TX, Amer. Meteor. Soc., P 12.5

Davies-Jones, R., R.J. Trapp, and H.B. Bluestein, 2001: Tornadoes and tornadic storms, *Severe Convective Storms, Meteor. Monogr.*, No. 50, Amer. Meteor. Soc., 167-222.

_____, 2006: Tornadogenesis in supercell storms-what we know and what we don't know, Symposium on the challenges of severe convective storms, 86th Annual Meeting, Amer. Meteor. Soc., Atlanta, GA, 2.2.

Donaldson, R. J., Jr., 1970: Vortex signature recognition by a Doppler radar. *J. Appl. Meteor.,* **9,** 661–670.

Doswell III, C.A., 1980: Synoptic-scale environments associated with high plains severe thunderstorms. *Bull. Amer. Meteor. Soc.*, **61**, no. 11, 1388-1400.

Dowell, D.C., and H.B. Bluestein, 2002A: The 8 June 1995 McLean, Texas, Storm. Part I: Observations of Cyclic Tornadogenesis. *Mon. Wea. Rev.*, **130**, 2626-2648.

Dowell, D C., and H.B. Bluestein, 2002B: The 8 June 1995 McLean, Texas storm, Part II: cyclic tornado formation, maintenance, and dissipation. *Mon. Wea. Rev.*, **130**, 2649-2670.

Edwards, R., and R.L. Thompson, 2001: RUC-2 Supercell proximity soundings, Part II: an independent assessment of supercell forecast parameters, adapted from Preprints, *20th Conf. on Severe Local Storms*, Orlando, FL, Amer. Meteor. Soc., 435-438.

_____, R.L. Thompson, and J.A. Hart, 2002A: Verification of Supercell Motion Forecasting Techniques. Preprints, *21st Conf. Severe Local Storms*, San Antonio, Amer. Meteor. Soc., JP 1.2.

_____, S.F. Corfidi, R.L. Thompson, J.S. Evans, J.P. Craven, J.P. Racy, D.W. McCarthy, M.D. Vescio, 2002B: Storm Prediction Center Forecasting Issues Related to the 3 May 1999 Tornado Outbreak. *Wea. and Forecasting*, **17**, no. 3, 544–558.

_____, R.L. Thompson, K.C. Crosbie, J.A. Hart, and C.A. Doswell III, 2004: Proposals for Modernizing the Definitions of Tornado and Severe Thunderstorm Outbreaks. Preprints*, 22nd Conf. Severe Local Storms*, Hyannis MA. [available online at http://www.spc.noaa.gov/publications/edwards/defpaper.pdf, accessed 2005].

FAA (Federal Aviation Administration), 2004: Freedom of Information Act (FOIA) request 2004-00629GL, US Department of Transportation, Great Lakes Region Flight Standards Division, Des Plaines, IL.

Falk, K.W., 1997: Techniques for issuing severe thunderstorm and tornado warnings with the WSR-88D Doppler radar. *NOAA Technical Memorandum NWS SR-185*, NOAA National Weather Service, Southern Region, Fort Worth, TX.

Finley, C.A., 2004: Preliminary results from Project ANSWERS 2003. Preprints*, 8th Annual Northern Plains Convective Workshop*, Sioux Falls, SD, April 2004.

Forbes, G.S.: 2006: Meteorological aspects of high-impact tornado outbreaks. Preprints, *Symposium on the challenges of severe convective storms*, 86th AMS Annual meeting, Atlanta, GA, P1.12. [available online at http://ams.confex.com/ams/pdfpapers/99383.pdf, accessed 2006].

Fujita, T.T., 1978: Manual of downburst identification for project NIMROD. SMRP Research Paper 156, University of Chicago, 104 pp.

Fujita, T.T., 1981: Tornadoes and downbursts in the context of generalized planetary scales. *J. Atmos. Sci.*, **38**, 1511-1534.

Galway, J.G., 1958: The lifted index as a predictor of latent instability, *Bull. Amer, Meteor. Soc.*, **37**, 398-401.

_____, 1975: Relationship of tornado deaths to severe weather watch areas. *Mon. Wea. Rev.*, **103**, 737-741.

_____, 1977: Some climatological aspects of tornado outbreaks. *Mon. Wea. Rev.*, **105**, 477-484.

Geerts B., and Q. Miao, 2005: The use of millimeter Doppler radar echoes to estimate vertical air velocities in the fair-weather convective boundary layer. Journal of Atmospheric and Oceanic Technology 22(3): 225. As summarized in *Bull. Amer Meteor. Soc*, April 2005, 491-492.

Glickman, T., editor, 2000: *Glossary of Meteorology*, 2nd edition. Amer. Meteor. Soc., Boston.

Grazulis, T.P., 1993: *Significant Tornadoes 1680-1991*. Environmental Films, St. Johnsbury, VT.

Grzych, M.L., B.D. Lee, C.A. Finley, and J. L. Schroeder: 2004: Thermodynamic characterization of supercell rear flank downdrafts in Project ANSWERS 2003. Preprints, *22nd Conf on Severe Local Storms*, Hyannis, MA, P11.1.

Hagemeyer, B.C., 1991: A lower-tropospheric thermodynamic climatology for March through September: Some implications for thunderstorm forecasting, *Weather and Forecasting*, Vol. 6, No. 2, 254-270 [available online at http://www.srh.noaa.gov/mlb/therm.html, accessed 2005].

Hart, J.A., 2003: SeverePlot: Historical Severe Weather Report Analysis Program, version 2.5. *Storm Prediction Center*, Norman, OK [available online at http://www.spc.noaa.gov/software/svrplot2/, accessed 2005].

Herald, P., and K. Drozd, 2001: Use of combined shear and spectrum width in tornado detection. NWS Central Region applied research paper 24-06, available online at NWS Central Region web site [accessed 2006].

Johns, R.H. and C.A. Doswell III, 1992: Severe local storms forecasting. *Wea. and Forecasting*, **7**, 588-612.

Koch, S.E. and C.A. Ray, 1997: Mesoanalysis of summertime convergence zones in central and

eastern North Carolina. *Wea.and Forecasting*, **12**, 56-77.

Lee, B.D., and C.A. Finley, 2002: High resolution numerical simulations of thunderstorm outflow boundaries. Preprints, *21ˢᵗ Conf. on Severe Local Storms*, San Antonio, Amer. Meteor. Soc., 81-84.

_____, _____, and P. Skinner, 2004: Thermodynamic and kinematic analysis of multiple RFD surges for the 24 June 2003 Manchester, SD cyclic tornadic supercell during Project ANSWERS 2003. *22ⁿᵈ Conf. Severe Local Storms*, Hyannis, MA, P 11.2

_____, 2004: June 24, 2003 - Eastern South Dakota - Manchester cyclic tornadic supercell, online at http://esci.unco.edu/faculty/lee/answers/manch030624.htm [accessed 2006].

Lemon, L.R. and C.A. Doswell III, 1979: Severe thunderstorm evolution and mesocyclone structure as related to tornadogenesis. *Mon. Wea. Rev.*, **107**, 1184-1197.

_____, 1998: The radar "three-body scatter spike": an operational large-hail signature. *Wea. and Forecasting*, **13**, 327-340.

_____, D. W. Burgess, 1993: Supercell deep convergence zone revealed by a WSR-88D. *Preprints*, 26ᵗʰ International Conf. on Radar Meteor., Paris, France, Amer. Meteor. Soc., 206-298.

_____, 2005 [accessed]: Operational uses of velocity spectrum width data. *Australian Sky and Weather*, online at http://www.stormchasers.au.com/lemon13.htm.

Maddox, R.A., 1976: An evaluation of tornado proximity wind and stability data. *Mon. Wea. Rev.*, **104**, 133-142.

Maddox, R.A., L.R. Hoxit, C.F. Chappell, 1980: A study of tornadic thunderstorm interactions with thermal boundaries. *Mon. Weather Rev.*, Vol. 108, 322-336.

Mahrt, L., 1977: Influence of low-level environment on severity of high-plains moist Convection, *Mon. Weather Rev.*, **105**, no. 10, 1315-1329.

Markowski, P.M, E.N. Rasmussen, and J.M. Straka, 1998: The occurrence of tornadoes in supercells interacting with boundaries during VORTEX-95. *Wea. and Forecasting*, **13**, 852-859.

Marquis, J.N., Y.P. Richardson, P.M. Markowski, J.M. Wurman, and J.C. Dowell, 2006: The maintenance of tornadoes observed with high-resolution mobile radars. Preprints, *23rd Conf on Severe Local Storms*, St. Louis, MO, 15.1.

Meted, 2006 [accessed]: Mesoscale aspects of the 05 June 1997 severe weather event. COMET/UCAR Professional competency unit 4, Instructional component W4.1, available online at http://meted.ucar.edu/convectn/w41/dmxcase/dmxcase1.htm.

Moller, A., 2001: Severe local storms forecasting, *Severe Convective Storms, Meteor. Monogr.*, No. 50, Amer. Meteor. Soc., 433-480.

Moncrieff, M.W., and M.J. Miller, 1976. The dynamics and simulation of tropical cumulonimbus and squall lines. *Q. J. R. Meteorol. Soc.*, 120, 373-394.

Naistat, R., 2004: The 24 June 2003 severe weather outbreak in the MPX CWA – an example of warning decision making using near storm environment parameters in Kandiyohi County, MN. Preprints, *8th Annual Northern Plains Convective Workshop*, Sioux Falls, SD, April 2004.

National Weather Service, Sioux Falls, SD (NWS-FSD), 2003: Public information statement, issued 0026 UTC, 26 June 2003.

National Weather Service, Norman, OK (NWS-OUN), 1999: The Central Oklahoma tornado outbreak of May 3, 1999 [online at http://www.srh.noaa.gov/oun/storms/19990503/, accessed 2005].

National Weather Service, Omaha, NE (NWS-OMA), 2003: Public information statement, 0305 UTC, 25 June 2003.

National Weather Service, Corpus Christi, TX (NWS-CRP), web published 2000: Hurricane Beulah, September 1967 [available online at http://www.srh.noaa.gov/crp/docs/research/hurrhistory/Beulah/beulah.html, accessed 2005].

NOAA News, 2003: Central plains storm produced largest hailstone in U.S.history, August, 2003 [available online at http://www.noaanews.noaa.gov/stories/s2008.htm, accessed 2004].

NOAA-HPC (Hydrometeorological Prediction Center), 2003: Daily weather map. [available online at http://www.hpc.ncep.noaa.gov/dwm/dwm.shtml, accessed 2004.]

NOAA-NWS, 1992: Advanced spotter's field guide (NOAA PA 92055) [available online at http://www.nws.noaa.gov/os/brochures/adv_spotters.pdf, accessed 2006.]

NOAA-SPC (Storm Prediction Center), cited 2003: Preliminary local Storm Reports [available online at http://www.spc.noaa.gov/climo/, accessed 2004].

OFCM (Office of the Federal Coordinator for Meterological Services and Supporting Research), 2005: Doppler radar meteorological operations, part B - Doppler radar theory and meteorology, FCM-H11B-2005, Federal meteorological handbook no. 11, Washington, DC.

Pautz, M.E., 1969: Severe local storm occurrences, 1955-1967. ESSA technical memo, WBTM FCST12, Washington, DC, 3-4.

Passner, J.E., and J.M. Noble, 2004: Acoustic energy measured from mesocyclones and tornadoes in June 2003. Preprints, *22$^{nd}$ Conf. on Severe Local Storms*, Hyannis, MA, Amer. Meteor. Soc., 1.3.

Patterson, R., and D. Cox, 2005: Visualization of an F-3 tornado within a simulated supercell thunderstorm. International conference on computer graphics and interactive techniques, proceedings of the Association for Computing Machinery, Los Angeles, CA.

Potts, S.L. and E.M Agee, 2002: Multiple vortex phenomena in thunderstorms and tornadoes: three scales for multiple vortices, *21st Conf. Sev. Local Storms*, Amer. Meteor. Soc., San Antonio, TX, 14.6.

RTNDA, 2004: "Making of a Murrow", DVD program produced by the Radio and Television News Directors Association, 1600 K Street NW, Suite 700, Washington, DC 20006-2838.

Ramsay, H., and C.A. Doswell III (2005): A sensitivity study of hodograph-based methods for estimating supercell motion. *Wea. and Forecasting*, **20**, 954-970.

Rasmussen, E.N., R.E. Peterson, J.E. Minor, and B.D. Campbell, 1982: Evolutionary characteristics and photogrammetric determination of windspeeds within the Tulia outbreak tornadoes 28 May 1980. Preprints, *12th Conf. Sev. Local Storms*, Amer. Meteor. Soc., San Antonio, TX, 301-304.

_____, 1995: VORTEX operations plan. 141 pp. [available from National Severe Storms Laboratory, 1313 Halley Circle, Norman, OK 73069].

_____, 2003: Refined supercell and tornado forecast parameters. *Wea. and Forecasting*, **18**, no. 3, 530–535.

Roebber, P.J., D.M. Schultz, and R. Romero, 2003: Synoptic regulation of the 3 May 1999 tornado outbreak. *Wea. and Forecasting*, **17**, 399-429.

Rotunno, R., and J.B. Klemp, 1985: On the rotation and propagation of simulated supercell thunderstorms. *J. Atmos. Sci.*, **42**, 271–292.

Samaras, T., 2004: Pressure measurements within a large tornado. Preprints, *84ᵗʰ*
     *Annual AMS Conf.,* Seattle, WA, Amer. Meteor. Soc., 4.9.

Speheger, D.A., C.A. Doswell, and G.J. Stumpf, 2001: The tornadoes of 3 May 1999: Event
     verification in central Oklahoma and related issues. *Wea. and Forecasting*, **19**, 362-381.

_____, and R.D. Smith, 2006: On the imprecision of radar signature locations and
     storm path forecasts. *Natl. Wea. Dig.*, **30**, 3-10.

Stumpf, G.J., A. Witt, E.D. Mitchell, P.L. Spencer, J.T. Johnson, M.D. Eilts, K.W. Thomas,
     and D.W. Burgess, 1998: The National Severe Storms Laboratory mesocyclone
     detection algorithm for the WSR-88D. *Wea. and Forecasting*, **13,** 304-326.

Sturtevant, J.S., 1995: *The severe local storm forecasting primer*, Weather Scratch Meteorological
     Services, 1ˢᵗ ed., 197 pp.

Thompson, R.L., 1998: Eta model storm-relative winds associated with tornadic and
     nontornadic supercells. *Wea. and Forecasting*, **13**, no. 1, 125-137 [available online at
     http://www.spc.noaa.gov/publications/thompson/sr.htm, accessed 2005.]

_____, and R. Edwards, 2000: An overview of environmental conditions and forecast
     implications of the 3 May 1999 tornado outbreak. *Wea. and Forecasting*, **15**, no. 6, 682–
     699.

_____, and _____, 2005 [accessed]: Forecasting supercell type. *Storm Track Mag.*,
     online at http://www.stormtrack.org/library/forecast/sctype.htm.

_____, _____, and C.M. Mead, 2004: An update to the supercell composite and
     significant tornado parameters. Preprints, *22nd Conf. Severe Local Storms*, Hyannis MA,
     Amer. Meteor. Soc. (CD ROM).

_____, cited 2003: Explanation of SPC severe weather parameters [available online at
     http://www.spc.noaa.gov/sfctest/s2/, accessed 2004.]

Togstad, W.E., S.J. Taylor, and J.L. Peters, 2004: An examination of severe thunderstorm discrimination skills from traditional Doppler radar parameters and near storm environment (NSE) factors at large radar range. *Preprints*, 22nd AMS Conf on Severe Local Storms, Hyannis, MA.

Trobec, J., 2003: Flight 1462. News report televised during "KELOLAND News at Ten", KELO-TV, Sioux Falls SD, 30 October 2003.

Verbout, S. M., L. M. Leslie, H. E. Brooks, and S. L. Bruening, 2004: Leveling the field for tornado reports through time: Inflation-adjustment of annual tornado reports and objective identification of extreme tornado reports. Preprints, *22nd Conference on Severe Local Storms*, Hyannis, MA, Amer. Meteor. Soc., Conference CD [available online at http://www.nssl.noaa.gov/users/brooks/public_html/papers/SLS22/verboutetal.pdf, accessed 2005.]

WDTB (NOAA Warning Decision Training Branch), 2002: Tornado warning guidance: Spring 2002, available online at http://www.wdtb.noaa.gov/modules/twg02/TWG2002.pdf, accessed 2006.

WW2010, 2004: An introduction to cyclic storms, University of Illinois at Urbana-Champaign, Department of Atmospheric Sciences, web-based weather program online at http://ww2010.atmos.uiuc.edu/(Gh)/guides/mtr/svr/torn/cyc/home.rxml.

Wakimoto, R.M., H.V. Murphey, D.C. Dowell, and H.B. Bluestein, 2003: The Kellerville tornado during VORTEX: Damage survey and Doppler radar analyses. *Mon. Wea. Rev.*, **131**, no. 10, 2197.

Wang, Y., T Yu, M. Yeary, A.M. Shapiro, S. Nemati, M. Foster, and D.L. Andra, 2006: Tornado identification using a neuron-fuzzy approach to integrate shear and spectral signatures, *23rd Conf. on Severe Local Storms*, Amer. Meteor. Soc., St. Louis, Mo, P9.1.

Weisman, M.L. and J.B. Klemp, 1982: The dependence of numberically simulated convective storms on vertical wind shear and buoyancy. *Mon. Wea. Rev.*, **110**, 504-520.

Weisstein, E.W., 2006 [accessed]: Mathworld web site, online at http://mathworld.wolfram.com.

Wicker, L.J. and D.C. Dowell, 2000: 7.6 A numerical study of cyclic tornadogenesis: The 8 June 1995 VORTEX . *20th Conf on Severe Local Storms*, Orlando, FL, Amer. Meteor. Soc., 7.6.

Wilson, G.S., and L.R. Lemon, 2000: Integration and application of multiple radars to May 3rd 1999 severe storms: an assessment of the "VIPIR" performance. Preprints: *20th Conf on Severe Local Storms*, Orlando, FL, Amer. Meteor. Soc., 3.4.

Wilson, J. W., and D. Reum, 1988: The flare echo: Reflectivity and velocity signature. *J. Atmos. Oceanic Tech.*, **5**, No. 2, 197-205.

Wilson, J.W., and W.E. Schreiber, 1986: Initiation of convective storms at radar-observed boundary-layer convergence lines. *Mon. Wea. Rev.*, **114**, no. 12, 2516-2536.

Wolf, R.A., 2000: Observations of a tornadic and non-tornadic circulation near the KDVN WSR-88D associated with the 18 June 1998 squall line. Preprints, *20th Conf. on Severe Local Storms*, Orlando, FL, Amer. Meteor. Soc., 7.2.

Young, G.S., and J.M. Fritch, 1989: A proposal for general conventions in analysis of mesoscale boundaries, *Bull. Amer. Meteor. Soc.*, **70**, 1412-1421.

Zeitler, J.W., and M.J. Bunkers, 2002: Anticipating and monitoring supercell motion for severe weather operations. Preprints, *21st Conf. on Severe Local Storms*, Amer. Meteor. Soc., J61-J64.

Zrnic, D. S ., 1987 : Three-body scattering produces precipitation signature of special diagnostic value. *Radio Sci.*, **22**, 76-86.

**APPENDIX A**

The following are local storm reports in South Dakota from the afternoon and evening of 24 June 2003, compiled by the National Climatic Data Center. Times listed are Local Standard Time (Daylight Saving Time -1). NCDC lists a total of 70 tornado reports, causing seven injuries and $13.46 million in damage. NCDC storm data available online at http://www4.ncdc.noaa.gov/cgi-win/wwcgi.dll?wwEvent~Storms, accessed 2004.

| Location or County | Time | Mag | Dth | Inj | PropDam | CropDam |
|---|---|---|---|---|---|---|
| 1 Mt Vernon | 04:15 PM | F0 | 0 | 0 | 0 | 0 |
| 2 Mt Vernon | 04:17 PM | F2 | 0 | 0 | 500K | 0 |
| 3 Vermillion | 04:58 PM | F0 | 0 | 0 | 0 | 0 |
| 4 Beresford | 05:17 PM | F0 | 0 | 0 | 0 | 0 |
| 5 Forestburg | 05:19 PM | F0 | 0 | 0 | 0 | 0 |
| 6 Lane | 05:23 PM | F1 | 0 | 0 | 10K | 0 |
| 7 Woonsocket | 05:26 PM | F3 | 0 | 0 | 500K | 0 |
| 8 Harrisburg | 05:30 PM | F0 | 0 | 0 | 0 | 0 |
| 9 Vermillion | 05:42 PM | F0 | 0 | 0 | 0 | 0 |
| 10 Vermillion | 05:42 PM | F0 | 0 | 0 | 0 | 0 |
| 11 Woonsocket | 05:45 PM | F0 | 0 | 0 | 0 | 0 |
| 12 Artesian | 05:55 PM | F0 | 0 | 0 | 0 | 0 |
| 13 Huron | 06:00 PM | F0 | 0 | 0 | 0 | 0 |
| 14 Huron | 06:00 PM | F0 | 0 | 0 | 0 | 0 |
| 15 Cavour | 06:16 PM | F0 | 0 | 0 | 0 | 0 |
| 16 Esmond | 06:27 PM | F0 | 0 | 0 | 0 | 0 |
| 17 Esmond | 06:29 PM | F4 | 0 | 4 | 3.0M | 0 |
| 18 Dalesburg | 06:30 PM | F0 | 0 | 0 | 0 | 0 |
| 19 Wakonda | 06:30 PM | F0 | 0 | 0 | 0 | 0 |
| 20 Wakonda | 06:32 PM | F0 | 0 | 0 | 0 | 0 |
| 21 Wakonda | 06:32 PM | F1 | 0 | 0 | 0 | 0 |

| 22 Centerville | 06:33 PM | F0 | 0 | 0 | 0 | 0 |
|---|---|---|---|---|---|---|
| 23 Wakonda | 06:33 PM | F0 | 0 | 0 | 0 | 0 |
| 24 Watertown | 06:35 PM | F0 | 0 | 0 | 0 | 0 |
| 25 Beresford | 06:38 PM | F0 | 0 | 0 | 0 | 0 |
| 26 Manchester | 06:52 PM | F0 | 0 | 0 | 0 | 0 |
| 27 Lake Andes | 06:54 PM | F0 | 0 | 0 | 0 | 0 |
| 28 Centerville | 06:55 PM | F0 | 0 | 0 | 0 | 0 |
| 29 Manchester | 06:58 PM | F2 | 0 | 0 | 200K | 0 |
| 30 Centerville | 07:00 PM | F2 | 0 | 0 | 0 | 0 |
| 31 Lake Andes | 07:03 PM | F1 | 0 | 0 | 50K | 0 |
| 32 De Smet | 07:05 PM | F1 | 0 | 0 | 0 | 0 |
| 33 Beresford | 07:10 PM | F1 | 0 | 0 | 0 | 0 |
| 34 Centerville | 07:10 PM | F0 | 0 | 0 | 0 | 0 |
| 35 Lake Andes | 07:10 PM | F1 | 0 | 0 | 0 | 0 |
| 36 De Smet | 07:17 PM | F0 | 0 | 0 | 0 | 0 |
| 37 De Smet | 07:19 PM | F0 | 0 | 0 | 0 | 0 |
| 38 Davis | 07:20 PM | F0 | 0 | 0 | 0 | 0 |
| 39 De Smet | 07:20 PM | F1 | 0 | 0 | 0 | 0 |
| 40 Lennox | 07:20 PM | F0 | 0 | 0 | 0 | 0 |
| 41 Viborg | 07:20 PM | F0 | 0 | 0 | 0 | 0 |
| 42 Davis | 07:22 PM | F2 | 0 | 0 | 500K | 0 |
| 43 De Smet | 07:28 PM | F0 | 0 | 0 | 0 | 0 |
| 44 Beresford | 07:30 PM | F1 | 0 | 0 | 200K | 0 |
| 45 Miller | 07:30 PM | F0 | 0 | 0 | 0 | 0 |
| 46 Willow Lake | 07:30 PM | F1 | 0 | 0 | 0 | 0 |
| 47 De Smet | 07:32 PM | F0 | 0 | 0 | 0 | 0 |
| 48 Centerville | 07:33 PM | F1 | 0 | 0 | 0 | 0 |
| 49 Bryant | 07:35 PM | F0 | 0 | 0 | 0 | 0 |
| 50 Lennox | 07:52 PM | F0 | 0 | 0 | 0 | 0 |
| 51 Armour | 07:55 PM | F0 | 0 | 0 | 0 | 0 |
| 52 Tea | 07:55 PM | F0 | 0 | 0 | 0 | 0 |

| | | | | | | |
|---|---|---|---|---|---|---|
| 53 Lennox | 08:00 PM | F1 | 0 | 0 | 0 | 0 |
| 54 Armour | 08:05 PM | F0 | 0 | 0 | 0 | 0 |
| 55 Harrisburg | 08:05 PM | F0 | 0 | 0 | 0 | 0 |
| 56 Harrisburg | 08:07 PM | F0 | 0 | 0 | 0 | 0 |
| 57 Tea | 08:09 PM | F0 | 0 | 0 | 0 | 0 |
| 58 Tea | 08:12 PM | F0 | 0 | 0 | 0 | 0 |
| 59 Cavour | 08:25 PM | F3 | 0 | 0 | 1.5M | 0 |
| 60 Parker | 08:30 PM | F2 | 0 | 0 | 3.0M | 0 |
| 61 Parker | 08:40 PM | F0 | 0 | 0 | 0 | 0 |
| 62 Pumpkin Center | 08:50 PM | F1 | 0 | 3 | 500K | 0 |
| 63 Hartford | 09:05 PM | F1 | 0 | 0 | 2.5M | 0 |
| 64 Yale | 09:05 PM | F2 | 0 | 0 | 0 | 0 |
| 65 De Smet | 09:13 PM | F1 | 0 | 0 | 0 | 0 |
| 66 Renner | 09:34 PM | F0 | 0 | 0 | 0 | 0 |
| 67 Viborg | 09:40 PM | F1 | 0 | 0 | 1.0M | 0 |
| 68 Wentworth | 09:40 PM | F0 | 0 | 0 | 0 | 0 |
| 69 Lennox | 09:47 PM | F0 | 0 | 0 | 0 | 0 |
| 70 Egan | 09:50 PM | F0 | 0 | 0 | 0 | 0 |

**APPENDIX B**

The following are included as background for the events described herein. The data are stored on the CD-ROM attached to this paper.

Broadcast.wmv - 97 MB, runs 8:47. Compilation of clips from television coverage of the tornado outbreak of 24 June 2003 broadcast on KELO-TV, Sioux Falls, SD.

Eyewitness.wav - 22 MB, runs 8:14. Recording of the 911 call placed at 03:28:22 UTC 25 June 2003 by storm chaser Jeff Piotrowski to Minnehaha County Metro Communications, in which he describes the tornadoes he sees and the jetliner that flew through them.

Radar.zip - 23 MB. Compressed Archive2 radar data from KFSD between 0313-0338 UTC 25 June 2003.

Tower.wav - 78 MB, runs 29:53. Audio of radio conversations between Sioux Falls airport tower and the cockpit of a passenger jet as it approached the runway and then aborted a landing at 0333 UTC 25 June 2003. Obtained by FOIA request 2004-00629GL from the Federal Aviation Administration, Great Lakes Region, Des Plaines, IL.
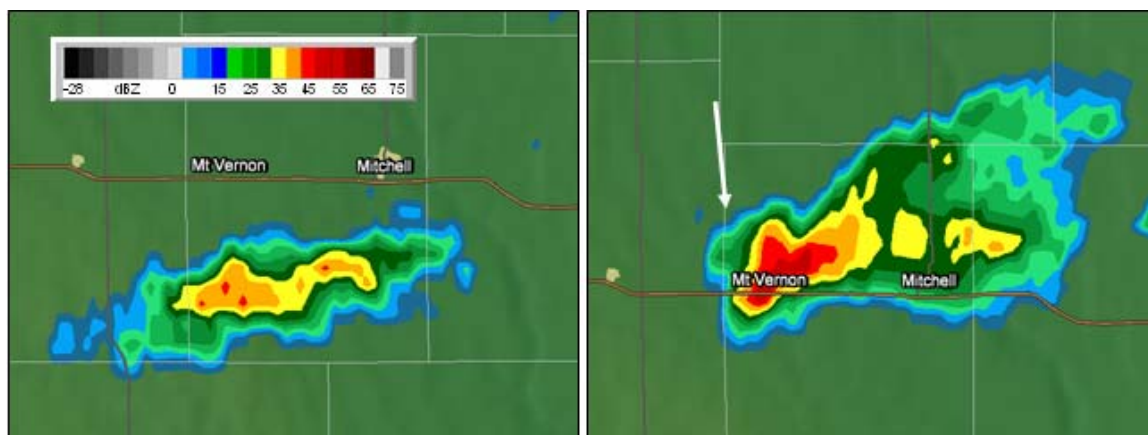
**Fig. 1a.** 2122 UTC Base reflectivity of developing storm south of Mount Vernon and Mitchell, moving north, as seen from the KFSD WSR-88D located 77 miles to the east. Beam elevation 0.5 deg, height 1798 m (5,900 ft) above radar level. **Fig. 1b** is the same storm at 2158 UTC at beam elevation 1.5 deg, height 4053 m (13,300 ft). Arrow indicates TBSS on westernmost portion of the cell, northwest of Mount Vernon. Baron Services reflectivity data smoothing applied.
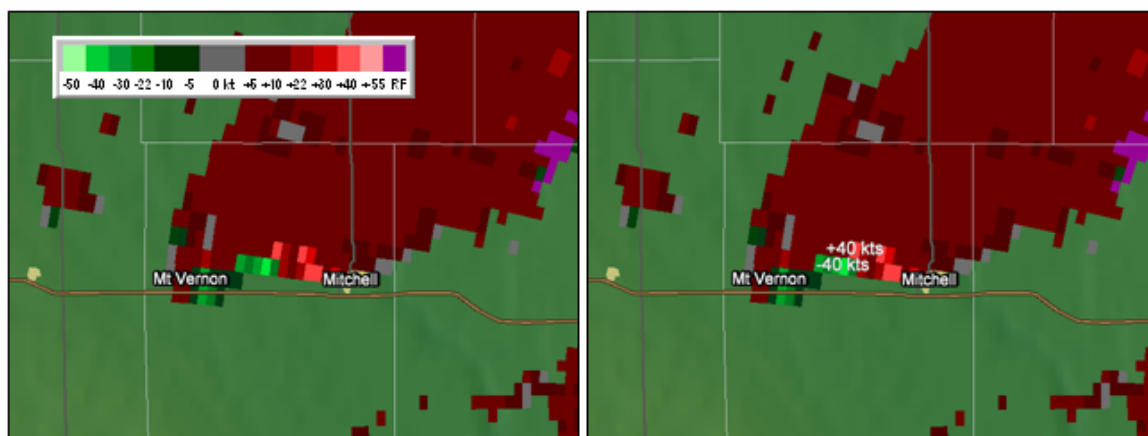


**Fig. 2a.** 2217 UTC Storm Relative Mean (SRM) velocity images from KFSD showing radar indicated rotation and convergence couplets between Mount Vernon and Mitchell. Beam elevation 0.5 deg, height 1920 m (6,300 ft). **Fig. 2b** is the same image with the inbound (green) and outbound (red) velocities indicated.
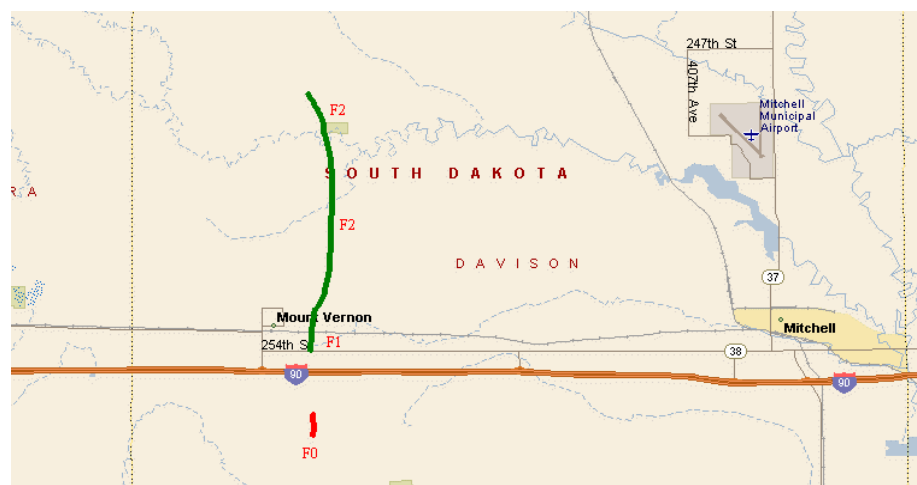
**Fig. 3**. Tornado damage path in Davison County (from NWS-FSD). F2 damage path length approximately 8.8 km (5.5 mi). View approx 35 km by 17 km.
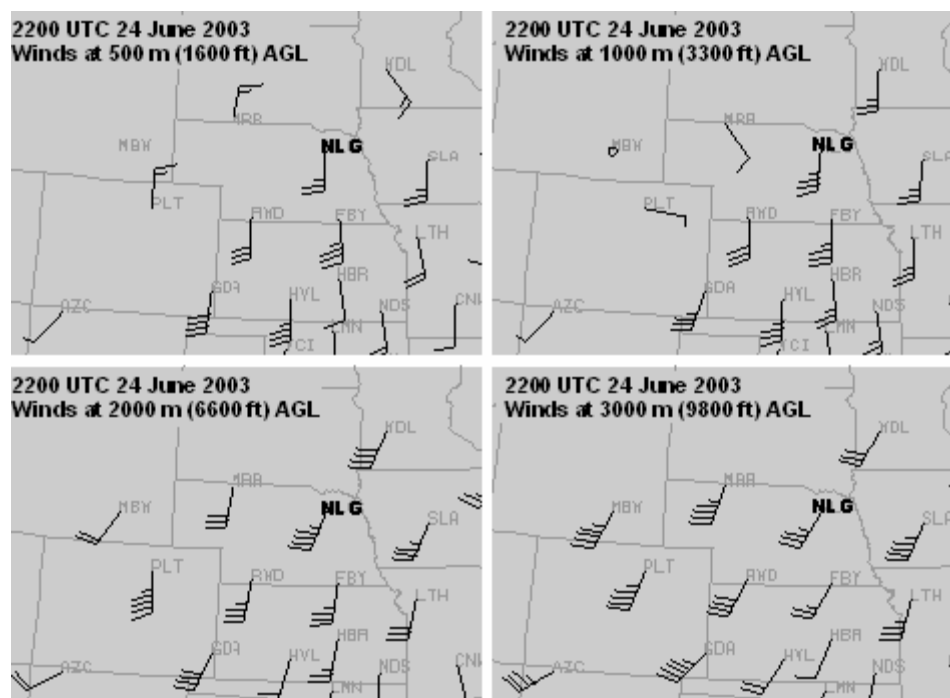


**Fig. 4.** Midwestern wind profilers at 2200 UTC, at 500 m, 1000m, 2000m, and 3000 m. Neligh is NLG (from UCAR, online at http://locust.mmm.ucar.edu/case-selection/).
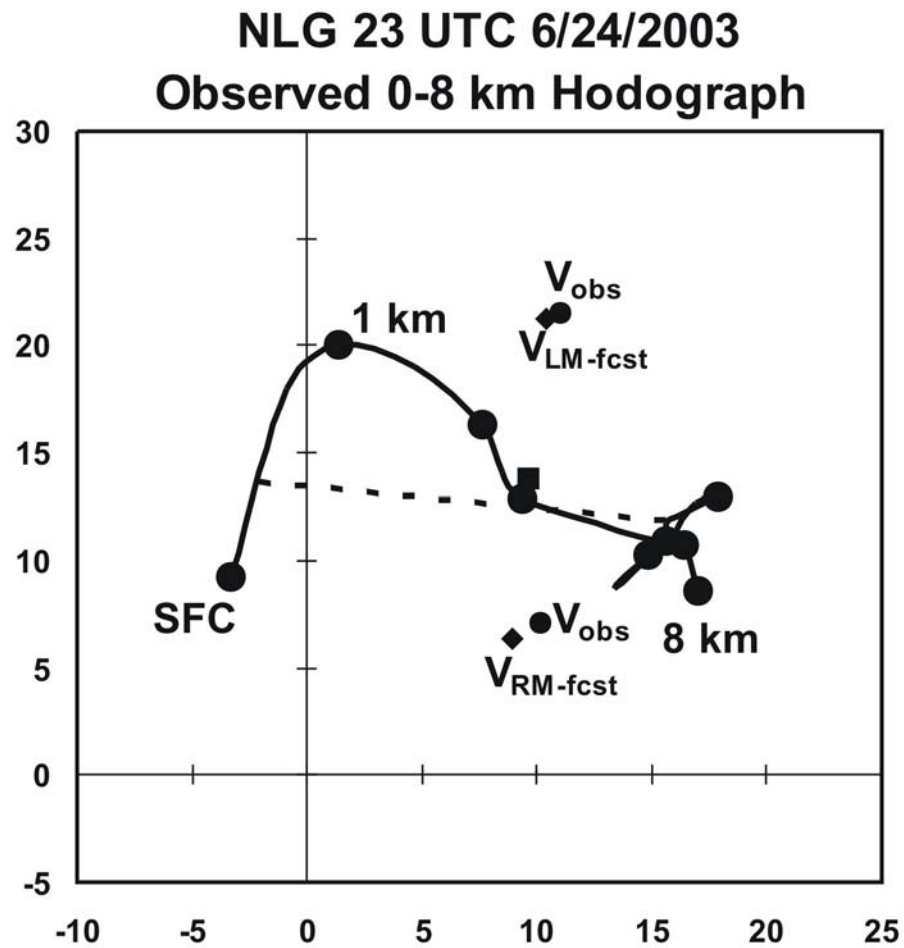
**Fig. 5.** Observed 0-8 km hodograph from Neligh (NLG) wind profiler at 2300 UTC (from Matt Bunkers, NWS UNR). $V_{RM-fcast}$ and $V_{LM-fcast}$ are the predicted direction and speed of right- and left-movers. $V_{obs}$ is the observed supercell movement observed with the initial supercells on 24 June 2003.
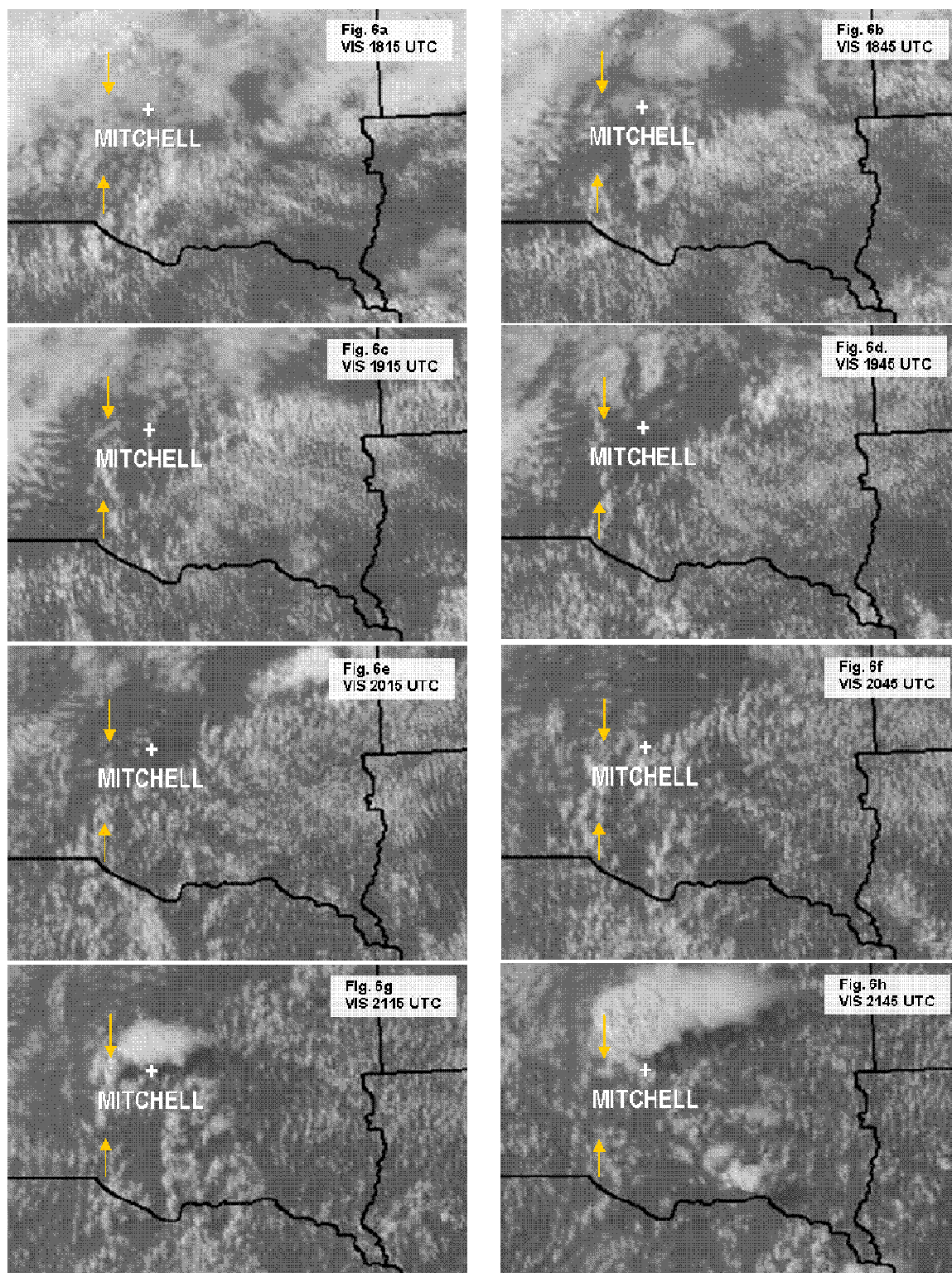
**Fig. 6a-6h.** GOES 1 km visible satellite images, with arrows added to indicate boundary where tornadic supercell formed (satellite image from Barker, 2003).

a) BREF 0.5 deg 2153 UTC
a) SRM 1.5 deg 2153 UTC
a) SRM 2.4 deg 2153 UTC
a) SRM 3.4 deg 2153 UTC

b) BREF 0.5 deg 2158 UTC
b) SRM 1.5 deg 2158 UTC
b) SRM 2.4 deg 2158 UTC
b) SRM 3.4 deg 2158 UTC

c) BREF 0.5 deg 2203 UTC
c) SRM 1.5 deg 2203 UTC
c) SRM 2.4 deg 2203 UTC
c) SRM 3.4 deg 2203 UTC
d) BREF 0.5 deg 2208 UTC
d) SRM 1.5 deg 2208 UTC
d) SRM 2.4 deg 2208 UTC
d) SRM 3.4 deg 2208 UTC

+13 m s$^{-1}$
-28 m s$^{-1}$

Mount Vernon
Mitc

20 km
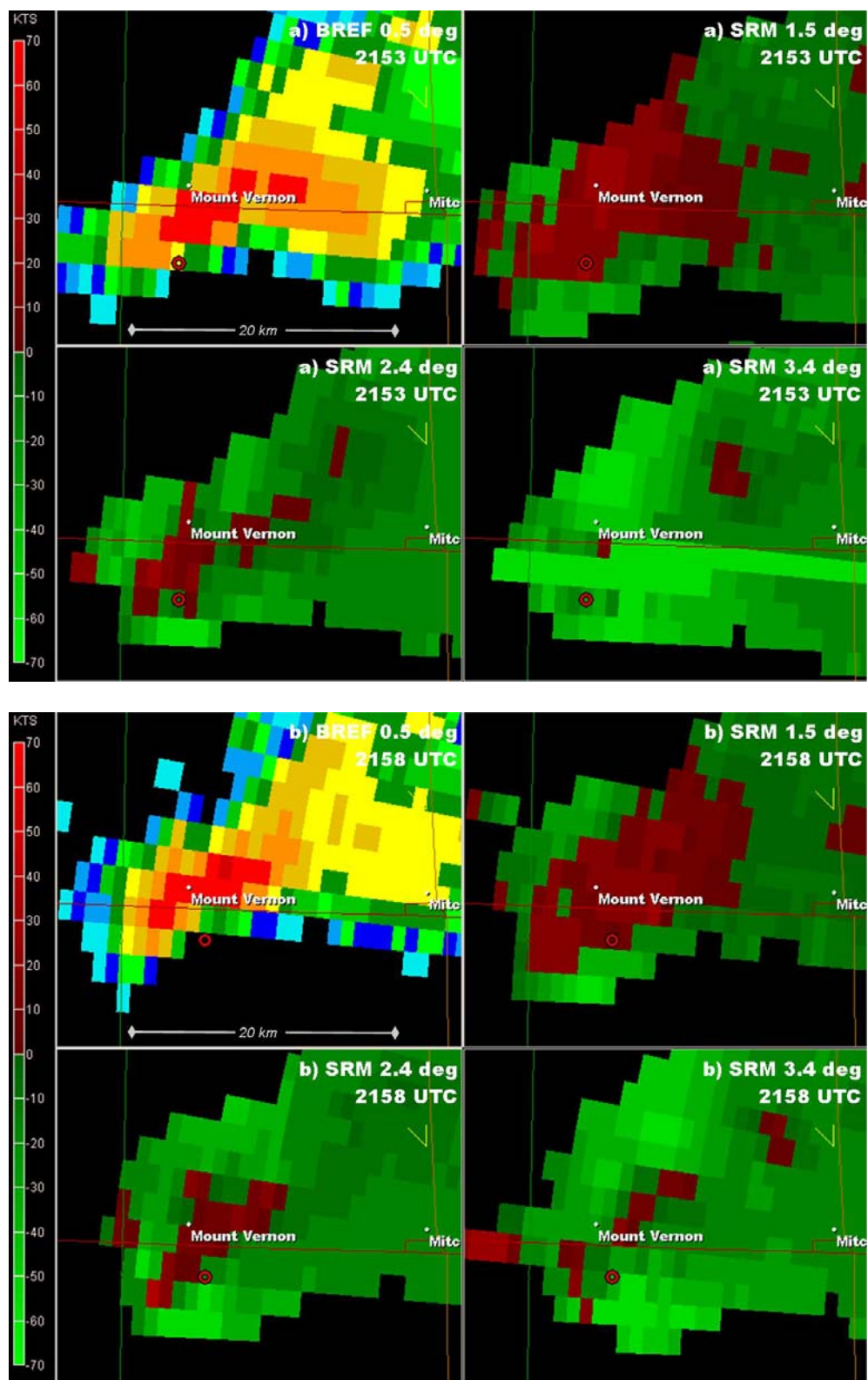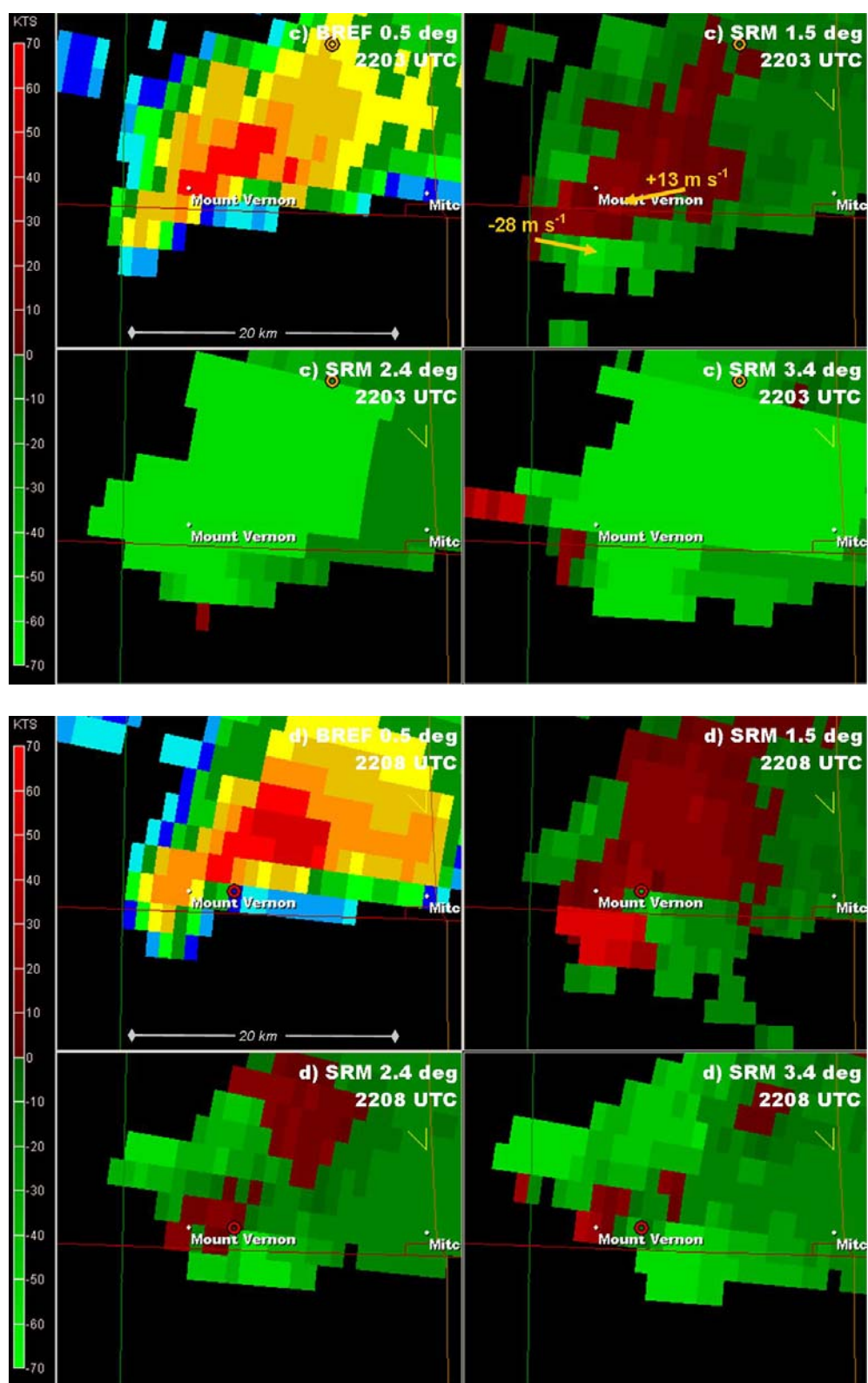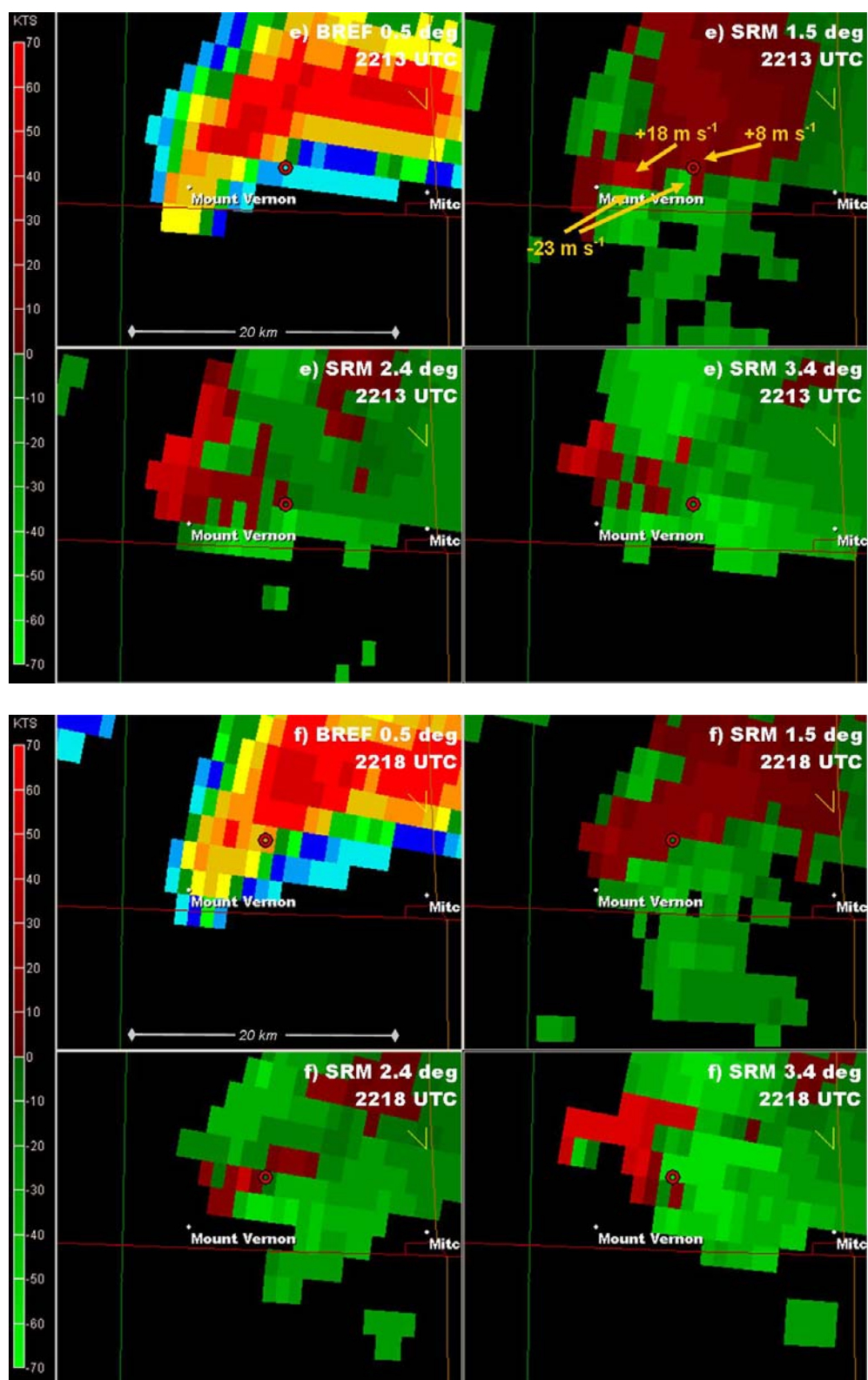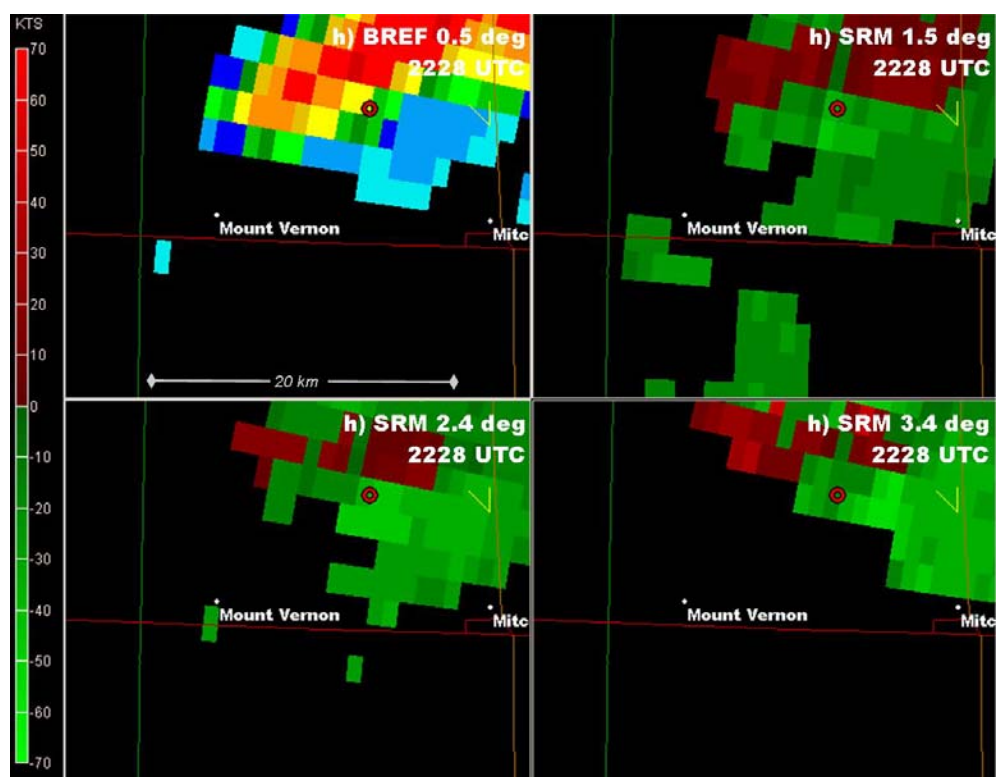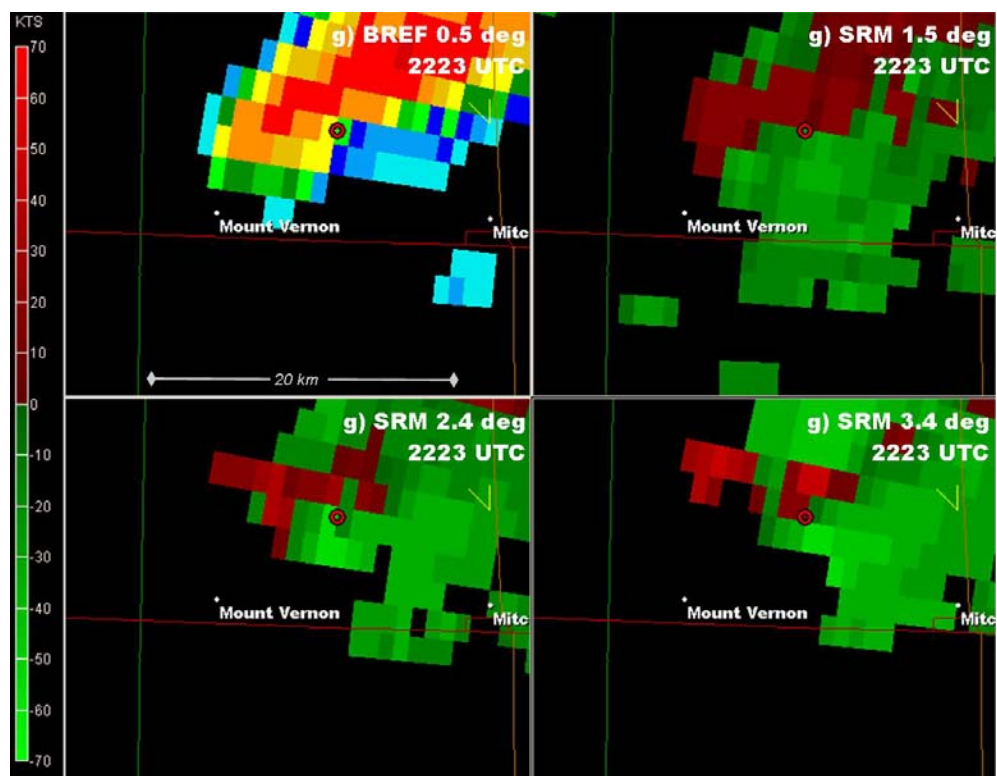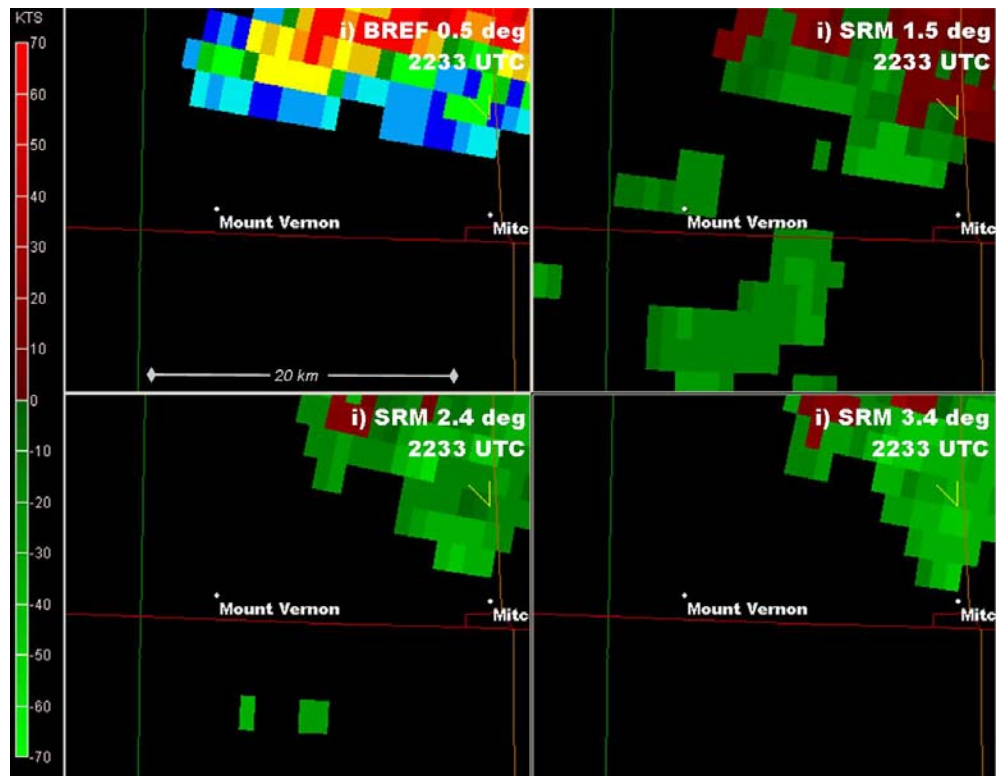
**Fig. 7a-7i.** Four panel radar display from KFSD from 2159-2233 UTC 24 June 2003. In each image, base reflectivity elevation 0.5 deg (unsmoothed) is in the upper left, followed by 1.5, 2.4, and 3.4 deg tilts of storm relative mean velocity products. The small red circles are the markers created by the MDA (mesocyclone detection algorithm). "V" symbol north of Mitchell is the position of runways at Mitchell airport. Displayed with level 3 data on Gibson Ridge viewer.
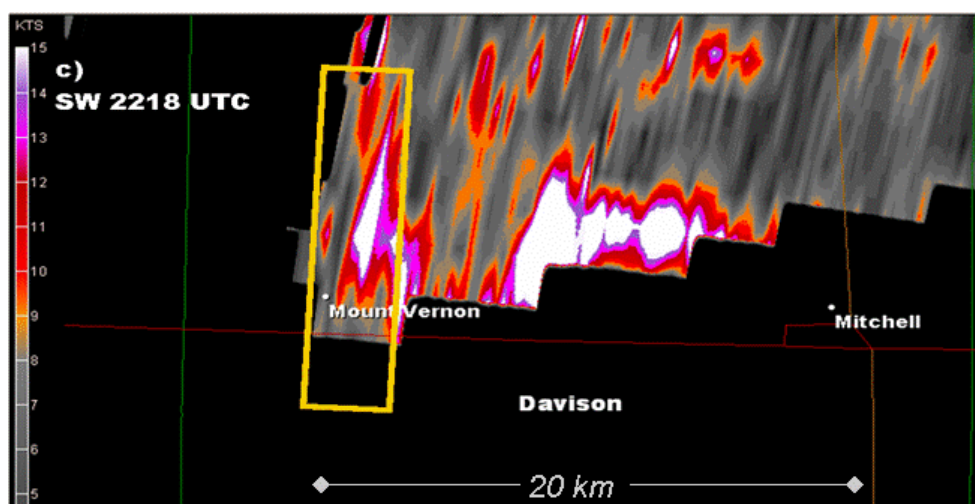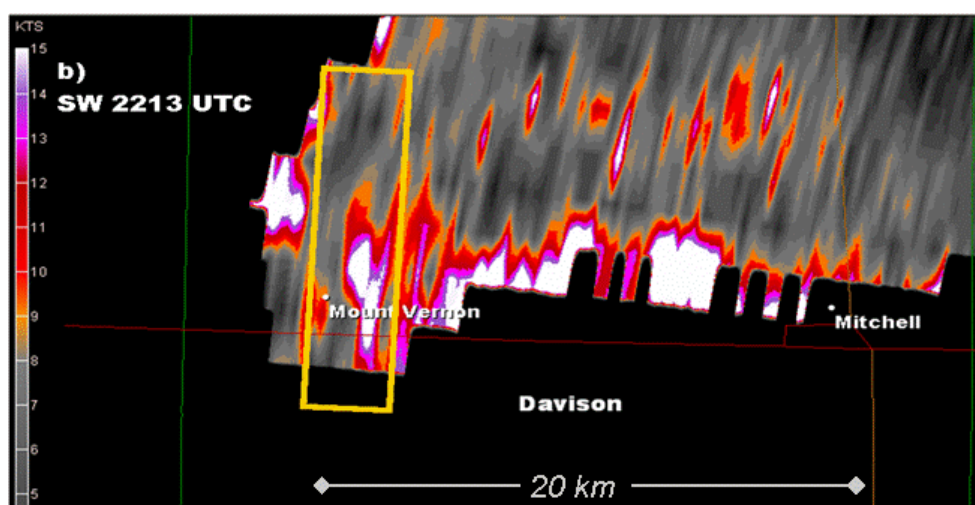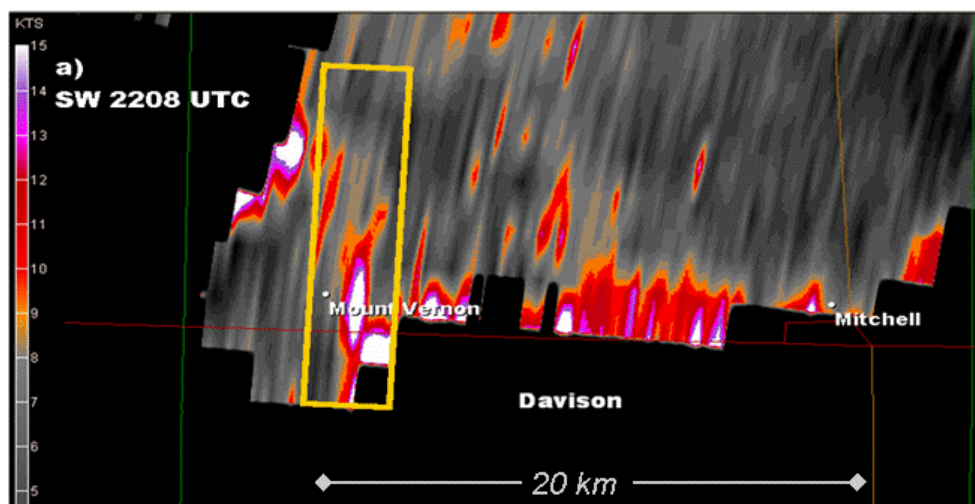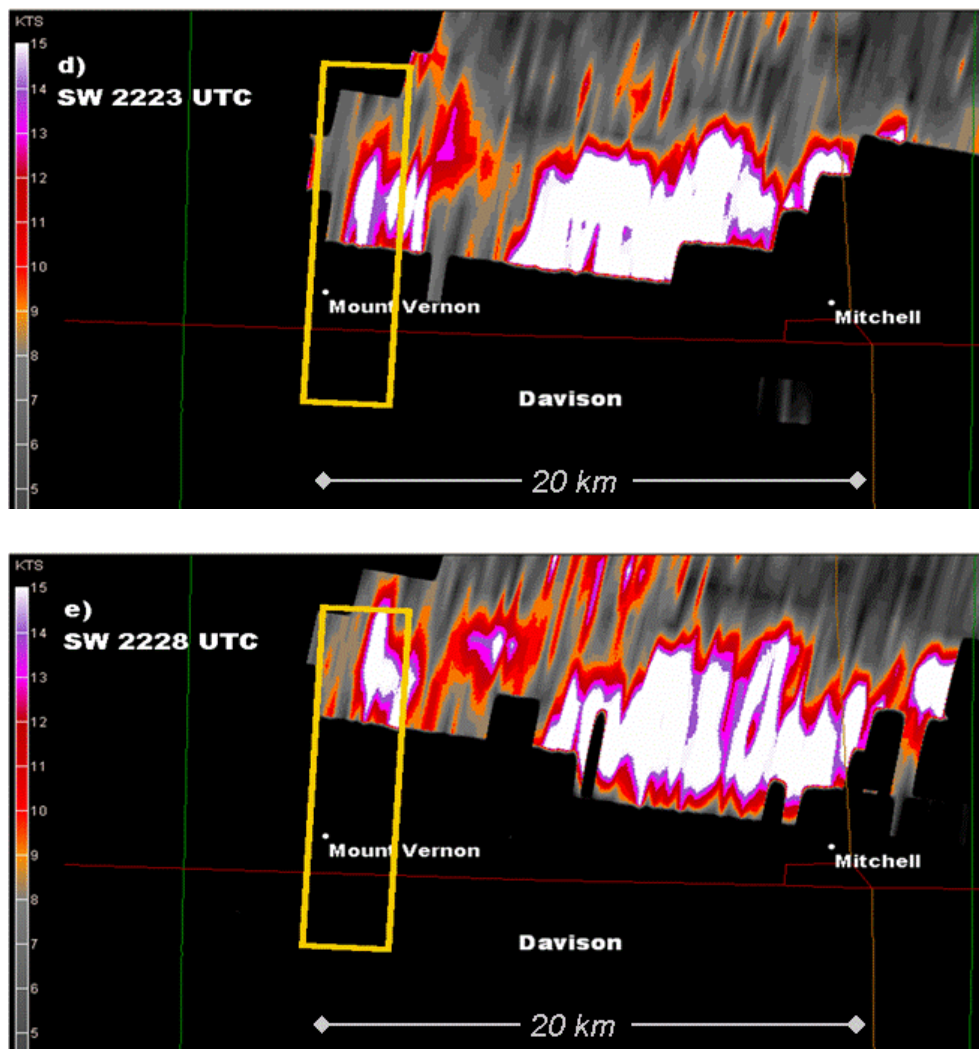
**Fig. 8a-8e.** Spectrum width at 0.5 deg from KFSD radar, displayed on Gibson Ridge level 2 viewer. View approximately the same as Fig 3. Yellow box added to highlight damage path from tornado on east side of Mount Vernon.
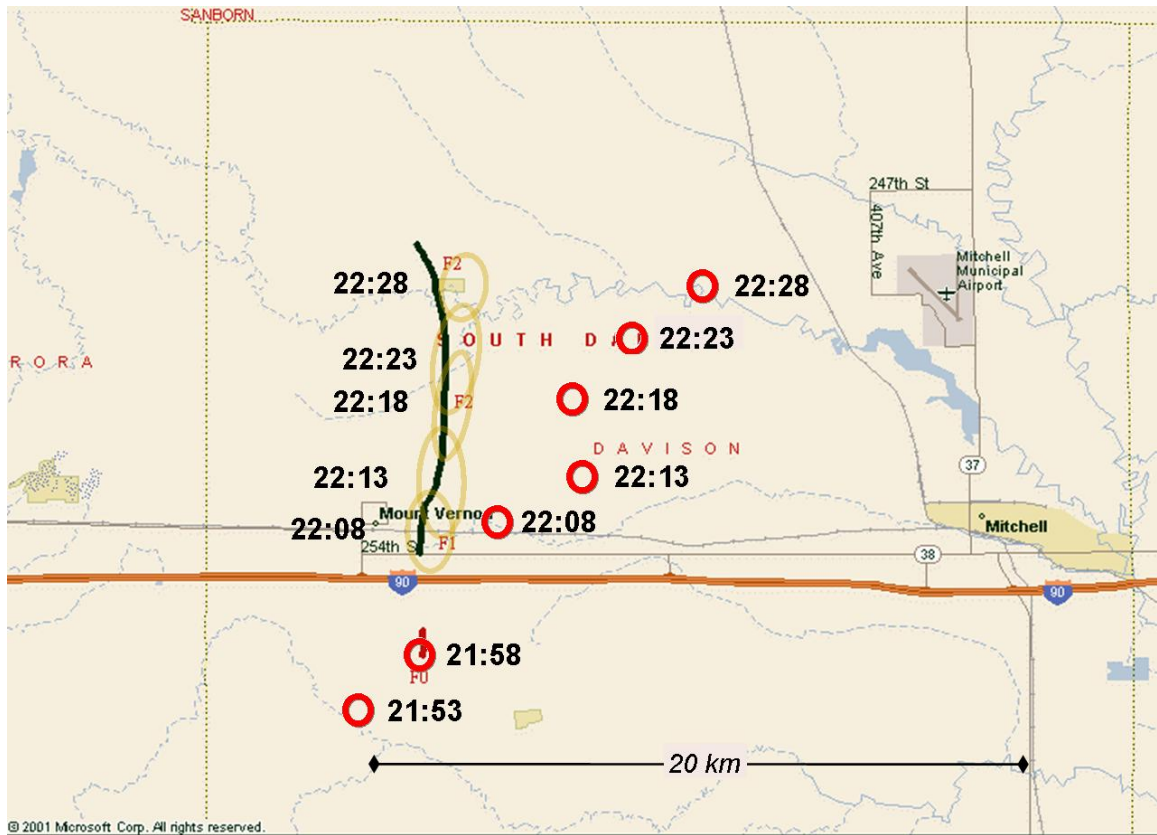
**Fig. 9.** Mosaic of NWS tornado damage path (green line), KFSD level 2 SW maxima (brown ovals) with time stamp, and NEXRAD mesocyclone markers (red circles) with time stamp.
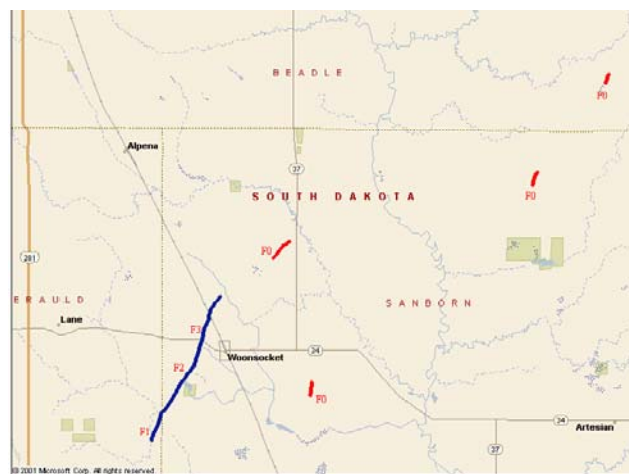


**Fig. 10.** Tornado damage paths near Woonsocket, from survey by NWS-FSD.
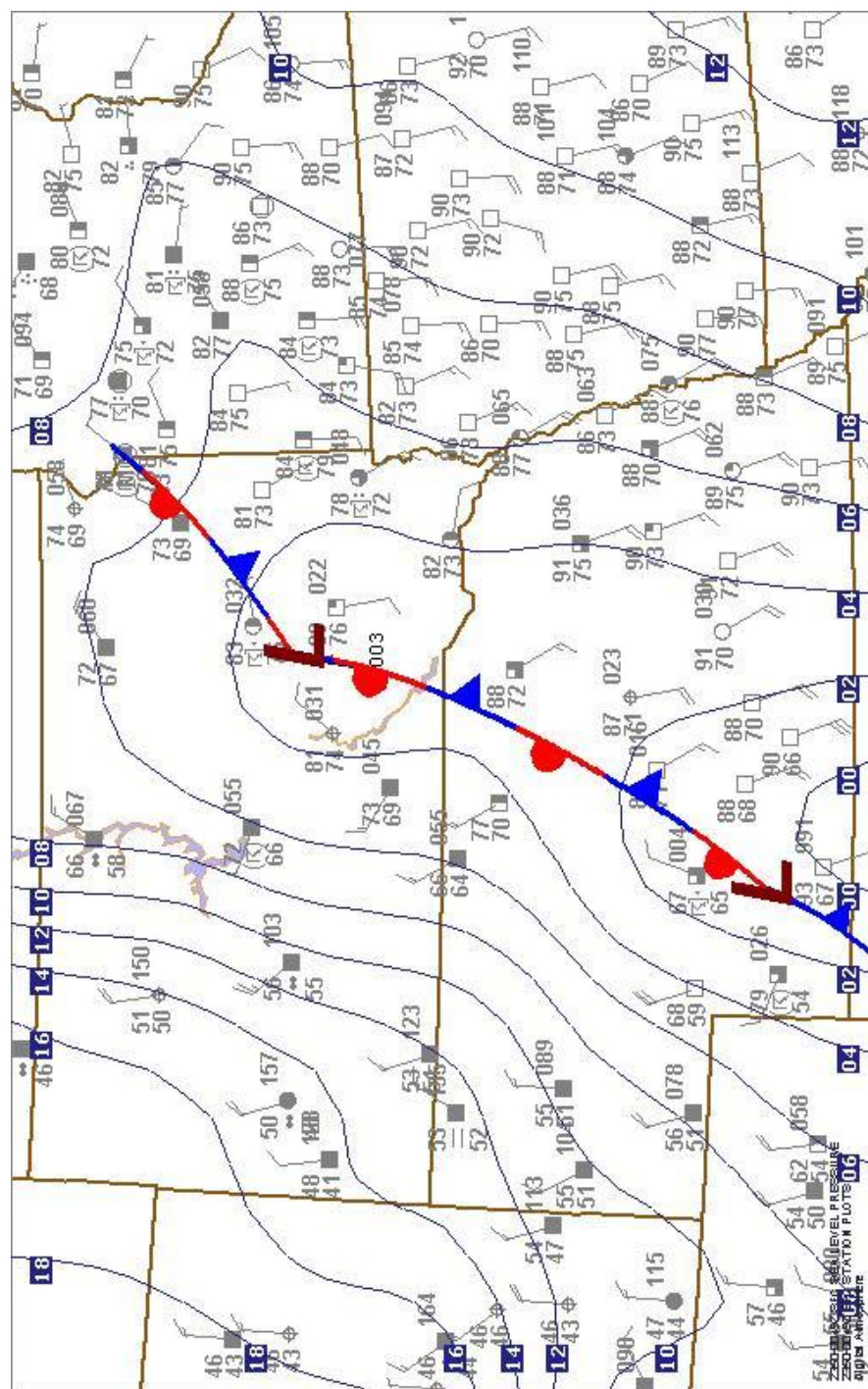
**Fig. 11a.** Subjective hand analysis of surface features at 0000 UTC on 25 June 2003. Isobar fields analyzed using Barnes method and plotted with Digital Atmosphere software program.
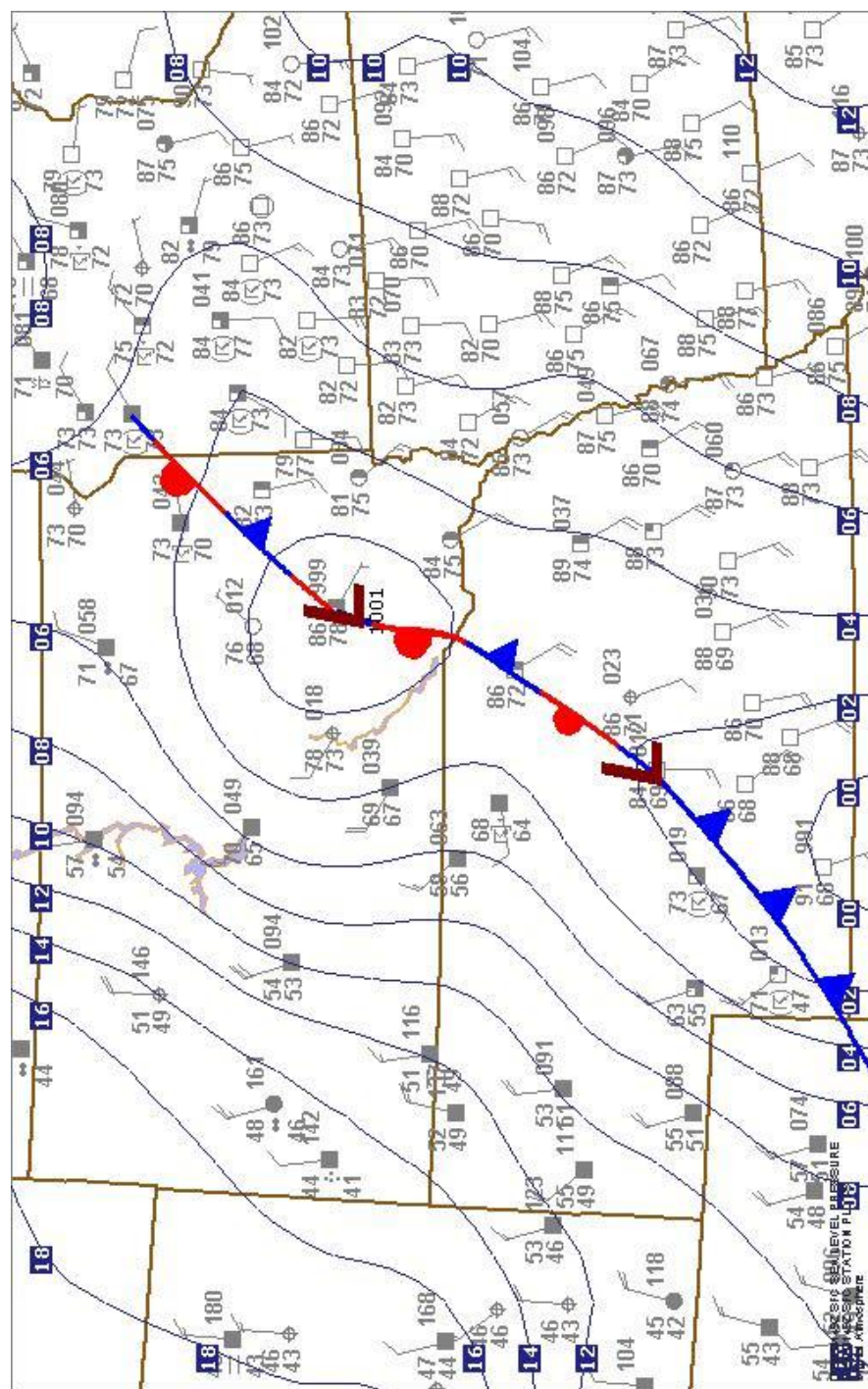
**Fig. 11b.** Same as 11a, except at 0100 UTC on 25 June 2003.
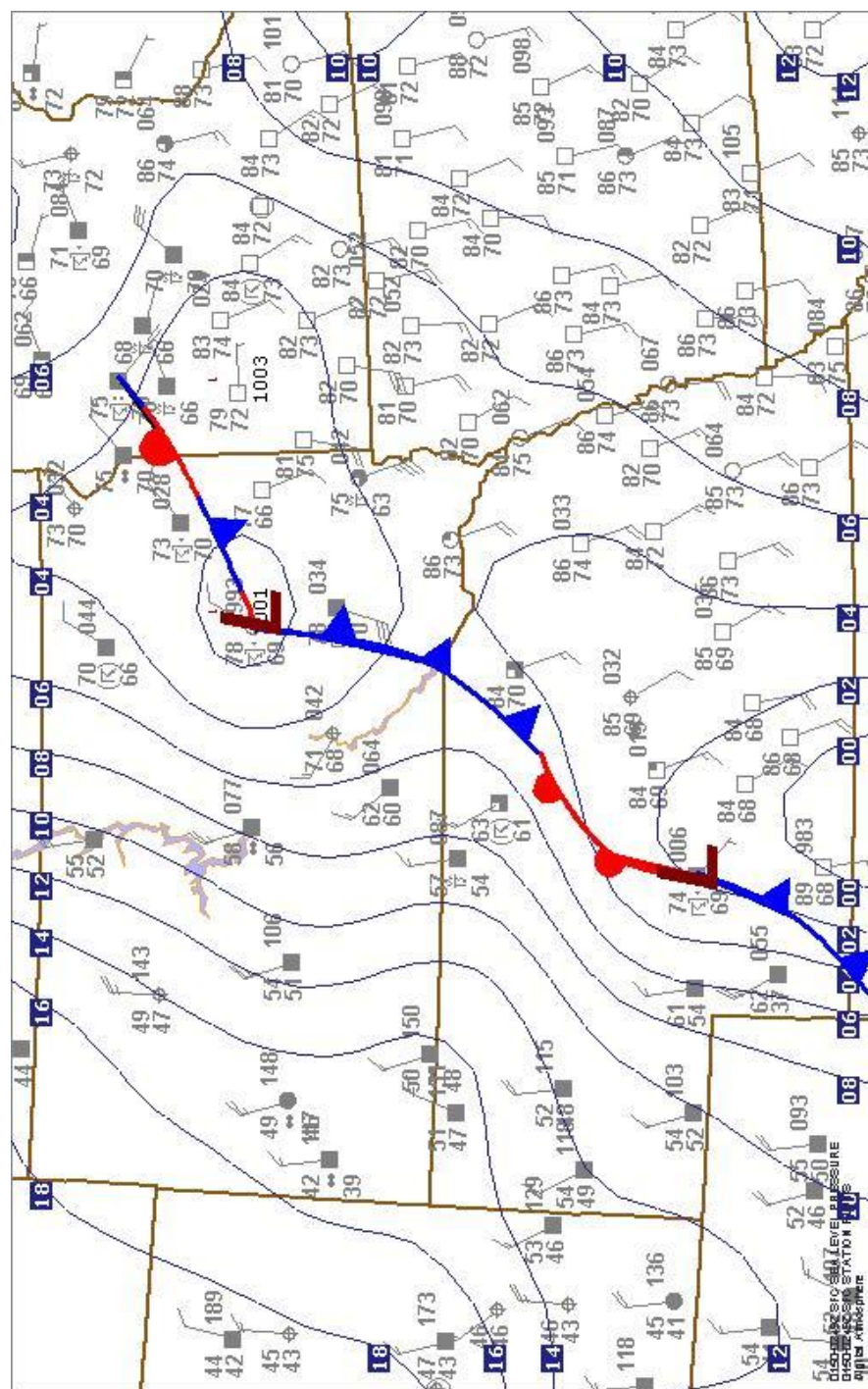
**Fig. 11c.** Same as 11a, except at 0200 UTC on 25 June 2003.

**Fig. 11d.** Same as 11a, except at 0300 UTC on 25 June 2003.
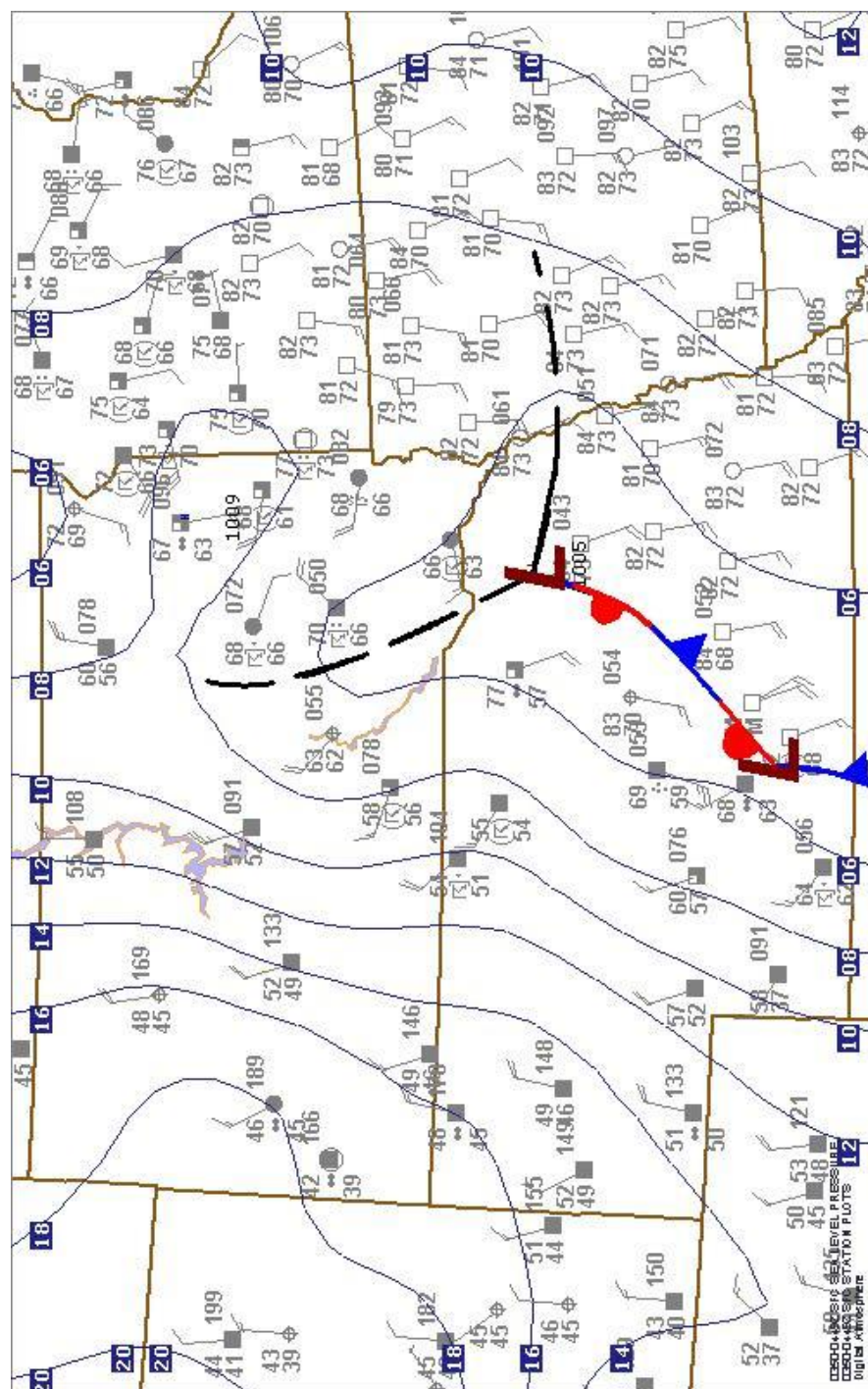
**Fig. 11e.** Same as 11a, except at 0400 UTC on 25 June 2003.

73
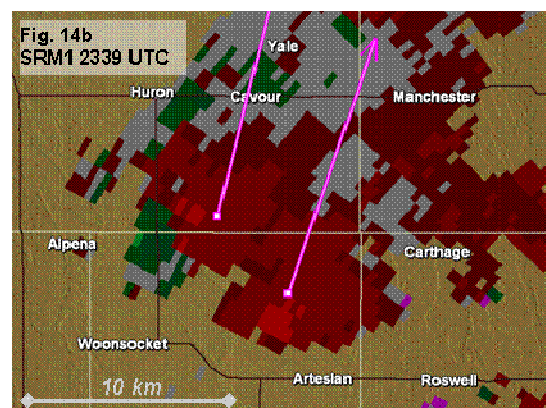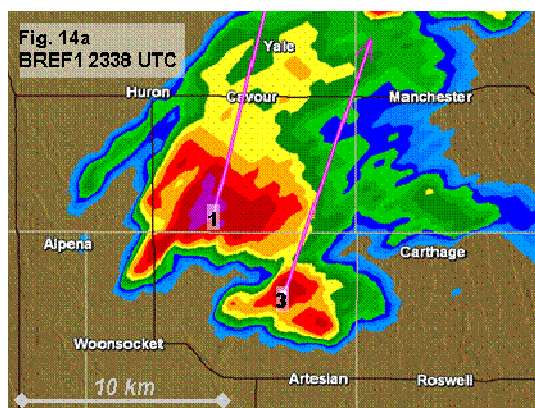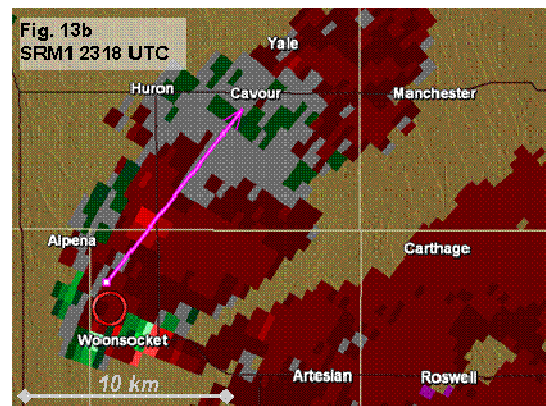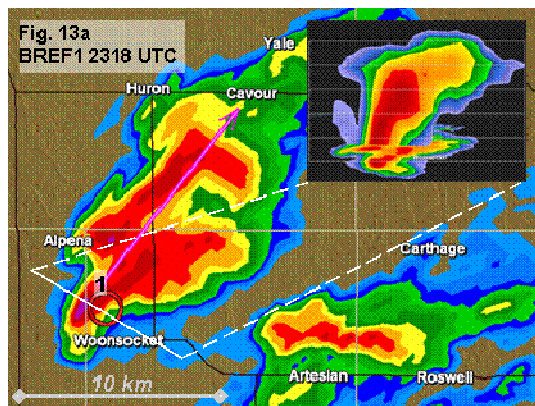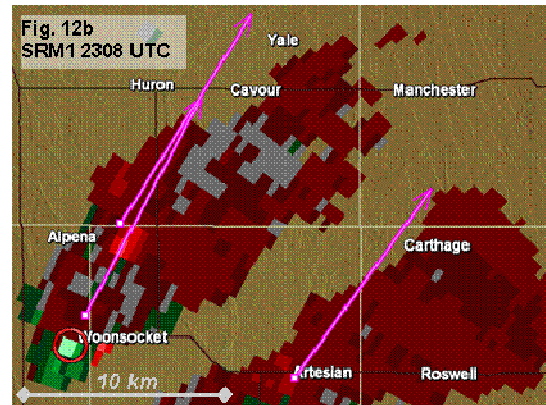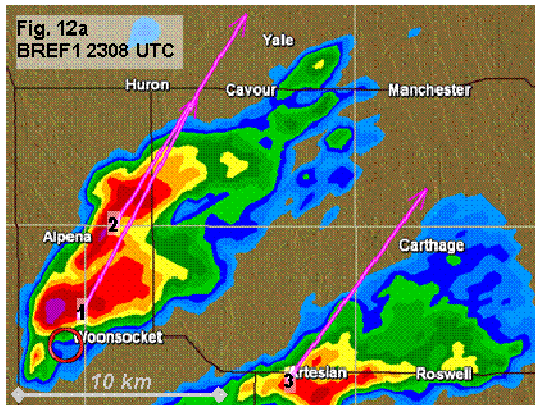


**Fig. 12-14.** 0.5 degree imagery from KFSD radar, base reflectivity (**a**) and SRM velocity (**b**). Arrows depict storm maximum reflectivity centroid and direction of movement from the NEXRAD attribute table. Red circles are Baron shear markers indicating areas of maximum cyclonic shear. Storms are 135-145 km from the KFSD RDA site, and the beam height at 0.5 deg is approximately 2238 m-2390 m (7,500-8,000 ft) AGL.
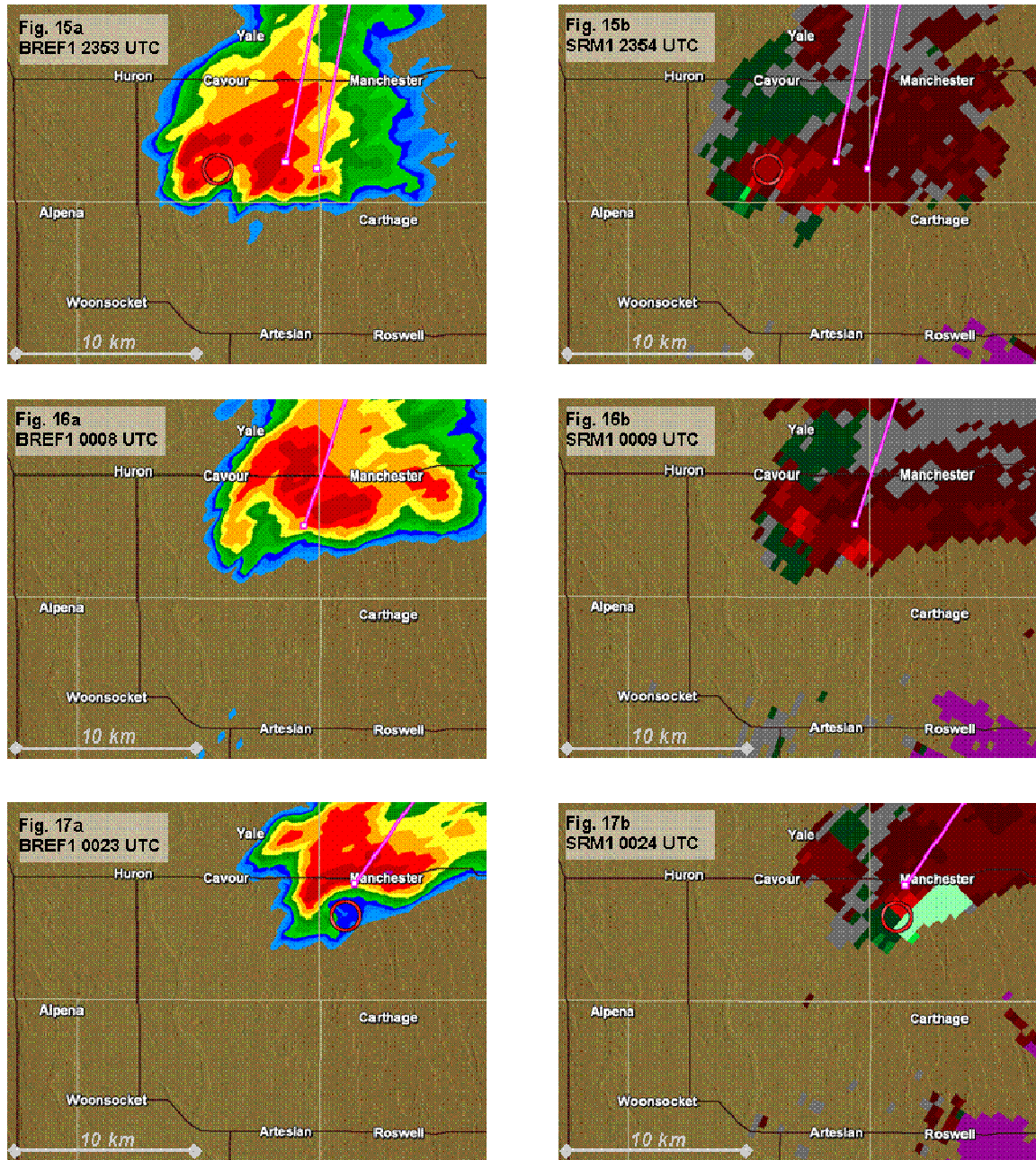
**Fig. 15-17.** 0.5 degree imagery from KFSD radar, base reflectivity (**a**) and SRM velocity (**b**). Arrows depict storm maximum reflectivity centroid and direction of movement from the NEXRAD attribute table. Red circles are Baron shear markers indicating areas of maximum cyclonic shear. Storms are 135-145 km from the KFSD radar, and the beam height at 0.5 deg is approximately 2260 m AGL.

**Fig. 18**. Schematic of a cyclic supercell from (WW2010, 2004).
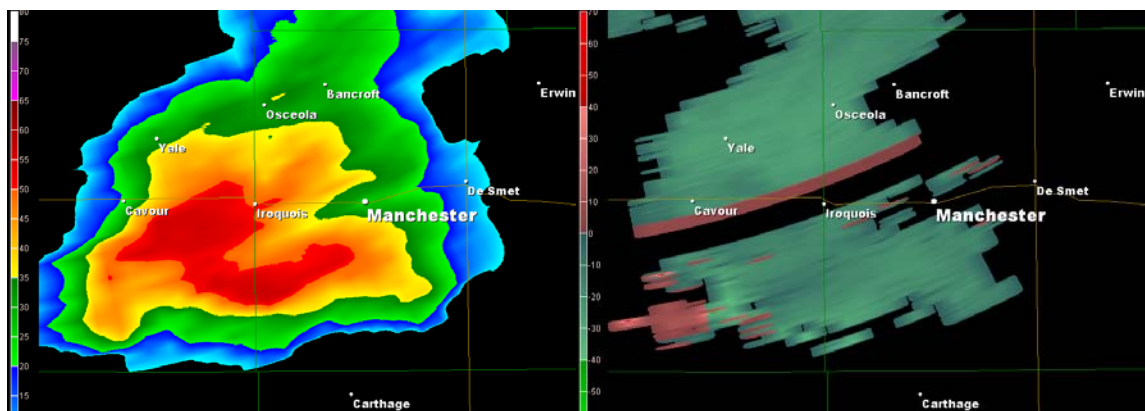


**Fig. 19.** KABR level 2 0.5 deg base reflectivty and SRM velocity, 0003 UTC (25 June 2003). Gibson Ridge data smoothing applied. View ~ 46 km x 65 km. Not dealiased.
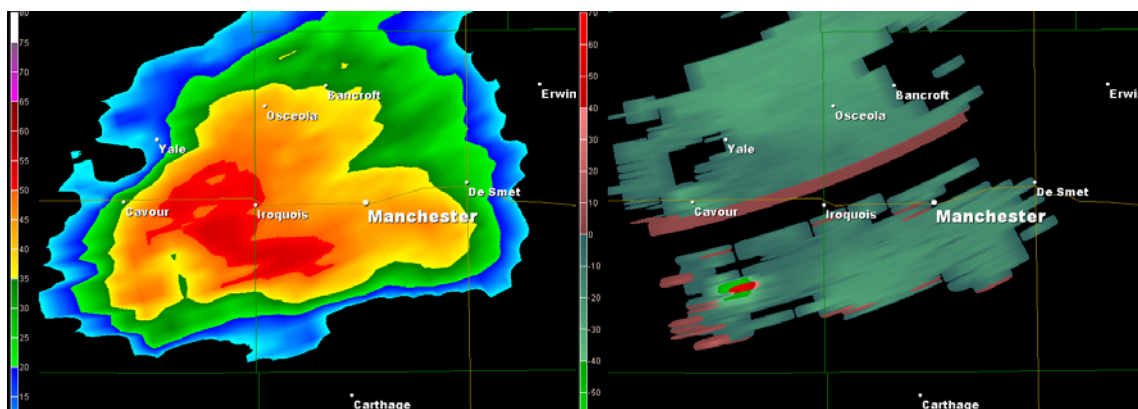
**Fig. 20.** KABR level 2 0.5 deg base reflectivty and SRM velocity, 0008 UTC (25 June 2003). Gibson Ridge data smoothing applied. View ~ 46 km x 65 km. Not dealiased.
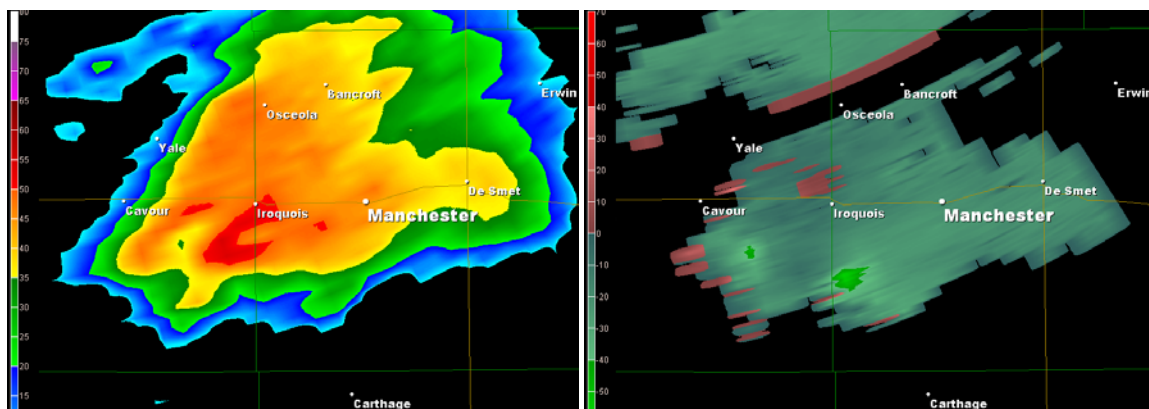


**Fig. 21.** KABR level 2 0.5 deg base reflectivty and SRM velocity, 0013 UTC (25 June 2003). Gibson Ridge data smoothing applied. View ~ 46 km x 65 km. Not dealiased.
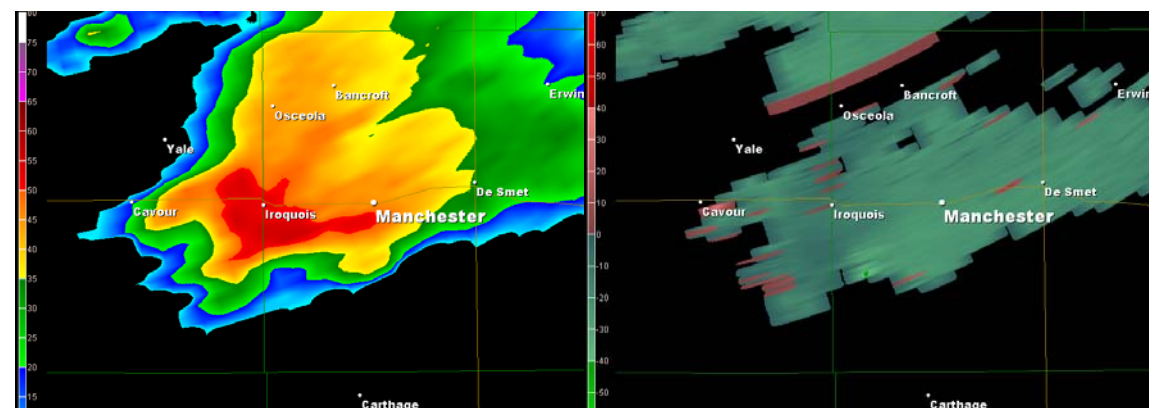


**Fig. 22.** KABR level 2 0.5 deg base reflectivty and SRM velocity, 0018 UTC (25 June 2003). Gibson Ridge data smoothing applied. View ~ 46 km x 65 km. Not dealiased.
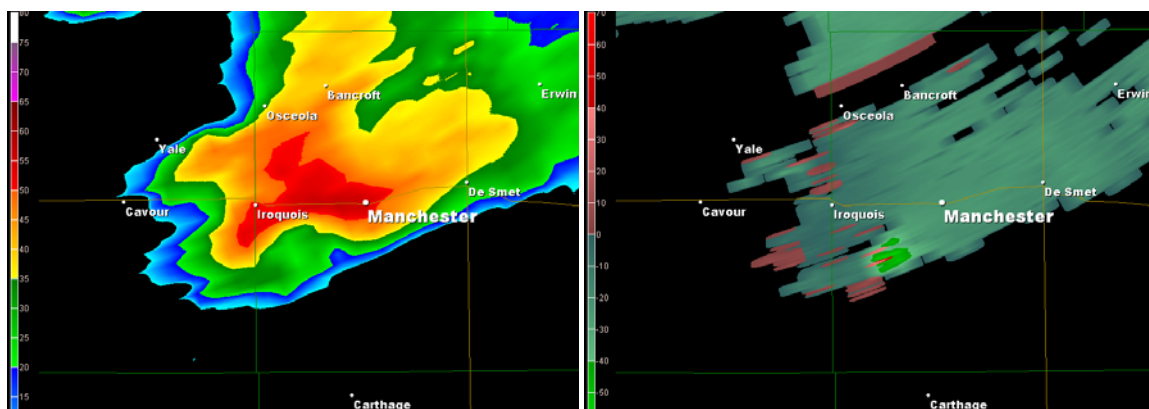
**Fig. 23.** KABR level 2 0.5 deg base reflectivty and SRM velocity, 0023 UTC (25 June 2003). Gibson Ridge data smoothing applied. View ~ 46 km x 65 km. Not dealiased.
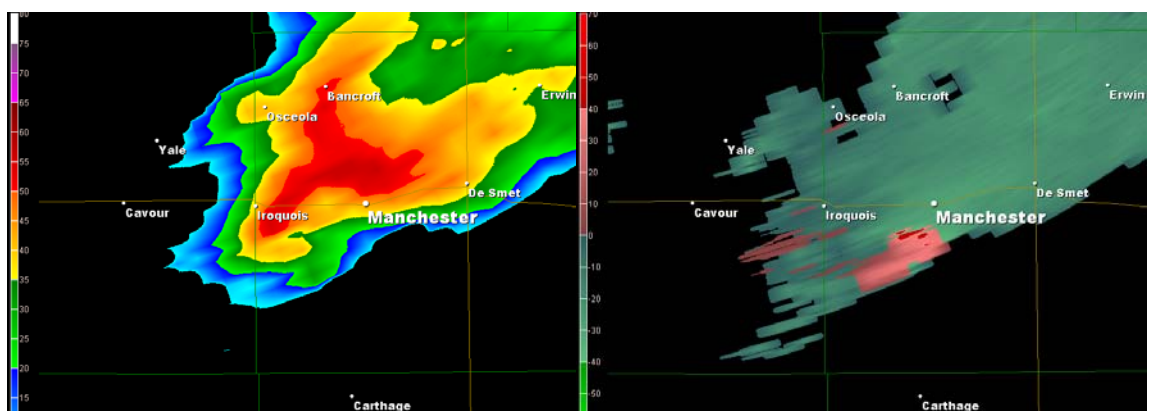


**Fig. 24.** KABR level 2 0.5 deg base reflectivty and SRM velocity, 0028 UTC (25 June 2003). Gibson Ridge data smoothing applied. View ~ 46 km x 65 km. Not dealiased.
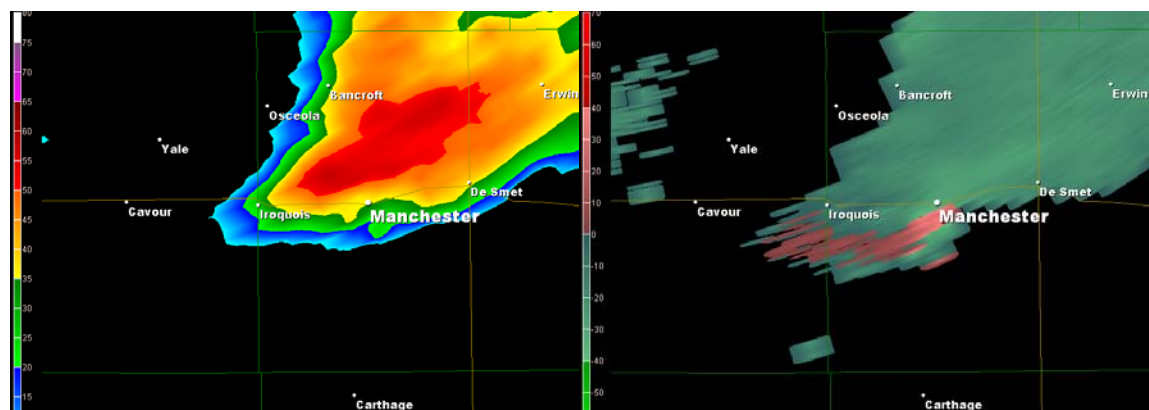


**Fig. 25.** KABR level 2 0.5 deg base reflectivty and SRM velocity, 0033 UTC (25 June 2003). Gibson Ridge data smoothing applied. View ~ 46 km x 65 km. Not dealiased.

2338 UTC
Max −12.8 m s⁻¹
+14.4 m s⁻¹

2343 UTC
Max −13.9 m s⁻¹
+17.5 m s⁻¹

2348 UTC
Max −12.8 m s⁻¹
+18.5 m s⁻¹

2353 UTC
Max −14.4 m s⁻¹
+22.6 m s⁻¹

2358 UTC
Max −12.8 m s⁻¹
+25.2 m s⁻¹

0003 UTC
Max −15.9 m s⁻¹
+20.6 m s⁻¹
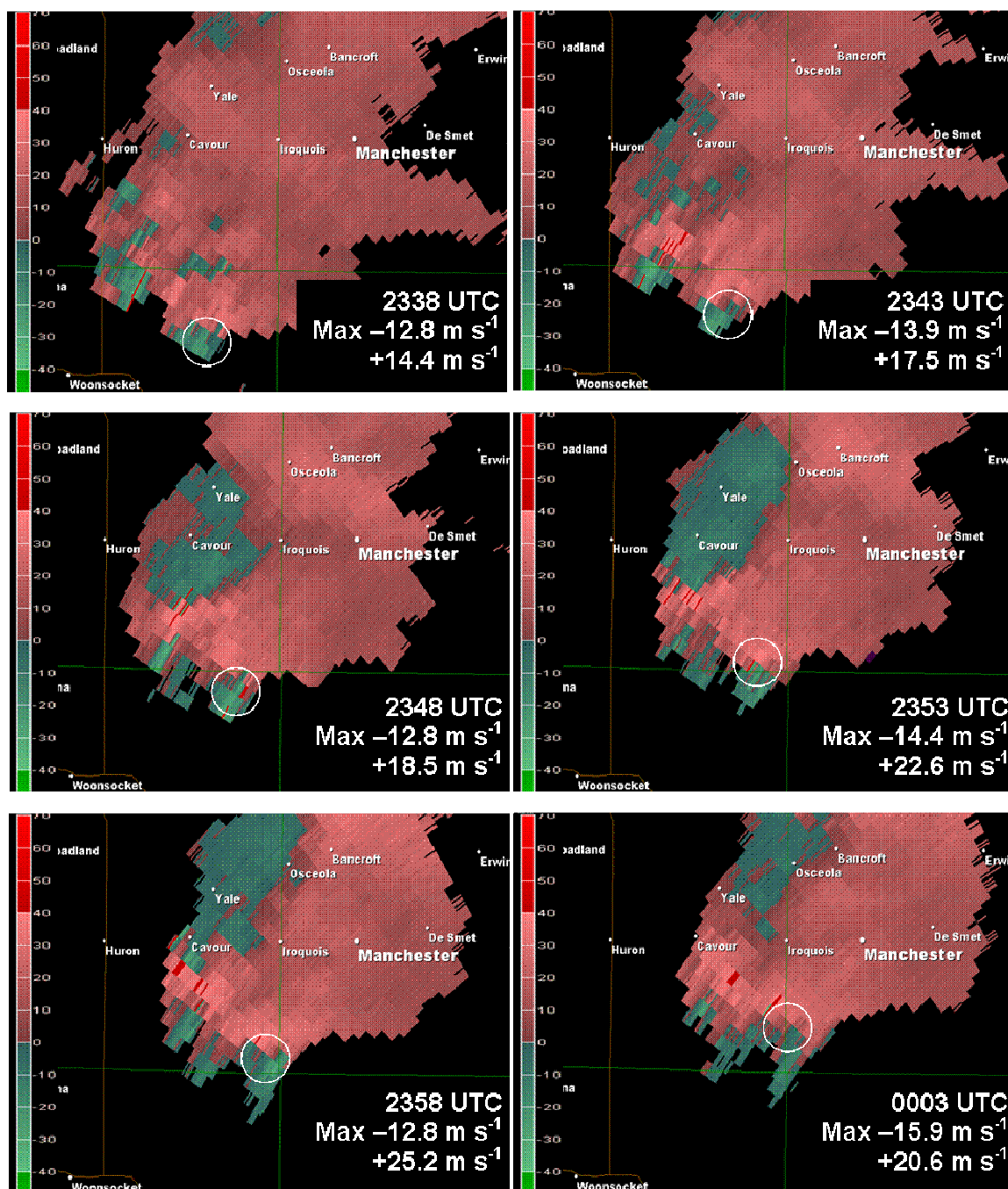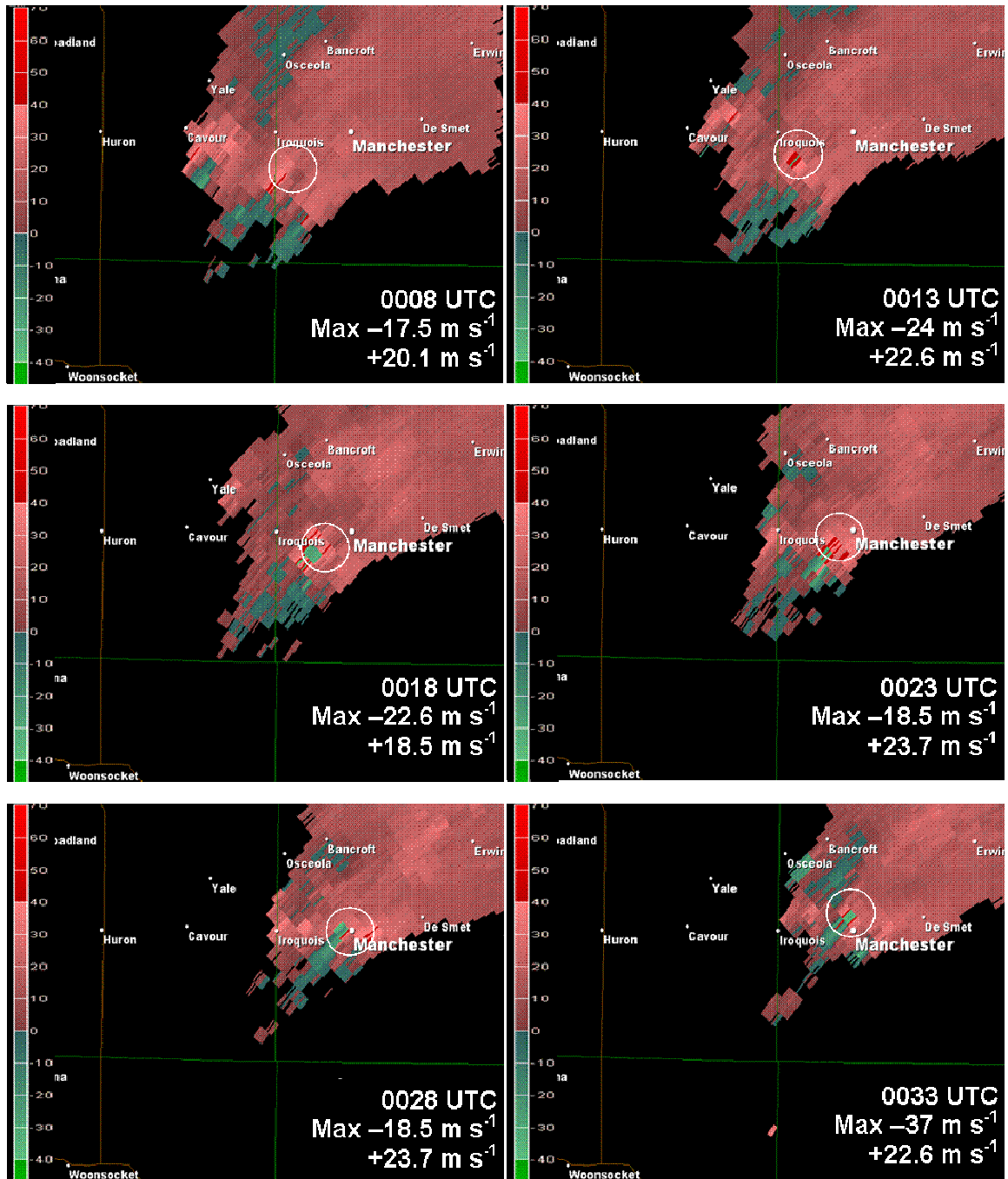
**Fig. 26.** SRM velocity at 1.5 deg KFSD radar from 2338 UTC 24 June 2003 to 0033 UTC 25 June 2003. Storm motion calculated from 240 deg at 10.3 m s$^{-1}$ (20 kt). Rings identify center of rotational shear with maximum range bin values noted. Image area ~87 km x 35 km. Beam height 3762 m AGL at distance 120 km from KFSD to shear maximum.
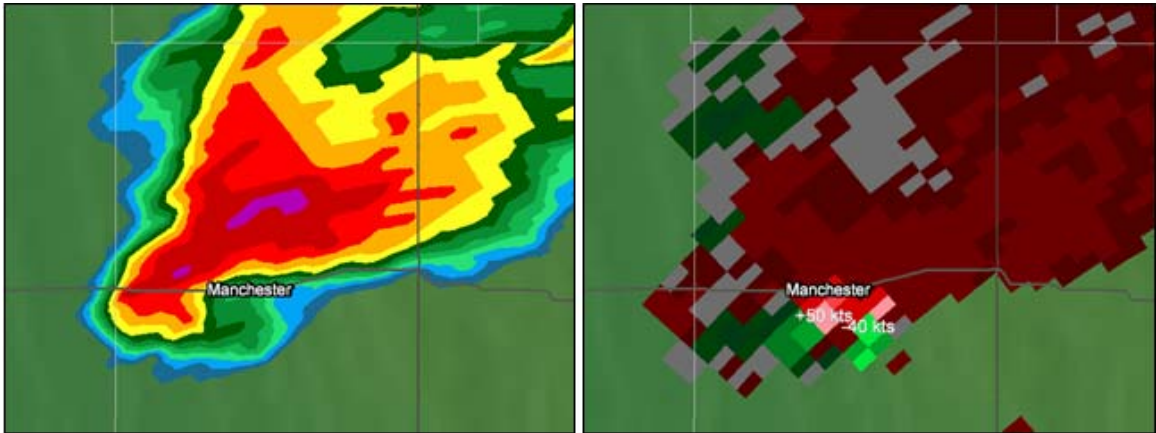
**Fig**. **27a.** KFSD level 3 0.5 deg base reflectivity, 0033 UTC (25 June 2003). Center beam height 1771 m AGL. **Fig. 27b** is the SRM product with velocities noted.
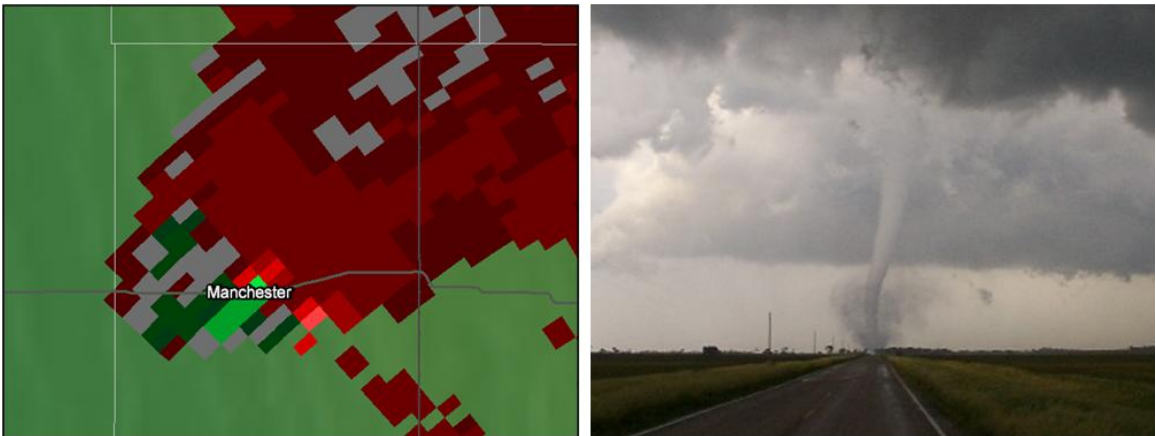


**Fig. 28a.** KFSD base velocity over Manchester at 0042 UTC (25 June 2003). **Fig. 28b.** Picture of tornado over Manchester at approximately the same time (photo by Shawn Cable, KELO-TV).

| Tilt (°) | Toward (kt) | Away (kt) |
|---|---|---|
| 3.5 | -50 | +36 |
| 2.5 | -50 | +26 |
| 1.5 | -36 | +36 |
| 0.5 | -36 | +36 |
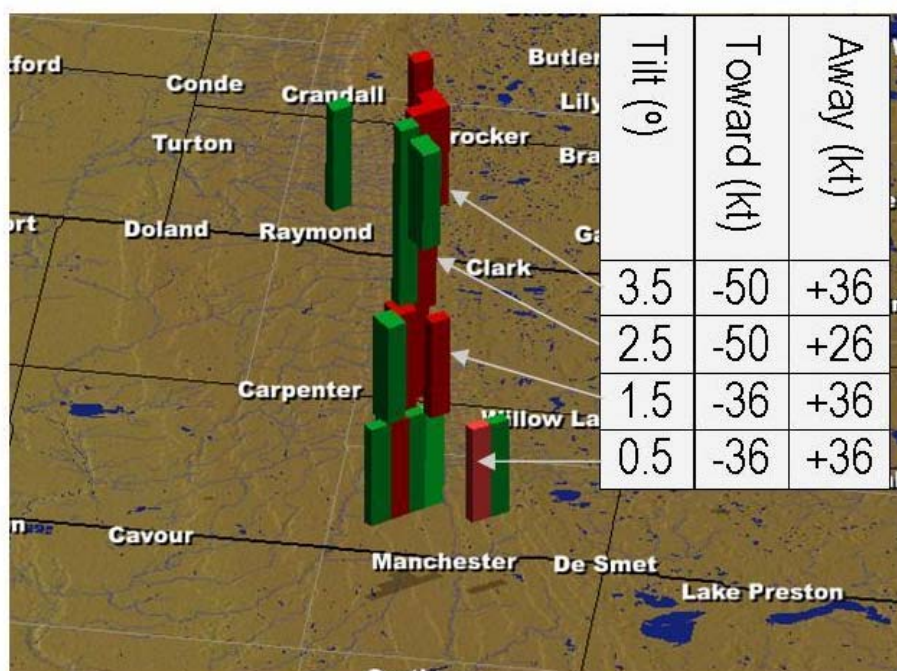
**Fig. 29.** Cross section (RHI) of 0034 UTC base velocity product from KFSD radar, tilt levels 0.5 deg, 1.5 deg, 2.5 deg, and 3.5 deg. Beam heights AGL over Manchester are approximately 1829 m (6,000 ft), 3871 m (12,700 ft), 5944 m (19,500 ft), and 7986 m (26,200 ft). In each case, gate-to-gate shear couplets are detected. Lower velocity gates are removed. Baron Services radar display. Inset: Maximum velocity gate values.

.
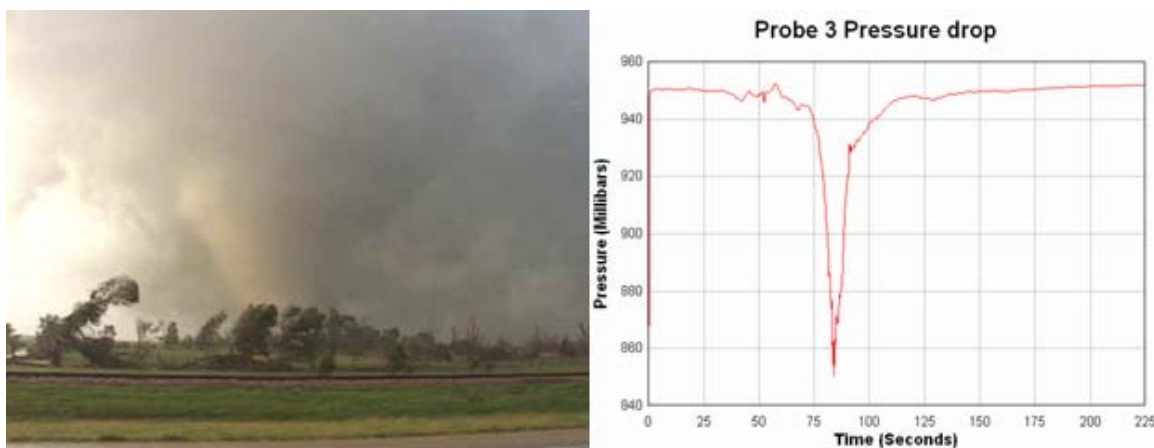


**Fig. 30a.** A wedge tornado went through Manchester (Roger Hill photo). **Fig. 30b.** Pressure trace from a Hardened In-Situ Tornado Pressure Recorder (HITPR) probe placed forty yards from a destroyed two-story farmhouse in Manchester (from Tim Samaras).
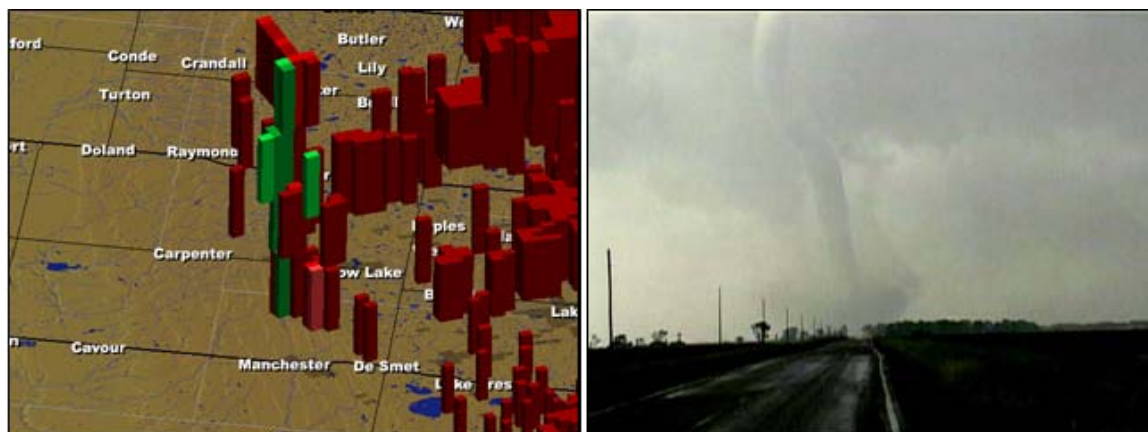
**Fig. 31a.** The next volume scan following Fig. 29. By 0039 UTC, velocities have increased in the higher levels, with shear now approaching 46.3 m s$^{-1}$ (90 kt) at 7945 m AGL. **Fig. 31b.** Tornado in rope stage (photo by Brian Karstens, KELO-TV).
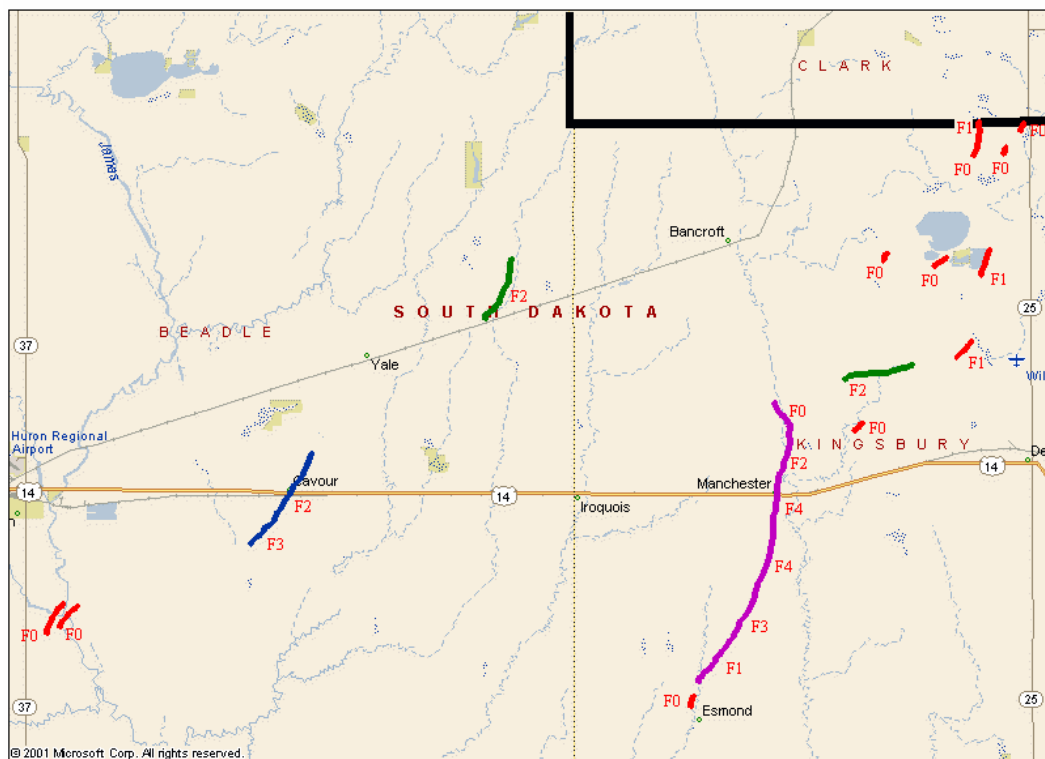


**Fig. 32.** Tornado damage paths near Manchester, from survey by NWS-FSD.
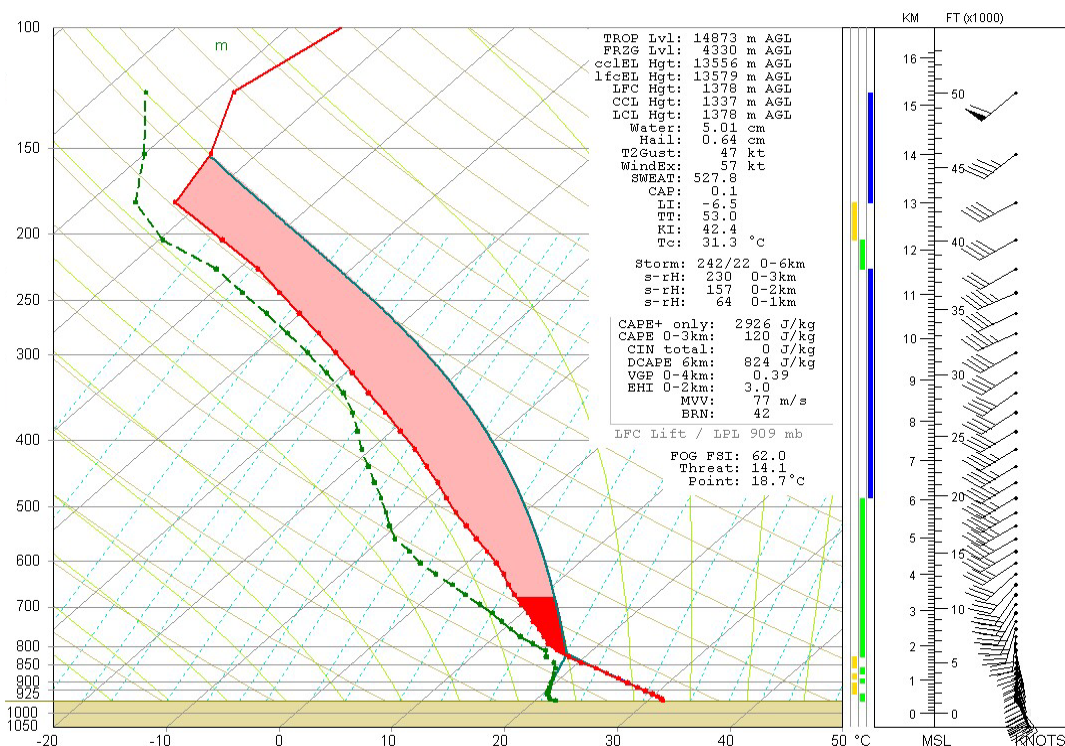
**Fig. 33.** Virtual sounding at KYKN (Yankton SD) valid at 0000 UTC 25 June 2003, from 1800 UTC 24 June 2003 meso-Eta forecast.

# Lapse rates (°C km$^{-1}$)

| Height (hPa) | 950 | 900 | 850 | 800 | 750 | 700 | 650 | 600 | 550 | 500 | 450 | 400 |
|---|---|---|---|---|---|---|---|---|---|---|---|---|
| 300 | 7.6 | 7.5 | 7.3 | 7.2 | 7.1 | 7 | 7.1 | 7.6 | 7.4 | 7.4 | 7.7 | 7.7 |
| 350 | 7.6 | 7.4 | 7.2 | 7.1 | 7 | 6.8 | 7 | 7.5 | 7.3 | 7.3 | 7.6 | 7.6 |
| 400 | 7.6 | 7.4 | 7.1 | 7 | 6.8 | 6.7 | 6.8 | 7.5 | 7.2 | 7.1 | 7.6 | |
| 450 | 7.6 | 7.3 | 7 | 6.9 | 6.7 | 6.4 | 6.6 | 7.5 | 7 | 6.5 | | |
| 500 | 7.8 | 7.5 | 7.1 | 6.9 | 6.7 | 6.4 | 6.6 | **8** | 7.5 | | | |
| 550 | 7.8 | 7.3 | 7.1 | 6.8 | 6.5 | 6 | 6 | **8.5** | | | | |
| 600 | 7.7 | 7.3 | 6.7 | 6.3 | 5.7 | 4.6 | 3.4 | | | | | |
| 650 | **8.6** | **8.2** | 7.7 | 7.4 | 7 | 5.9 | | | | | | |
| 700 | **9.2** | **8.8** | **8.3** | **8.2** | **8.2** | | | | | | | |
| 750 | **9.5** | **9.1** | **8.4** | **8.1** | | | | | | | | |
| 800 | **10** | **9.6** | **8.6** | | | | | | | | | |
| 850 | **10.8** | **10.6** | | | | | | | | | | |
| 900 | **11** | | | | | | | | | | | |

**Height (hPa)**

**Table 1.** Lapse rates within selected pressure surface layers at KYKN (Yankton SD) at 2200 UTC from meso-Eta 1800 UTC forecast 24 June 2003. Red numbers are lapse rates >8°C km$^{-1}$. Coordinates are pressure surfaces in hPa.

**Fig 34.** Tornado damage paths though eastern Turner County and western Lincoln County, from survey by NWS-FSD.



**Fig. 35.** 0000 UTC 25 June 2003 RUC 1 hour surface conditions (Barker, 2003).
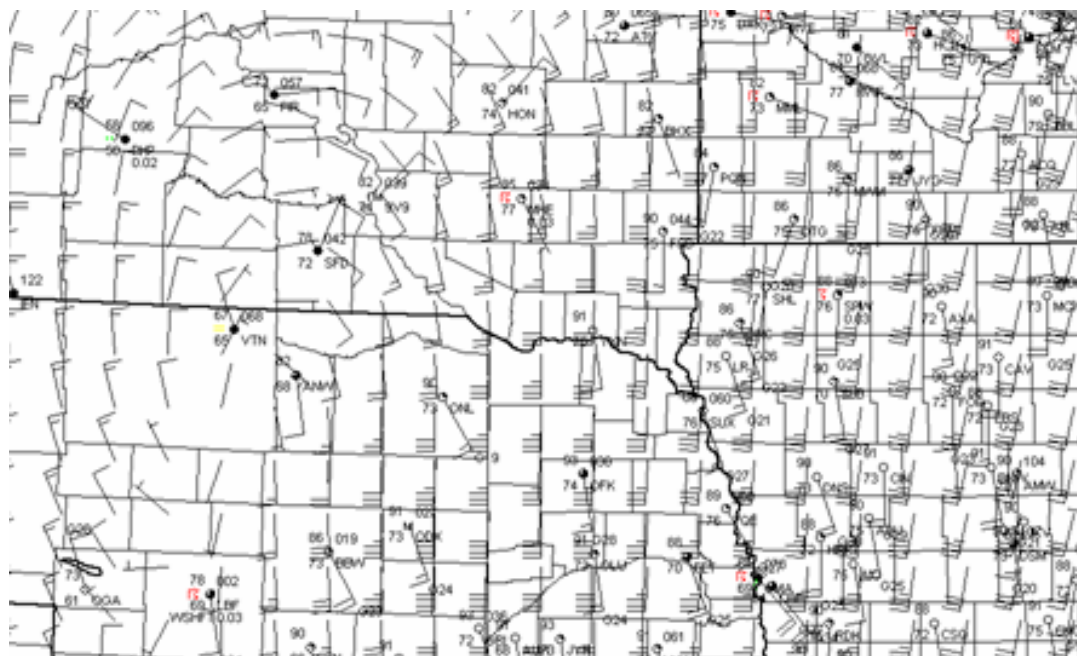
**Fig. 36.** 2300 UTC RUC 850 hPa 1hour forecast (Barker, 2003).
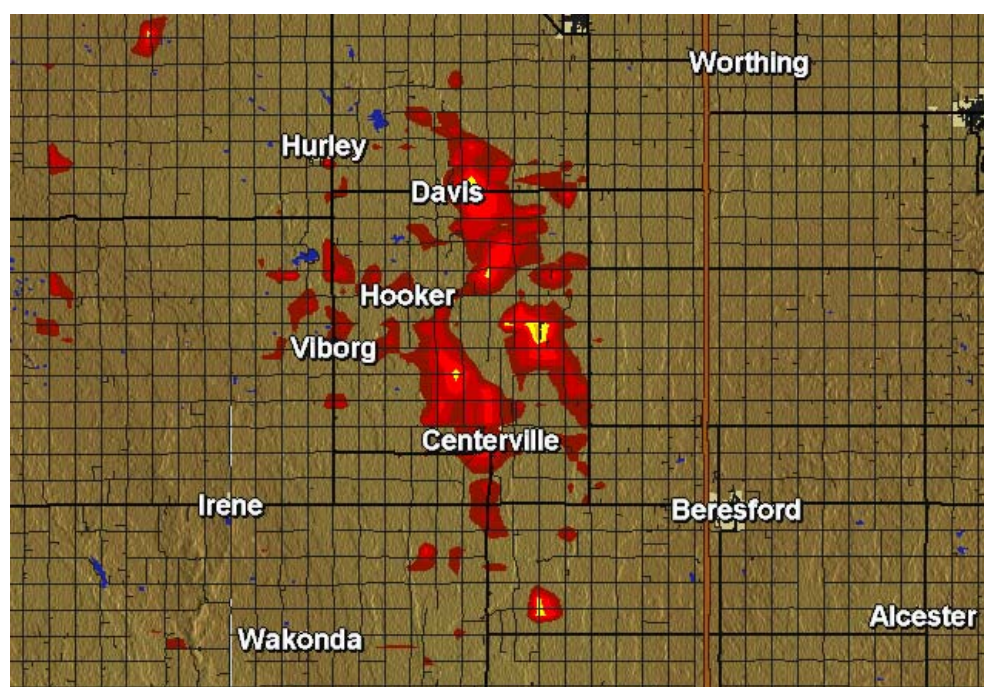


**Fig. 37.** Mosaic of maximum cyclonic shear from KFSD radar between 0040 and 0140 UTC (25 June 2003). Areas plotted indicate shear between 30.8 and 51.4 m s$^{-1}$ (60 and 100 kt) from the Baron shear algorithm (similar to a mosaic of the CS-Combined Shear product from the WSR-88D). Highest values indicated with the yellow color. View approximately the same as Fig. 34.
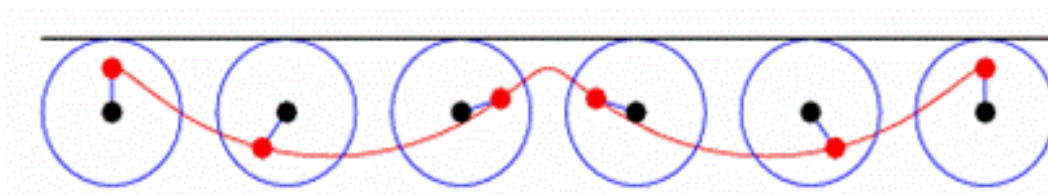
**Fig. 38.** Diagram of a curtate cycloid. When applied to tornadic storms, the blue circle would represent the cyclonically rotating mesocyclone, the red spot the tornado vortex, and the red line the tornado damage path. From mathworld.wolfram.com with permission.
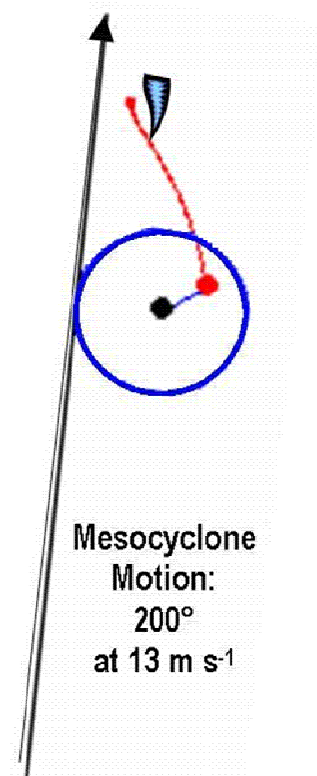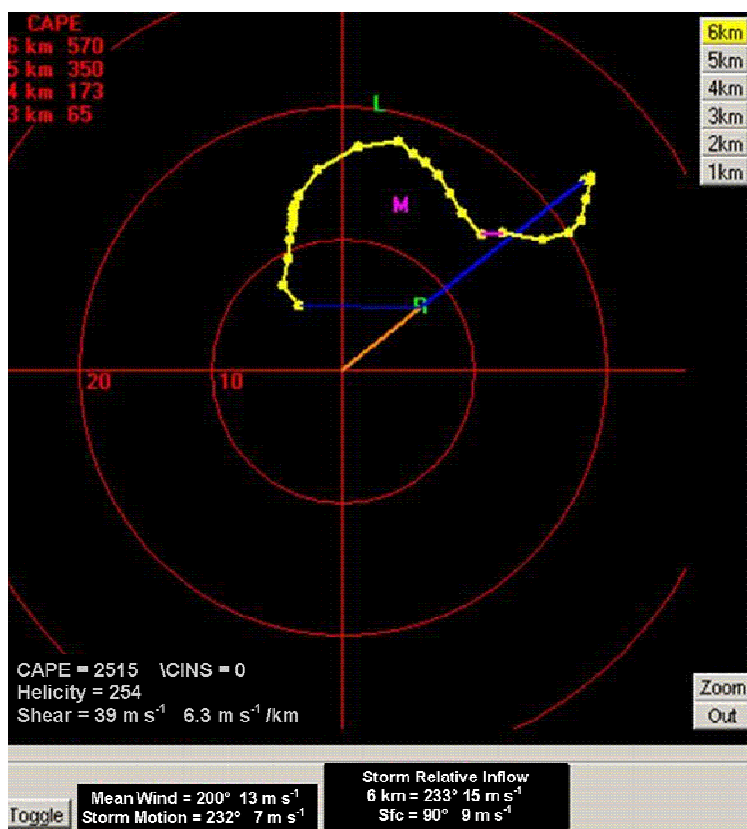


**Fig. 39.** Hodograph of BUFKIT wind profile at KYKN at 01 UTC (25 June 2003) based upon afternoon meso-Eta forecast. Mean 0-6 km wind 200 deg at 13 m s$^{-1}$. Curtate cycloid movement would result in some tornadoes leaving damage path from southeast to northwest.
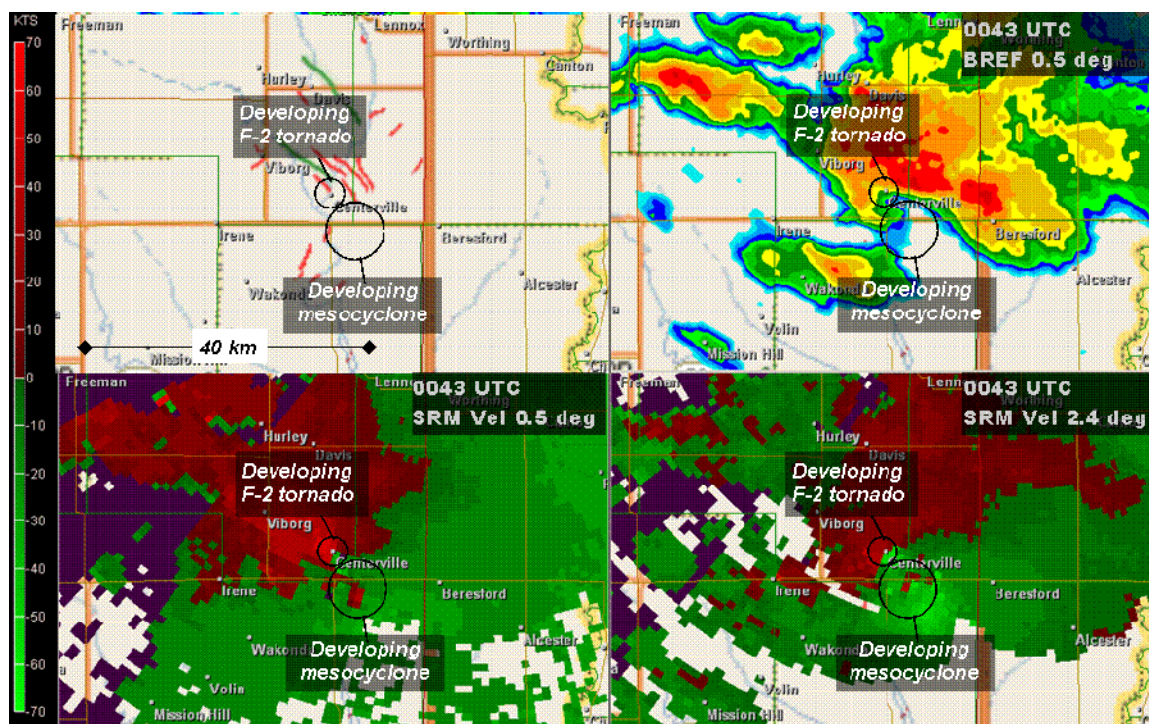
**Fig. 40.** KFSD level 3 data, 0043 UTC 25 June 2003. Clockwise from upper left: NWS damage paths, reflectivity 0.5 deg, SRM velocity 2.4 deg, and SRM velocity 0.5 deg.
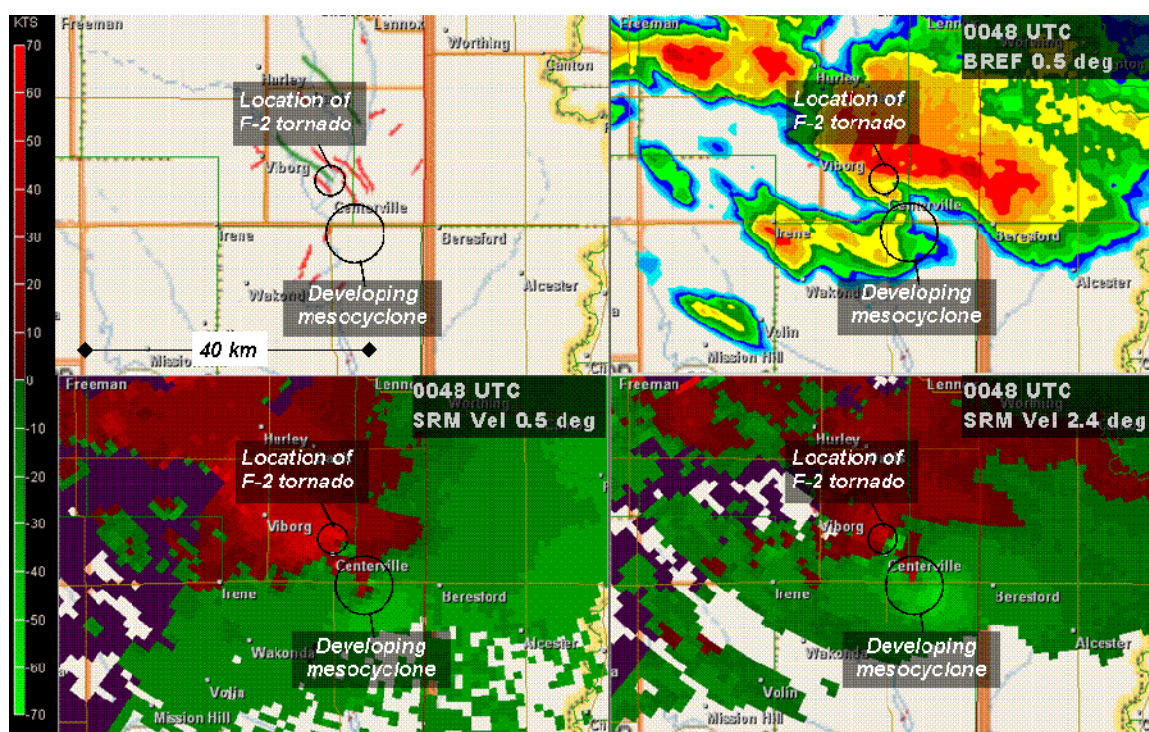


**Fig. 41.** Same as Fig. 40, except 0048 UTC 25 June 2003.
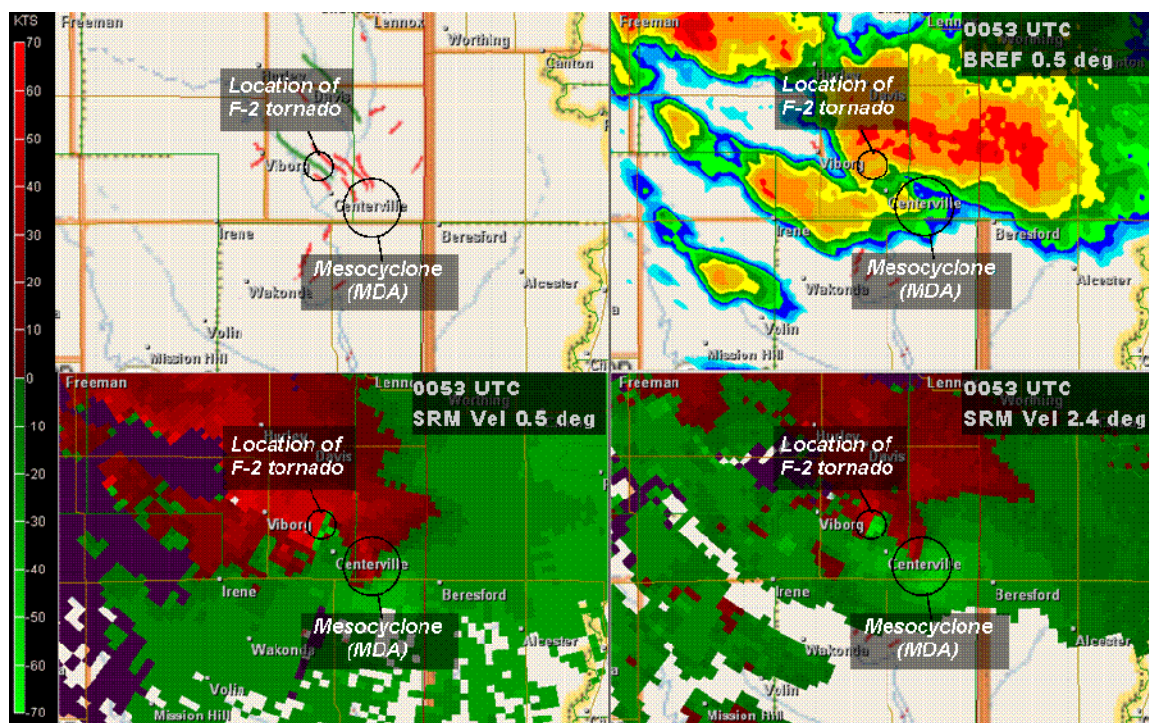
**Fig. 42.** Same as Fig. 40, except 0053 UTC 25 June 2003.
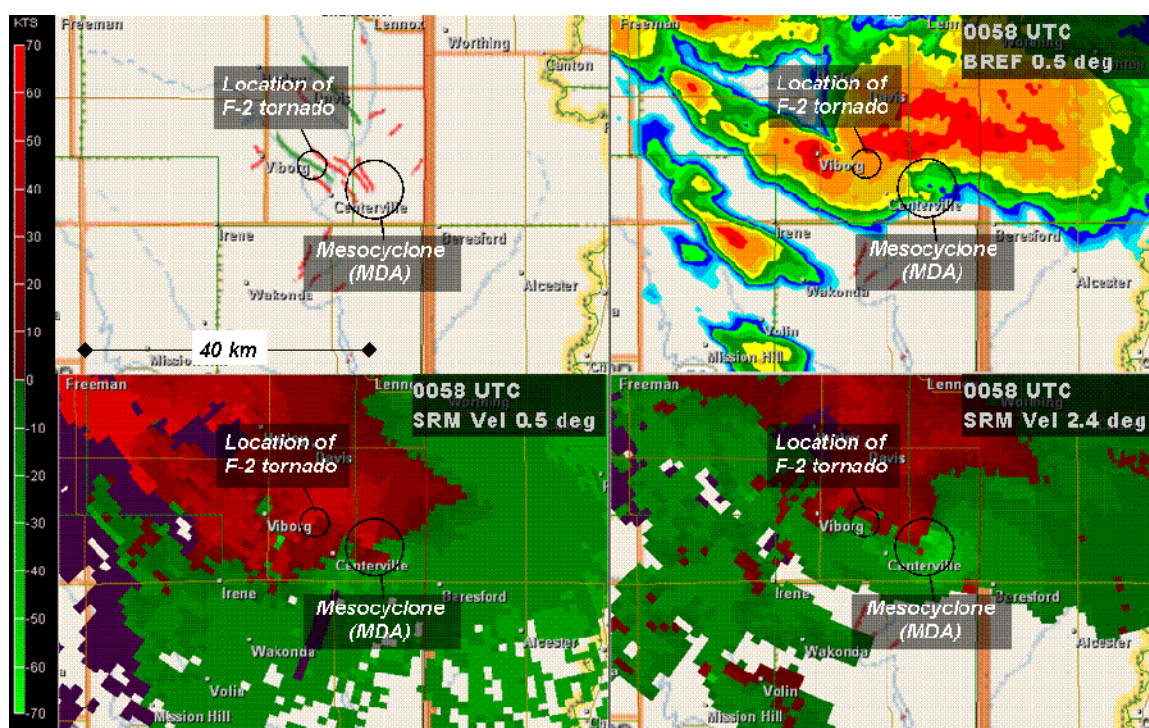


**Fig. 43.** Same as Fig. 40, except 0058 UTC 25 June 2003.
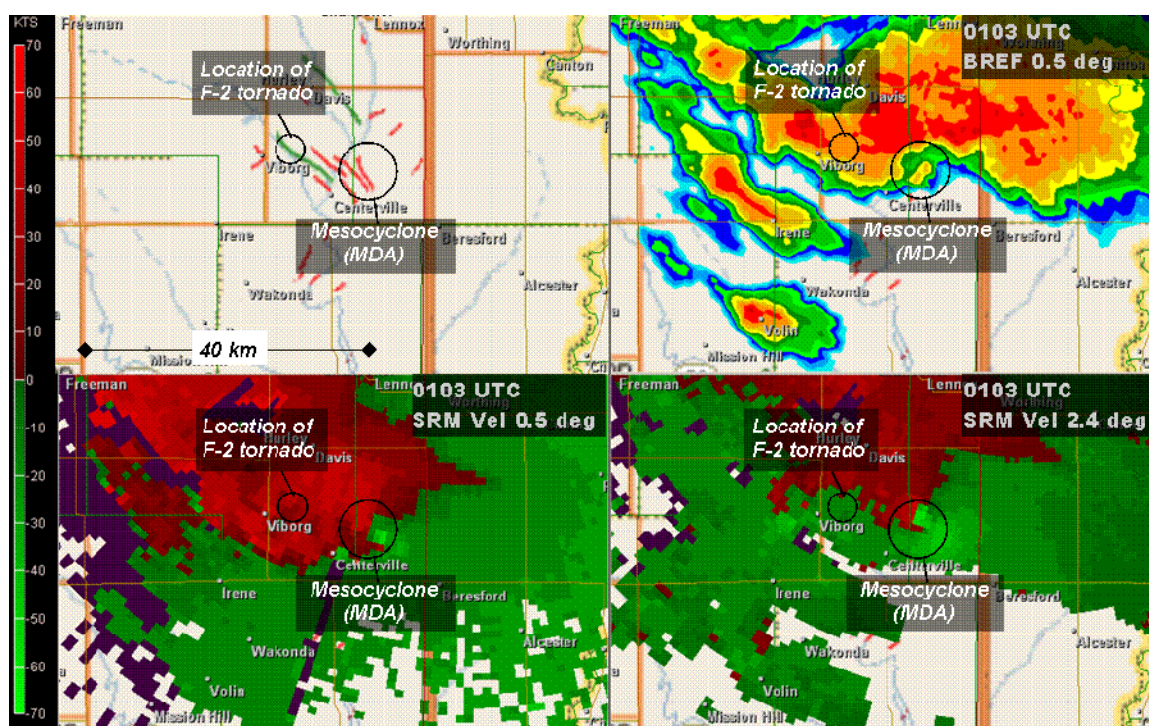
**Fig. 44.** Same as Fig. 40, except 0103 UTC 25 June 2003.
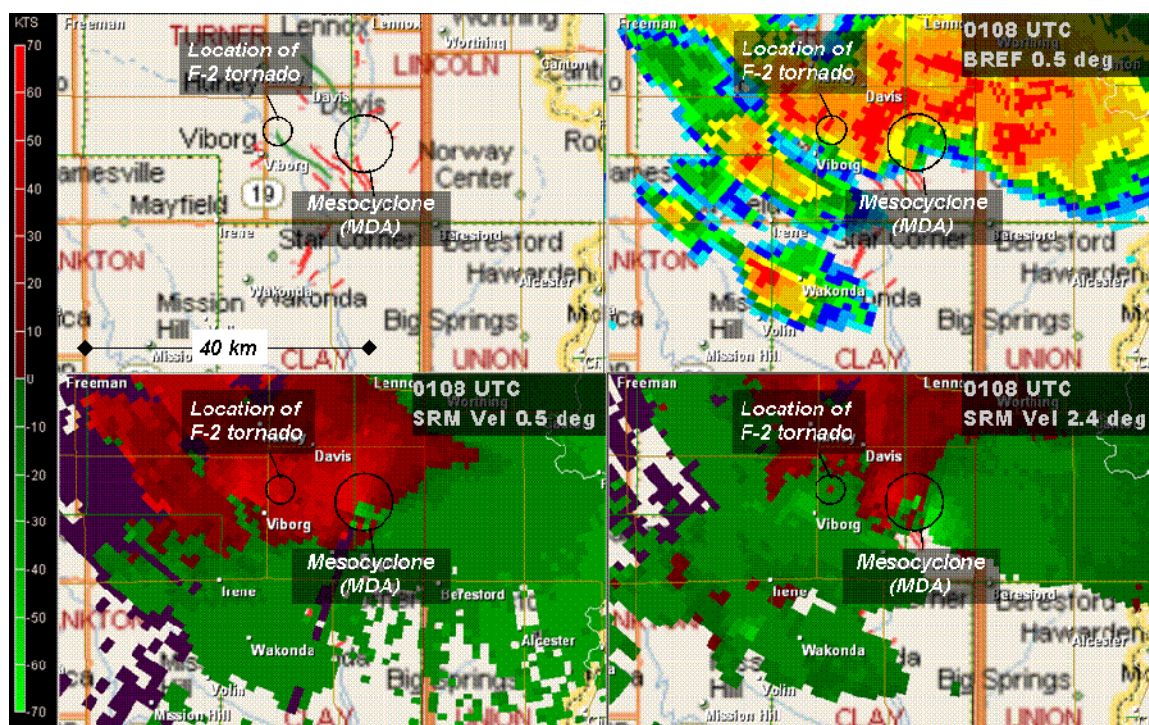


**Fig. 45.** Same as Fig. 40, except 0108 UTC 25 June 2003.
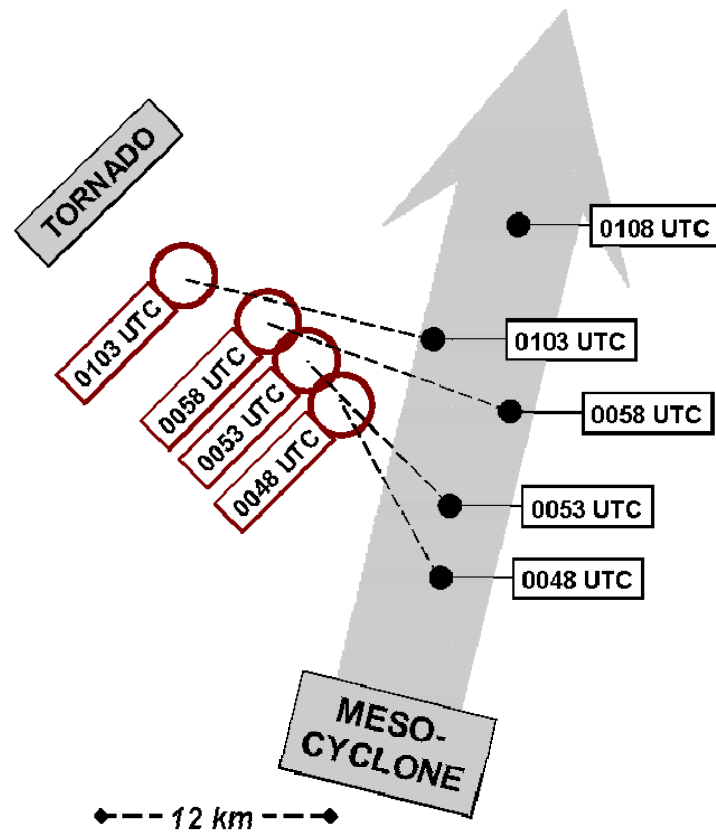
**Fig. 46.** Diagram of the relative positions of radar-indicated mesocyclone circulation centers and associated tornadoes in Turner Co, South Dakota on 24 June 2003.
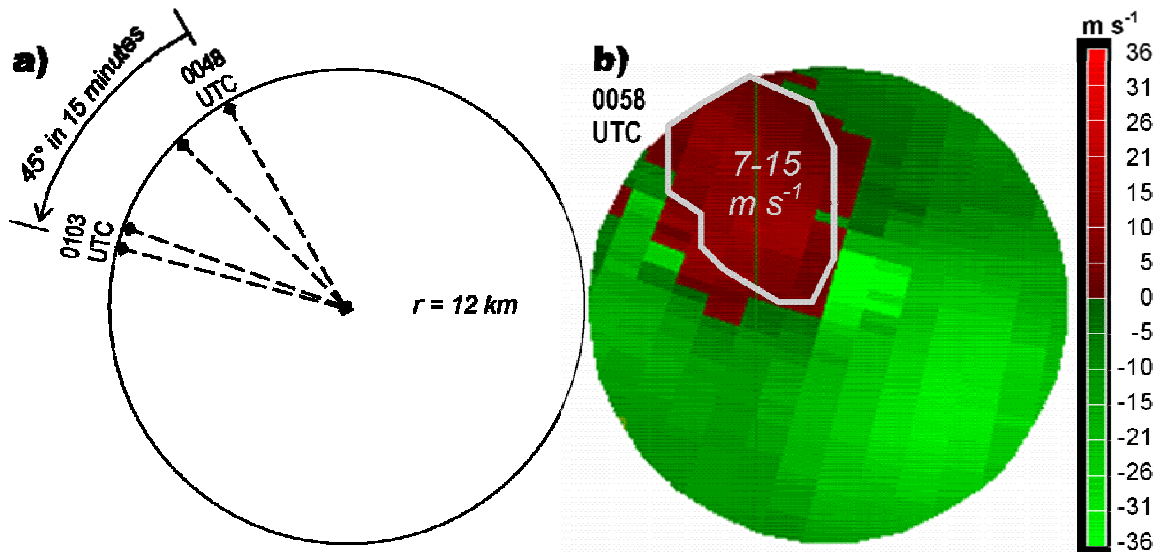


**Fig. 47a.** Storm-relative tornado positions compared to mesocyclone centers in Fig. 46. Vector rotates 45 deg in 15 min. **Fig. 47b.** Base velocity from KFSD radar at 0058 UTC, viewed over circulation center at 3.3 deg (3048 m AGL). Scale same as Fig. 46.
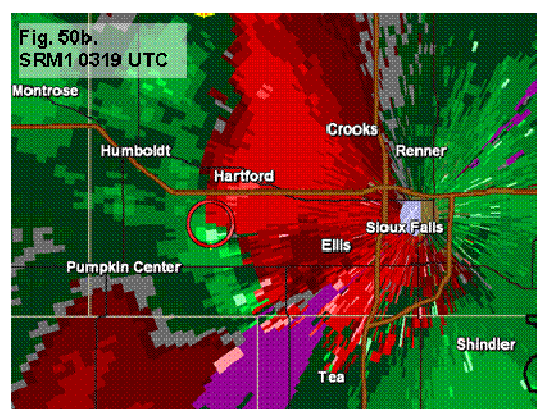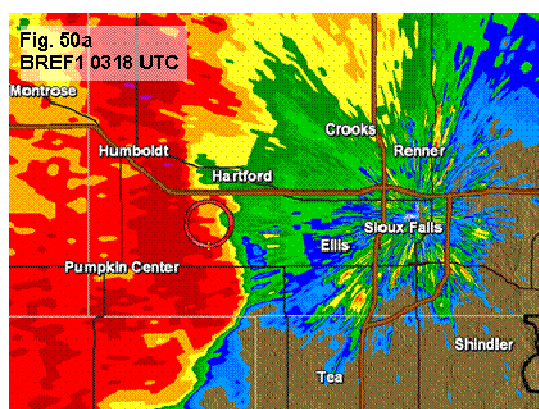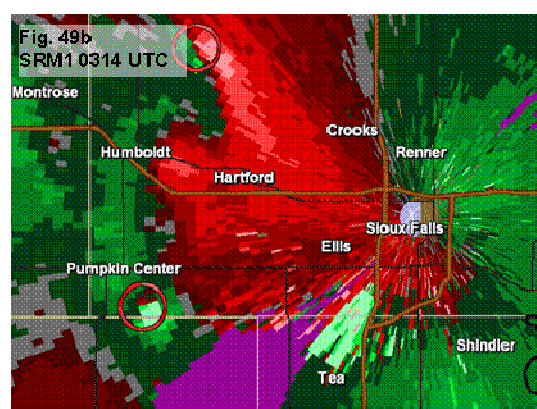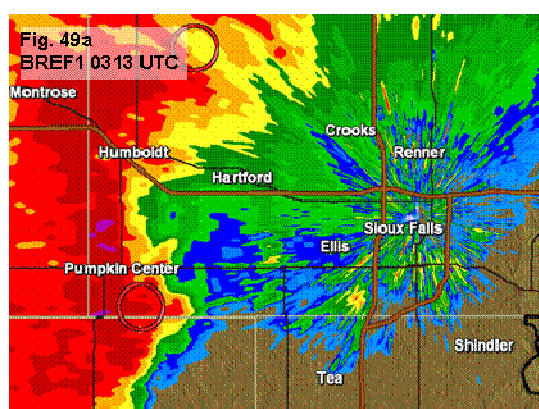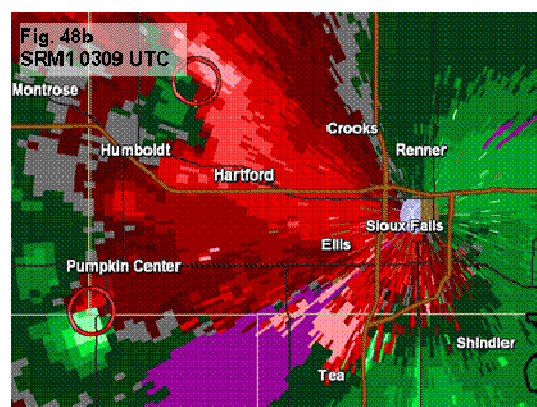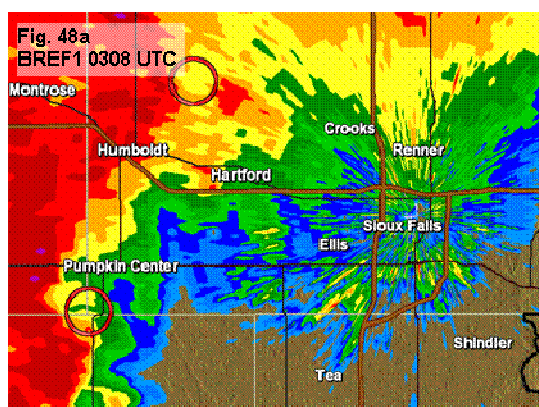
**Fig. 48-50.** 0.5 degree level 3 imagery from KFSD radar, base reflectivity (**a**) and storm-relative mean velocity (**b**). Red circles are Baron shear markers indicating areas of maximum cyclonic shear. Shear maximums are <30 km from the KFSD radar site. Purple indicates radar range folding.
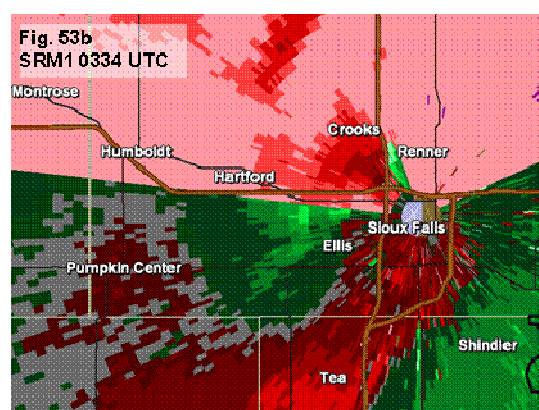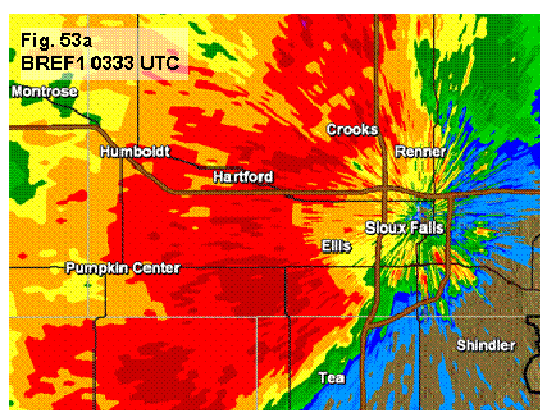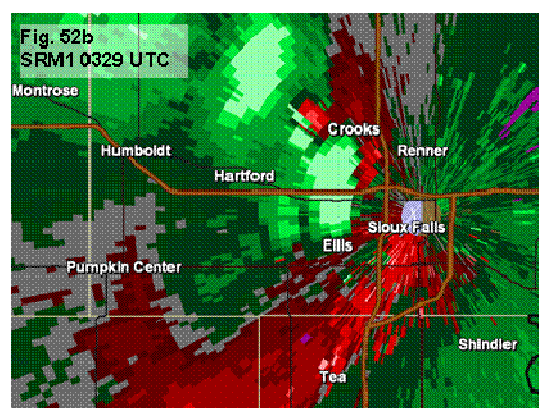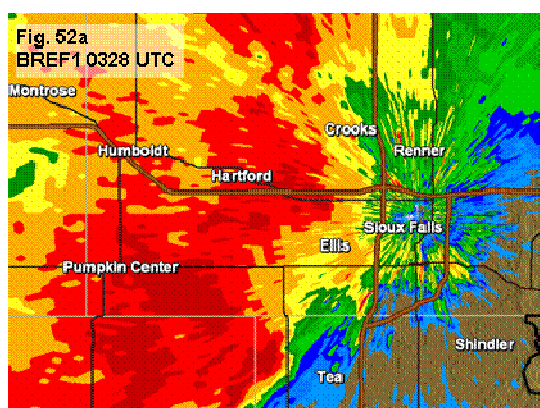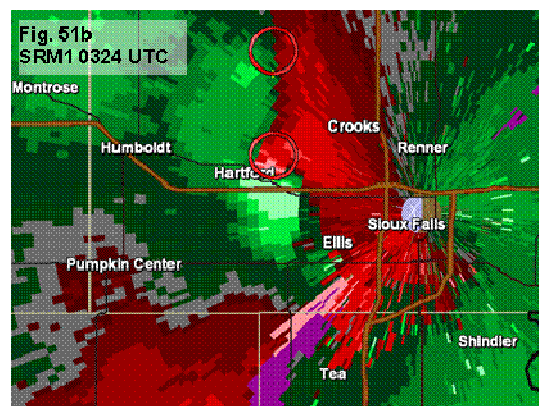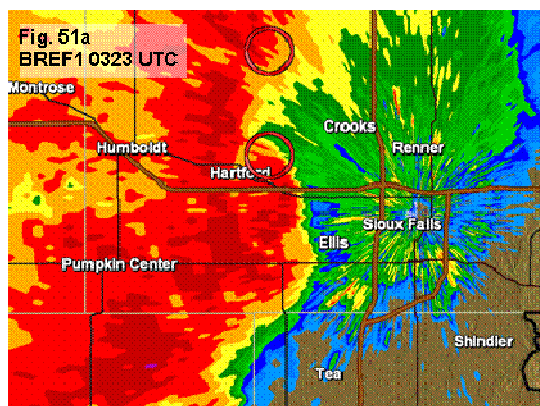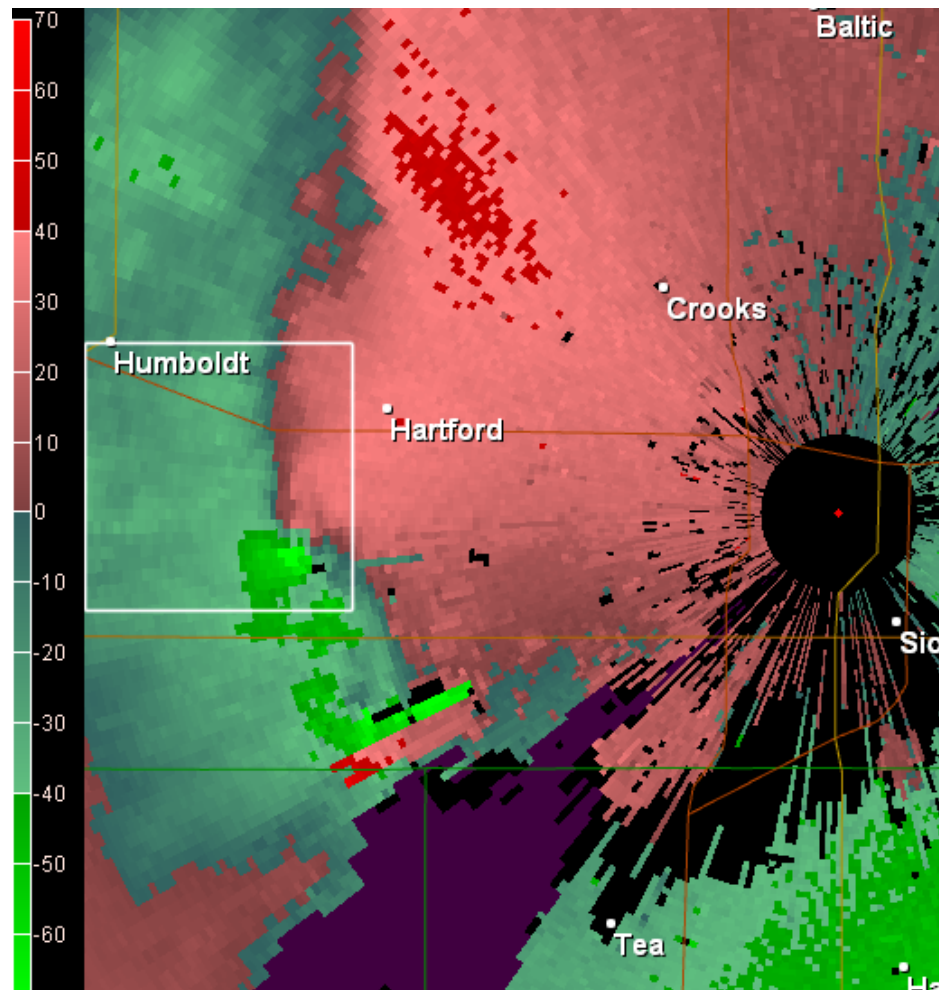
**Fig. 51-53.** 0.5 degree level 3 imagery from KFSD radar, base reflectivity (**a**) and storm relative mean velocity (**b**). Red circles are Baron shear markers indicating areas of maximum cyclonic shear. Shear maximums are <18 km from the KFSD radar site. Purple indicates radar range folding.
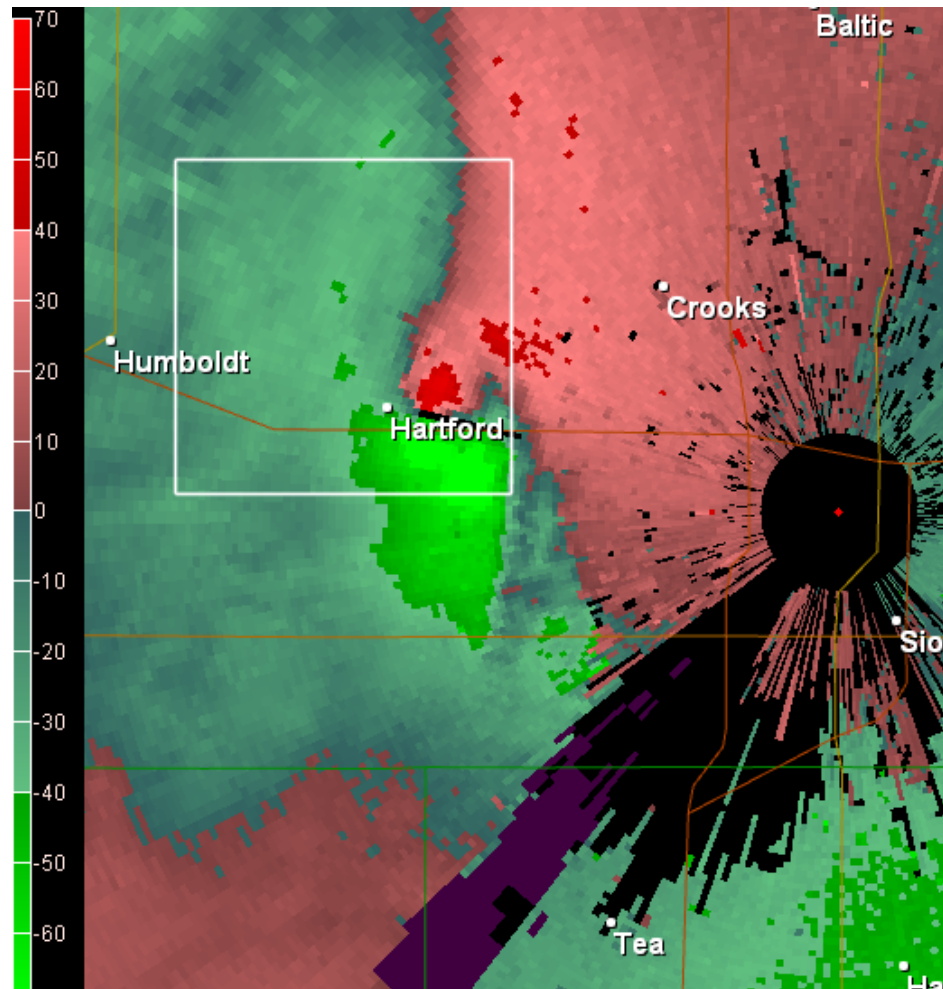
**Fig. 54.** KFSD level 2 velocity data at 0318 UTC (25 June 2003) with storm motion of 240 deg at 10.3 m s$^{-1}$ (20 kt) assumed to create storm relative velocity. Gibson Ridge dealiasing algorithm applied, with maximum of -43.2 m s$^{-1}$ (-84 kt) green inbound and +15.4 m s$^{-1}$ (+30 kt) red outbound inside 10 km x 10 km box. The box also indicates area shown in succeeding volumetric views.
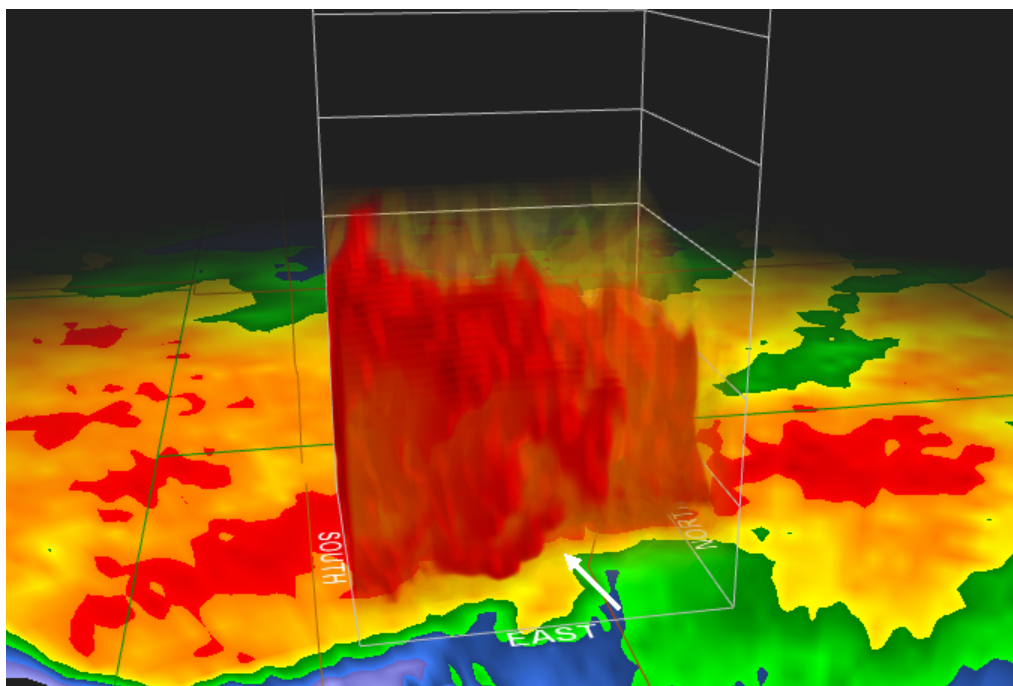
**Fig. 55.** KFSD reflectivity data at 0318 UTC (25 June 2003). Box depicts 10 km x 10 km area noted in Fig. 54 as viewed from the east, with height lines in increments of 10k ft. Yellow color ≥ 40 dBZ, red color ≥ 50 dBZ. Arrow points to reflectivity notch.
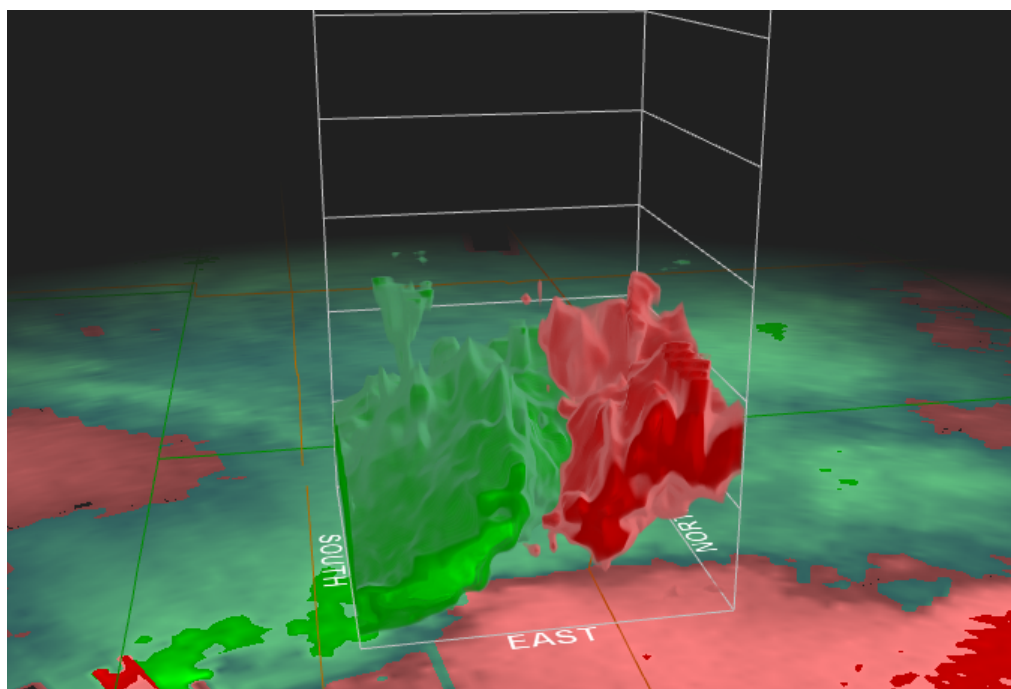


**Fig. 56.** Storm relative velocity 40 kt isosurfaces. Same scale, view, and time period (0318 UTC 25 June 2003) as in Fig. 55. Pink values in lowest level show storm inflow, and stronger green inbounds show incoming north side of the squall line.

**Fig. 57.** KFSD level 2 velocity data at 0323 UTC (25 June 2003) with storm motion of 240 deg at 10.3 m s$^{-1}$ (20 kt) assumed to create storm relative velocity. Gibson Ridge dealiasing algorithm applied, with maximum of 40.1 m s$^{-1}$ (-78 kt) green inbound and 24.7 m s$^{-1}$ (+48 kt) red outbound inside 10 km x 10 km box. The box also indicates area shown in succeeding volumetric views.
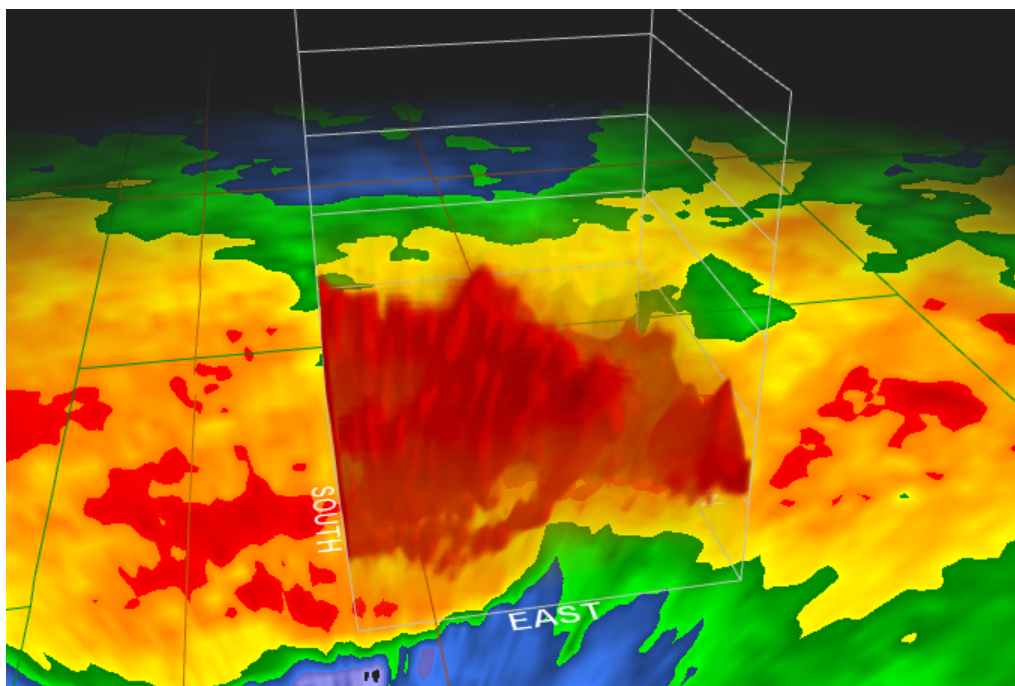
**Fig. 58.** KFSD reflectivity data at 0323 UTC (25 June 2003). Box depicts 10 km x 10 km area noted in Fig. 57 as viewed from the east, with height lines in increments of 10k ft. Yellow color ≥40 dBZ, red color ≥50 dBZ.
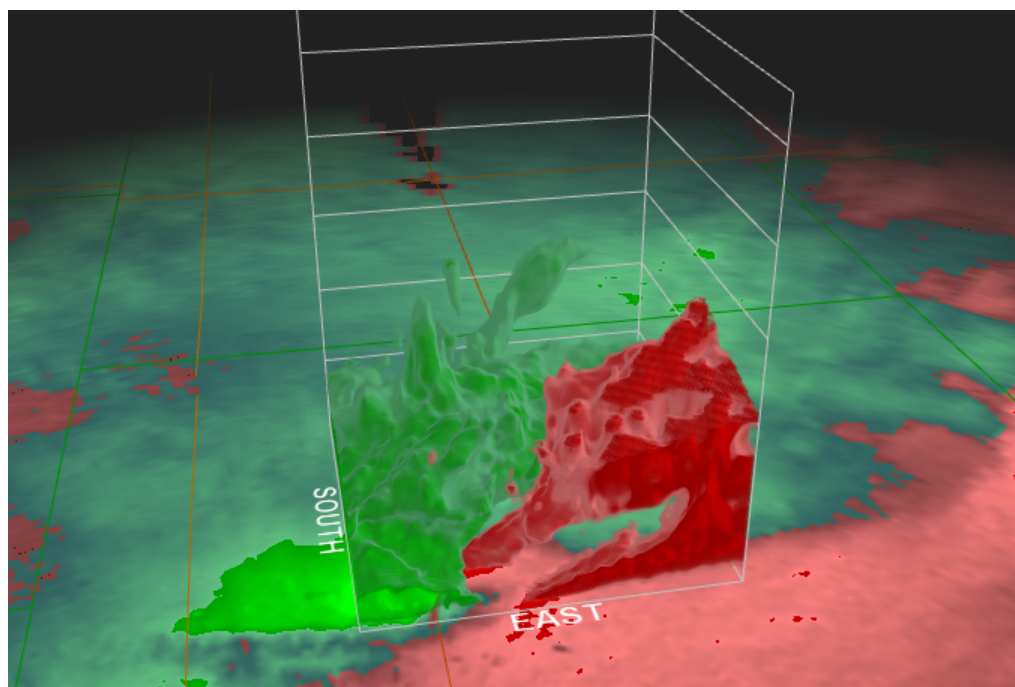


**Fig. 59.** Storm relative velocity 40 kt isosurfaces. Same scale, view, and time period (0323 UTC 25 June 2003) as in Fig. 58. Pink values in lowest level show storm inflow, and stronger green inbounds show incoming north side of the squall line.
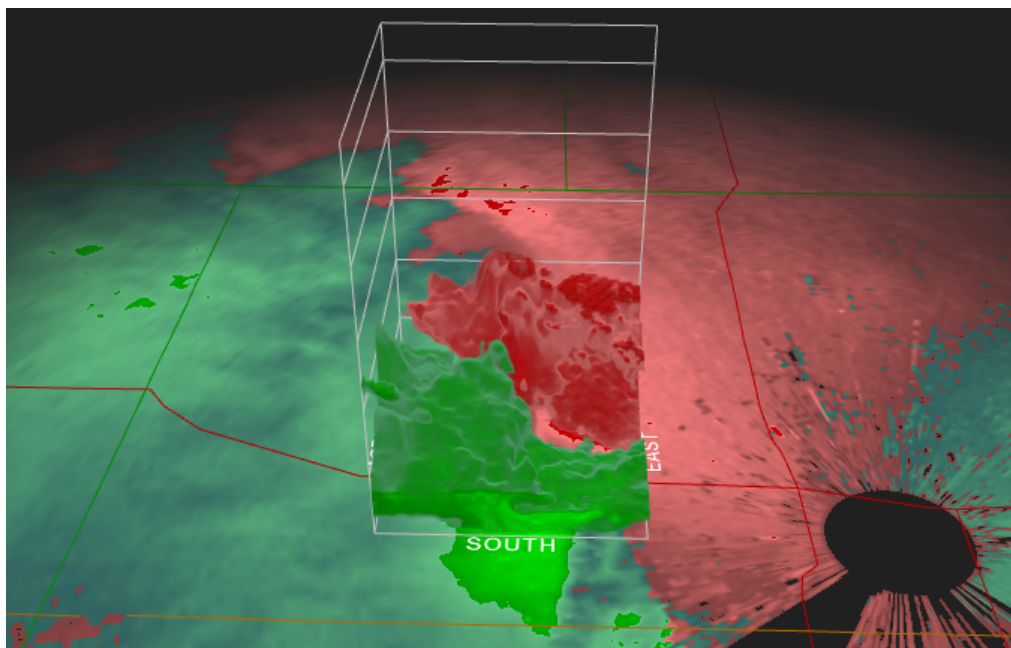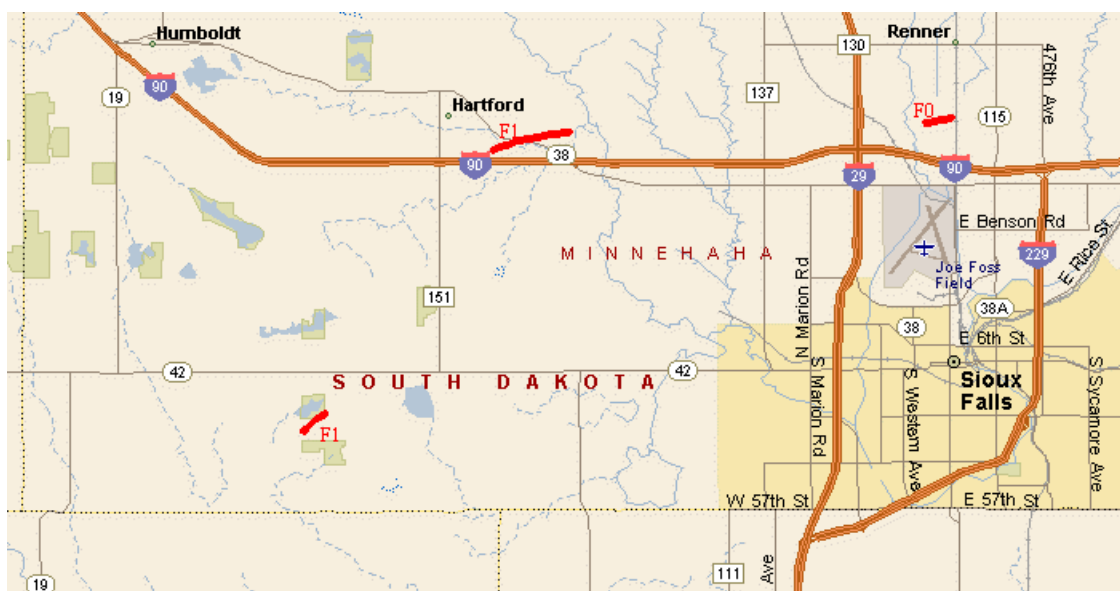
**Fig. 60.** Same as Fig. 59, except viewed from the south.



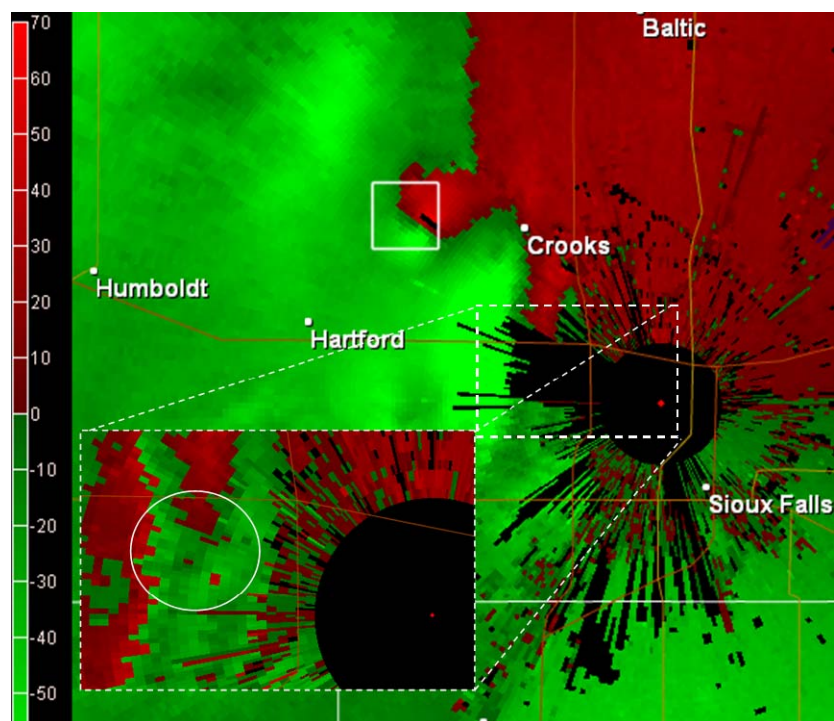**Fig. 61.** Tornado damage paths in Minnehaha County, from survey by NWS-FSD.

**Fig. 62.** Base velocity 0.5 deg, 0328 UTC. Solid box 4.5 km x 4 km. Dash inset shows raw Nyquist velocities. Many >15.4 m s$^{-1}$ (>30 kt) gates inside circle near gust front.
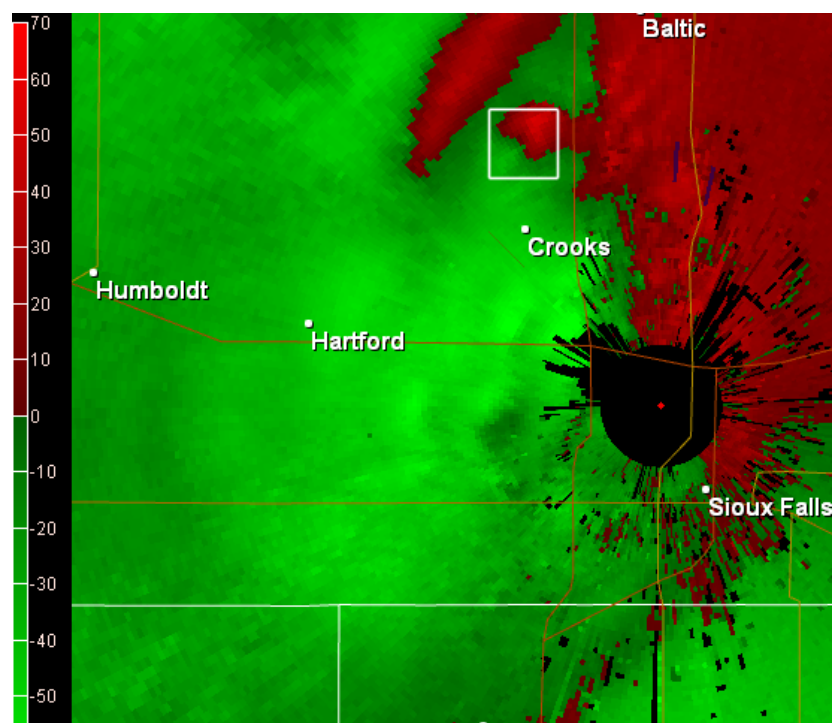


**Fig. 63.** Base velocity 0.5 degree, 0333 UTC. Solid box 4 km x 4 km.
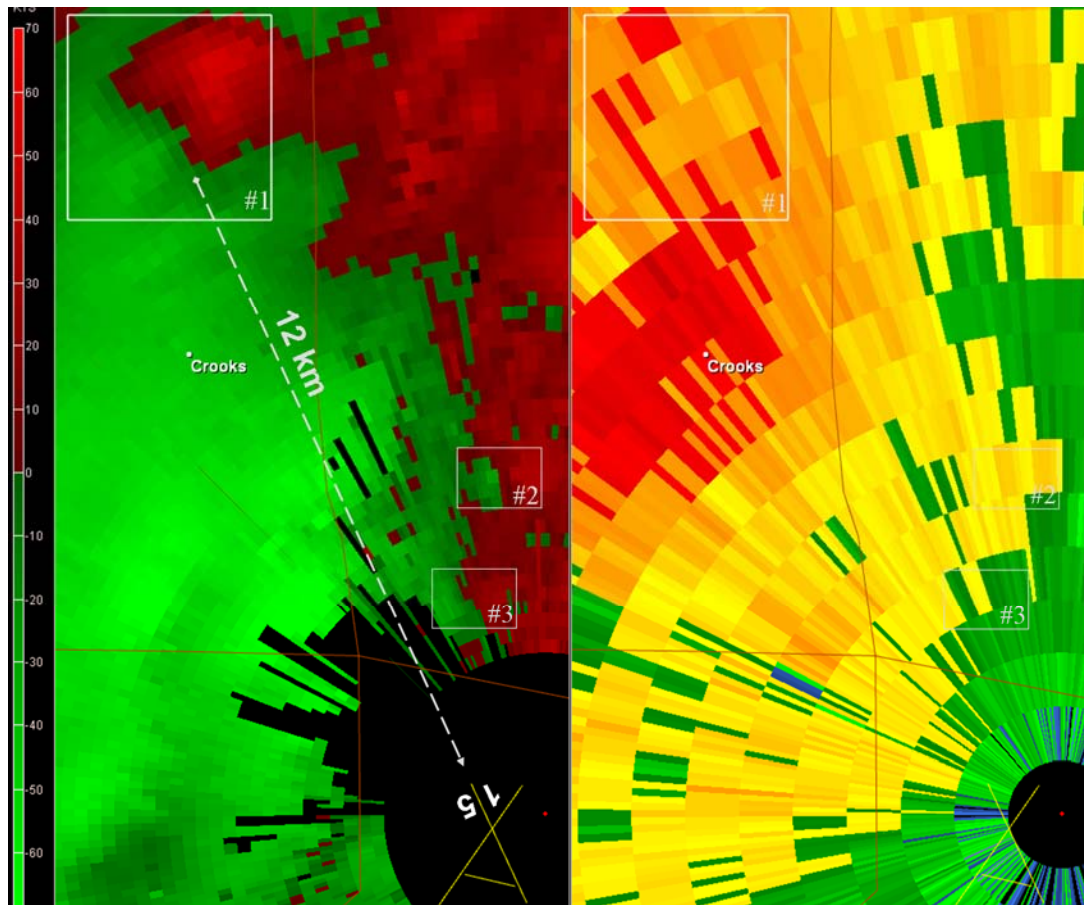
**Fig. 64.** Base velocity (left) and base reflectivity (right) from KFSD at 0033 UTC (25 June 2003). The distance from circulation #1 to runway 15 at Sioux Falls airport is 12 km.

**Conclusions**

The record outbreak known as "Tornado Tuesday" in South Dakota provided us the occasion to research past single-day tornado outbreaks in the state. We found the historical record for such outbreaks, similar to tornado report records in other parts of the country, contains flaws. Additionally, since the 67 tornadoes confirmed on 24 June 2003 is more than double any previous outbreak in South Dakota, we suggest the large number of tornadoes in this outbreak is more due to the efficiency of modern reporting methods than meteorological causes. Yet given a compilation of notable tornado days in South Dakota, we found a precursor link: in 70 percent of the significant outbreaks since 1950, tornado generation was preceded by rapid advection (<72 h) of air parcels from the Arkansas-Louisiana-Texas region – normally a source region for warm, moist maritime tropical (mT) air.

A close examination of the 2003 outbreak shows that thermodynamic parameters were exceptionally favorable for severe thunderstorm formation for three days from 22 June-24 June. One factor that favored the third day, on which the tornadoes occurred, was strong positive vorticity advection. We also found that the meso-Eta forecast model (now the North American Mesoscale model) under predicted surface dew points at the location of the first tornado of the outbreak. It resulted in an underestimation of surface-based CAPE by 3000 J kg-1 and overestimation the height of the level of free convection by 960 m. This situation serves as a reminder to monitor observed dew points when forecasting late-day thunderstorms in a region in which morning convection occurred. The resultant supercell

initiation here appears to have occurred near fine lines of low-level convergence detected on satellite and weather surveillance radar.

Another key finding for those concerned with operational forecasting is the dissimilarity of tornado paths and supercell paths of motion. While it has long been known that tornado motion and motion of its parent supercell cannot be assumed to be identical, here we documented two cases where there was substantial deviation. In the first tornado of the outbreak, the tornado vortex appeared to move north while the supercell moved in a forecasted northeasterly direction near the rear-flank downdraft. Later in the event, warm sector tornadoes moved in an unusual southeast to northwest direction – the result, we hypothesize, of tornadoes swirling cyclonically around large, northeast-moving mesocyclones. In both cases the tornadoes moved to the left of supercell motion (left-moving tornadoes, not left-moving supercells), demonstrating a limitation of the accuracy of tornado pathcasts by radar in public warning situations. It is important to consider these effects, particularly in high-instability, weak-shear conditions such as those described in this event.

One final question: Given the conditions outlined in these papers, how predictable was this historic outbreak? Certainly the severe weather that occurred was well-forecast. South Dakota was identified as a tornado risk area days ahead of time, the tornado watch was posted hours ahead of time, and most of the tornado warnings were in effect several minutes ahead of time. But what about the quantitative magnitude of the outbreak, should that have been anticipated?

Most forecasters are cautious about issuing a forecast that includes record-setting phenomena. In this case, caution would have been justified. The SPC did not even declare it a "particularly dangerous situation" until 0135 UTC – more than three hours into the six-hour outbreak. A record number of tornadoes was not assured even at that point, when you consider that over half of the outbreak's tornadoes occurred in the least-likely area - not near the surface low nor along the warm front, but in the warm sector, where directional shear was minimal and mid-level flow was weak. These were not supercell tornadoes in the traditional sense – they were small, updraft-driven vortexes that multiplied in number. But without them, there would have been no single-day record tornado outbreak of 24 June 2003.